DEVELOPMENT AND EXPERIMENTAL VERIFICATION OF A PARAMETRIC MODEL OF AN AUTOMOTIVE DAMPER

A Thesis

by

KIRK SHAWN RHOADES

Submitted to the Office of Graduate Studies of
Texas A&M University
in partial fulfillment of the requirements for the degree of

MASTER OF SCIENCE

August 2006

Major Subject: Mechanical Engineering

DEVELOPMENT AND EXPERIMENTAL VERIFICATION OF A PARAMETRIC MODEL OF AN AUTOMOTIVE DAMPER

A Thesis

by

KIRK SHAWN RHOADES

Submitted to the Office of Graduate Studies of
Texas A&M University
in partial fulfillment of the requirements for the degree of

MASTER OF SCIENCE

Approved by:

Co-Chairs of Committee,	Make McDermott
	Gerald Morrison
Committee Members,	Daejong Kim
	Glen Williams
Head of Department,	Dennis O'Neal

August 2006

Major Subject: Mechanical Engineering

ABSTRACT

Development and Experimental Verification of a

Parametric Model of an Automotive Damper. (August 2006)

Kirk Shawn Rhoades, B.S., University of New Mexico

Co-Chairs of Advisory Committee: Dr. Make McDermott
Dr. Gerald Morrison

This thesis describes the implementation of a parametric model of an automotive damper. The goal of this research was to create a damper model to predict accurately damping forces to be used as a design tool for the Formula SAE racecar team. This study pertains to monotube gas charged dampers appropriate to Formula SAE racecar applications.

The model accounts for each individual flow path in the damper, and employs a flow resistance model for each flow path. The deflection of the shim stack was calculated from a force balance and linked to the flow resistance. These equations yield a system of nonlinear equations that was solved using Newton's iterative method.

The goal of this model was to create accurately force vs. velocity and force vs. displacement plots for examination. A shock dynamometer was used to correlate the model to real damper data for verification of accuracy. With a working model, components including the bleed orifice, piston orifice, and compression and rebound shims which were varied to gain an understanding of effects on the damping force.

ACKNOWLEDGEMENTS

I would like to express my sincere gratitude to Dr. Make McDermott for the opportunity to perform this research. Your time and help in this project is greatly appreciated. A special thanks to Shaun Lide and Brian Auer for guidance in testing procedures.

Thank you to the remaining members of my thesis committee for all guidance and assistance in the project and thesis.

To my parents, your love has always been the thing that kept me going when I needed a push. I hope I have made you proud.

Great thanks to my friend, Andy, for enduring graduate school alongside me. It was an experience neither of us will ever forget. To my old friends, Jon and Brad, thanks for all the support. Finally to my friend, Rebecca, you always kept the smiles coming. It will never be forgotten.

TABLE OF CONTENTS

Page

Page

LIST OF FIGURES

FIGURE Page

FIGURE Page

FIGURE Page

LIST OF SYMBOLS

Symbol	Definition, Units
A	Area, in^2
A_b	Area of the bleed orifice valve, in^2
A_c	Area of compression side of piston, in^2
A_{dyno}	Amplitude of sine wave for dynamometer motion, in
A_{gp}	Area of gas piston, in^2
A_o	Area of piston orifice, in^2
A_r	Area of rebound side of piston, in^2
A_{rod}	Area of the piston rod, in^2
A_v	Area of valve on which the pressure acts, in^2
$A_{v,\ flow}$	Area through which valve flow occurs, in^2
B	Clearance between piston seal and cylinder inner wall, in
C_D	Dynamic discharge coefficient
$C_{D,b}$	Dynamic discharge coefficient for the bleed orifice
$C_{D,v}$	Dynamic discharge coefficient for the valve orifice
C_f	Momentum adjustment coefficient
D_b	Diameter of bleed orifice, in
D_o	Diameter of piston orifice, in
D_p	Diameter of piston, in
D_v	Diameter of the valve, in
E	Modulus of Elasticity, lbs/in^2

Symbol	Definition, Units
F	Damping Force, lbs
F_{dyno}	Frequency of sine wave for dynamometer motion, Hz
Symbol	Definition, Units
F_f	Friction force from piston seal, lbs
F_m	Momentum force on valve caused by direction change of fluid, lbs
F_{sp}	Preload force on shims, lbs
k	Shim stiffness, lbs/in
l	Length of piston leakage gap, in
L_g	Length of the gas chamber, in
m_{gp}	Mass of the gas piston, lbm
m_p	Mass of the piston/rod assembly, lbm
p	Pressure, lbs/in^2
p_c	Pressure in the compression chamber, lbs/in^2
p_f	Final pressure in ideal gas equation, lbs/in^2
p_i	Initial Pressure in ideal gas equation, lbs/in^2
p_g	Pressure in the gas chamber, lbs/in^2
p_{gi}	Initial pressure in the gas chamber, lbs/in^2
Q	Total volumetric flow rate, in^3/sec
Q’	Equivalent flow rate due to the rod insertion, in^3/sec
Q_b	Bleed orifice flow rate, in^3/sec
Q_{lp}	Piston leakage flow rate, in^3/sec

Symbol	Definition, Units
Q_v	Valve orifice flow rate, in^3/sec
V_i	Initial volume of gas chamber, in^3
V_f	Final volume of gas chamber, in^3
x	Displacement of Piston, in
$\dot{x}$	Velocity of Piston, in/sec
$\ddot{x}$	Acceleration of piston, in/sec^2
y	valve opening distance, in
z	Displacement of gap piston, in
$\ddot{z}$	Acceleration of gas piston, in/sec^2
α	Area flow correction factor
β	Fluid compressibility, ft^2/lb
β'	Effective compressibility including cylinder wall compliance, ft^2/lb
Δp_{po}	Pressure drop across the piston orifice, lbs/in^2
Δp_{valve}	Pressure drop across the valve shim, lbs/in^2
ΔV	Volume change in gas chamber, in^3
μ	Dynamic viscosity, lbs*s/in^2
ρ	Density, lbs/in^3

INTRODUCTION

In any design endeavor with limited time for research and development, tools that increase productivity or decrease necessary testing are crucial for success. The Formula SAE student design competition is no exception. In most cases, teams have one year to design and fabricate all systems of a racecar. This gives rise to a need for development tools such as computer models of suspension, chassis, and engine systems. Because of schedule constraints, the suspension design of most Formula SAE racecars is based primarily on steady state analysis.

An often underutilized area of development is the suspension dampers, which are commonly referred to as shock absorbers. The majority of data for dampers is experimental. Damper design and performance is fully understood by few in the field. A damper model or design tool is not commonly employed, but a valid model could aid in the choice of dampers and save hours of trial and error testing of damper orifice designs and shim stack combinations.

The primary objective of this research is to create and validate a parametric model for use as a stand alone damper design tool. This model will calculate Force vs. Velocity curves given input parameters characterizing the damper. Parameters required included dimensions of damper components, properties of hydraulic fluid, and known internal gas pressures. It can be used to experiment virtually with tunable aspects of an existing damper, or aid in choice or design of a new damper.

This thesis follows the style of the Journal of Automobile Engineering.

The secondary objective was to gain an insight into the hysteretic behavior of dampers that appears in characteristic Force vs. Velocity graphs. Understanding this phenomenon will provide valuable insight into the inner working of racecar dampers and is a necessary first step in any attempt to minimize this effect.

FUNCTIONAL DAMPER CHARACTERISTICS

The first step in understanding the operation of a damper is to understand how the components interact to create the damper force. A brief discussion of damper components and functionality is given in this section. The characteristics of damper are usually presented graphically in Force vs. Velocity and Force vs. Displacement graphs. A detailed description of these graphs is contained in this section.

GENERAL CONFIGURATION OF DAMPER

There are many types of automotive suspension dampers, which are commonly referred to as shock absorbers. This is a misnomer because the damper does not actually absorb the shock. That is the function of the suspension springs. As is well known, a spring/mass system without energy dissipation exhibits perpetual harmonic motion with the spring and the mass exchanging potential and kinetic energy, respectively. For the purpose of this paper, the term damper will be used. The function of the damper is to remove the kinetic energy from the system and to convert it into thermal energy.

There are numerous configurations of dampers: twin tube, monotube with or without reservoir, and even a rod through damper type. For the purpose of this thesis, a monotube damper without a separate reservoir will be examined.

Another major distinction in damper types is the feature of external adjustability, i.e. if the damping can be adjusted after the damper is assembled. Automotive applications generally use a nonadjustable damper. In contrast, many dampers for racing applications have some degree of adjustability. Since the main focus of this research is

to aid in racecar suspension design, the monotube damper chosen has adjustable damping.

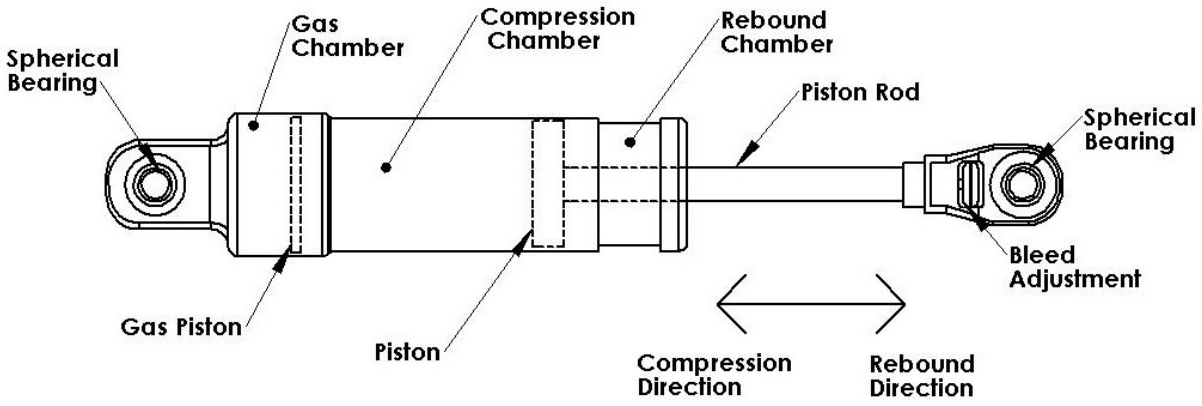

Figure 1: Components of Monotube Adjustable Damper

Figure 1 displays the major components of a monotube style, externally adjustable damper. The damper is comprised of a piston assembly that moves inside a fluid filled cylinder. The outer housing of the damper contains all internal components. A fully assembled damper is partitioned into three pressure chambers: gas, rebound and compression. The gas chamber is separated from the compression chamber by a floating piston. This floating piston separates the gas in the gas chamber from the fluid, typically oil, in the compression and rebound chambers. The gas used for most damper applications is dry nitrogen because it does not react with oil. It is relatively insensitive to temperature and contains no water vapor.

The compression chamber is the volume between the floating gas piston and the piston attached to the rod. The rebound chamber is the volume on the rod side of the piston. The compression and rebound chambers are completely filled with oil, typically 5W weight oil designed for this application.

The piston is connected to the piston rod which exits the housing through a rod seal that retains the oil. The rod seal also prevents dirt and other contaminates from entering the rebound chamber and affecting internal flow of oil. The piston also has a seal between its outer diameter and the inner diameter of the outer housing. This seal separates the compression and rebound chambers.

The spherical bearings shown in Figure 1 are for mounting the damper to the vehicle. They allow for some degree of misalignment in mounting without imposing bending loads on the damper. For racing applications, the piston rod of the damper is usually mounted to the wheel suspension, while the cylinder side is connected to the frame of the vehicle in order to minimize the unsprung weight.

GENERAL OPERATION OF DAMPER

There are two modes of operation in a damper: compression and rebound. Each of these modes will be examined individually. The compression operation mode is shown in Figure 2.

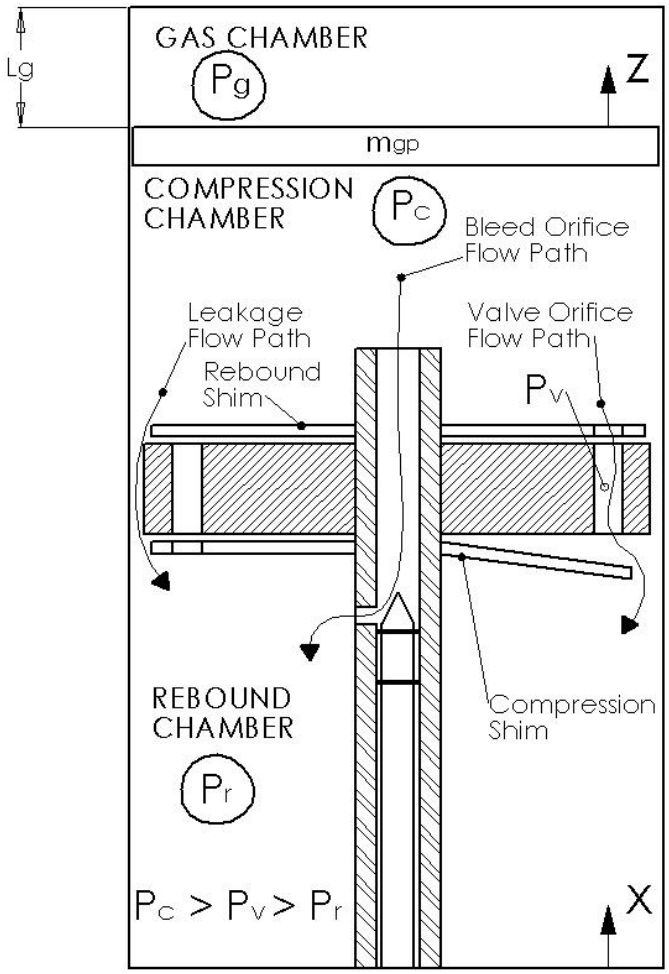

Figure 2: Compression Stroke Flow Diagram

During the compression stroke, fluid flows from the compression chamber into the rebound chamber. Since the oil is effectively incompressible, as the piston rod enters the rebound chamber the sum of the volumes of the oil and the rod in the rebound and compression chambers must increase. To accommodate this volume increase, the gas piston compresses the nitrogen in the gas chamber to decrease the gas volume by an amount equal to the volume of the inserted rod. Monotube dampers also have the

advantage of pressurizing the gas chamber to maintain an elevated pressure on the oil, which helps prevent oil cavitation. Model analysis has shown only a four to ten psi change in the gas chamber pressure for one inch of piston rod displacement, depending on initial gas pressure value. This small pressure change means an almost uniform pressure exerted on the hydraulic oil in the compression chamber. The pressure in the gas chamber is denoted P_g.

A gas spring effect is also present due the pressure in the gas chamber. A force equal to the area of the rod times the gas pressure, P_g, will be on the rod at all times. Gas spring effect is independent of piston velocity, but strongly dependant on displacement and very weakly dependant on acceleration. The gas spring force increases during the compression stroke.

Total flow during compression is comprised of flow through three flow paths. These flows are related to the pressure differences in the pressure chambers. Pressure in the rebound chamber is denoted as P_r and pressure in the compression chamber is denoted P_c. During compression P_c is greater than P_r; this pressure difference drives the flow from the compression chamber to the rebound chamber and generates the damping force. Flow paths and chamber pressures are shown in Figure 2 and explained below.

The first path is the flow through the bleed orifice. The bleed orifice flow path begins at the end of the piston rod in the compression chamber and ends out of the side of the piston rod in the rebound chamber. The bleed orifice size can be adjusted by moving the needle valve inside the piston rod in Figure 2. The needle valve is adjusted in or out using the bleed adjustment shown in Figure 1. The bleed flow orifice can be

adjusted from fully open for less damping to fully closed for increased damping. Modifications to the geometry of the needle value or size of the bleed orifice can change the bleed orifice flow also. The bleed orifice dominates the low speed damping because this orifice is always open, regardless of piston velocity.

The second flow path is the valve orifice flow path. Valve orifice flow travels through constant diameter holes in the piston and past thin washer-like shims that deflect to allow flow. Valve flow is controlled by the compression shim or shims. For simplicity, only one shim is shown in Figure 2. The flow into the compression valve travels through a hole in the rebound shim. This hole in the rebound shim eliminates the need to machine a flow path in the piston and is a simple way of allowing valve flow and decreasing complexity of piston manufacture.

Increased velocity decreases the pressure in the rebound chamber and increases the flow rate. The pressure differential also triggers shim. The compression shim, located in the rebound chamber, limits the area for flow depending on the velocity of the piston. With increased velocity, shim deflection increases and valve flow area increases. P_v is defined as pressure inside the exit of the orifice in the piston.

The third flow path is the leakage flow around the piston-cylinder wall seal. Leakage flow is at least an order of magnitude less then other two flows, but is difficult to eliminate completely. With prolonged usage the seal may degrade, increase the leakage flow, and lessen the damping force from the damper. The piston cylinder seal should be replaced periodically so that the leakage flow does not become significant in comparison to the other flow paths.

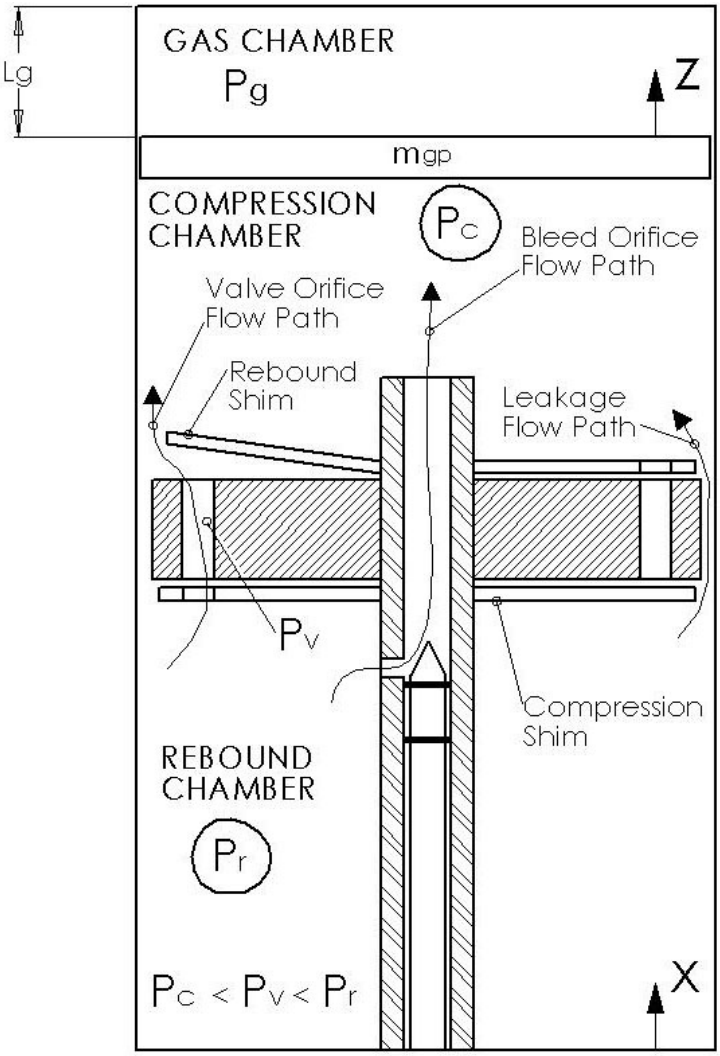

Figure 3: Rebound Stroke Flow Diagram

Rebound operation is shown in Figure 3. During the rebound stroke, the piston rod is being withdrawn from the fluid filled cylinder, causing flow from the rebound to the compression chamber. The combined volume of oil plus the rod in the compression and rebound chambers is now decreasing due to the removal of the rod, and the gas in the gas chamber expands.

The flow in rebound is from the rebound chamber to the compression chamber. All the valve, bleed, and leakage flow paths discussed previously still exist, only their directions have reversed.

The bleed orifice flow now begins at the side inlet hole in the piston rod, and exits out the end of the piston rod into the compression chamber. All the properties of low speed damping dominated by the bleed are retained in the transition from compression to rebound.

The valve orifice flow path is conceptually the same as for compression, only the specific orifice is different. During rebound the pressure relationships are $P_r > P_v > P_c$. The valve flow now travels through the appropriate hole in the compression shim and initiates the deflection of the rebound shim in the compression chamber. As before, an increase in rebound velocity will result in increased shim deflection and valve flow area.

The leakage flow is of the same magnitude and travels through the same axisymmetric gap between the piston seal and the outer cylinder. Only the direction in rebound is opposite of that in compression.

After examination of the rebound and compression stroke, it can be seen that physical operation of the damper is complex. Dampers are displacement, velocity and acceleration dependant. The equations relating pressures, shims deflections, flows, etc. will be the basis for modeling the behavior of a damper.

CHARACTERIZATION OF DAMPER OPERATION

Since the position and velocity of a damper in any automotive or racing application is in constant state of change, it is hard to define and interpret damper performance. To evaluate the performance of a damper, testing on a damper dynamometer has become the norm. The damper dynamometer used in this research is a Roehrig 2VS. This damper dynamometer imposes a sinusoidal input for displacement. The displacement is defined by specifying the amplitude and the frequency. The first and second derivatives of the displacement are the velocity and acceleration, respectively.

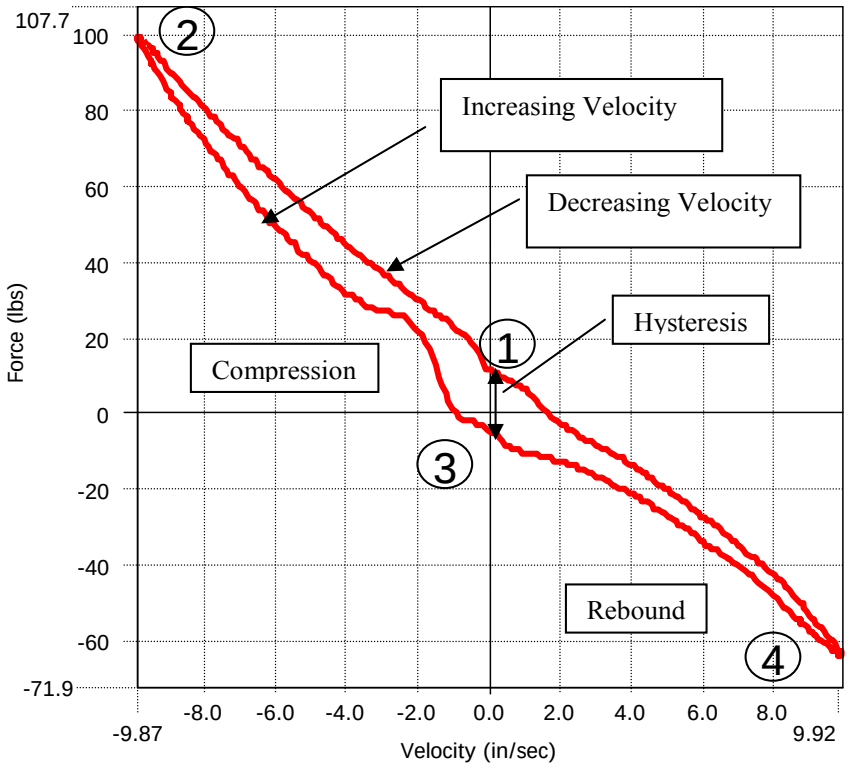

Figure 4: Full Cycle Force vs. Velocity Plot

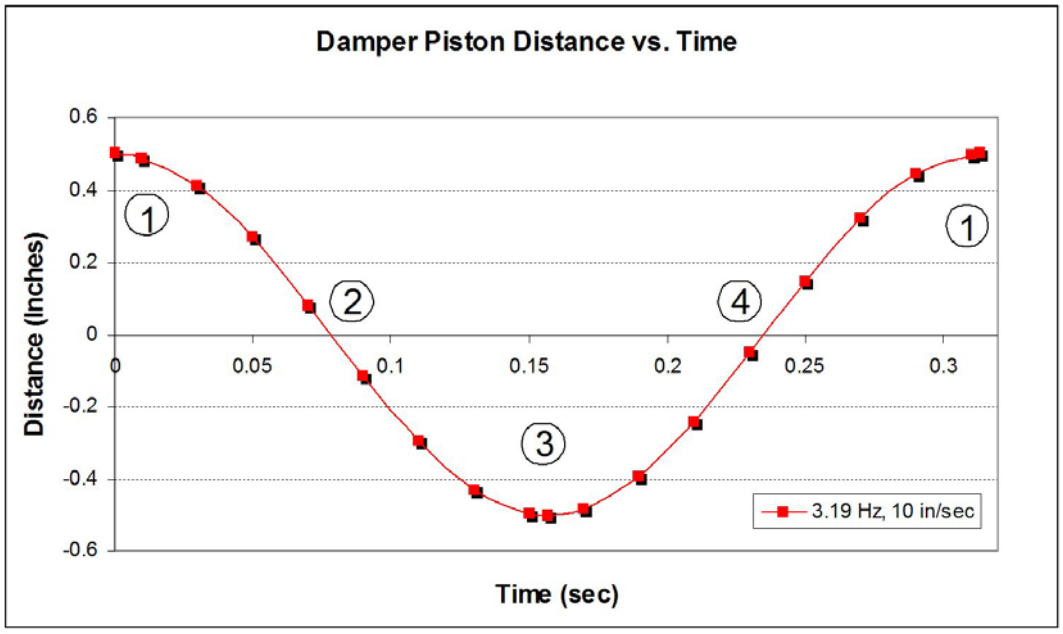

Figure 5: Damper Piston Distance vs. Time Corresponding to FV Plot

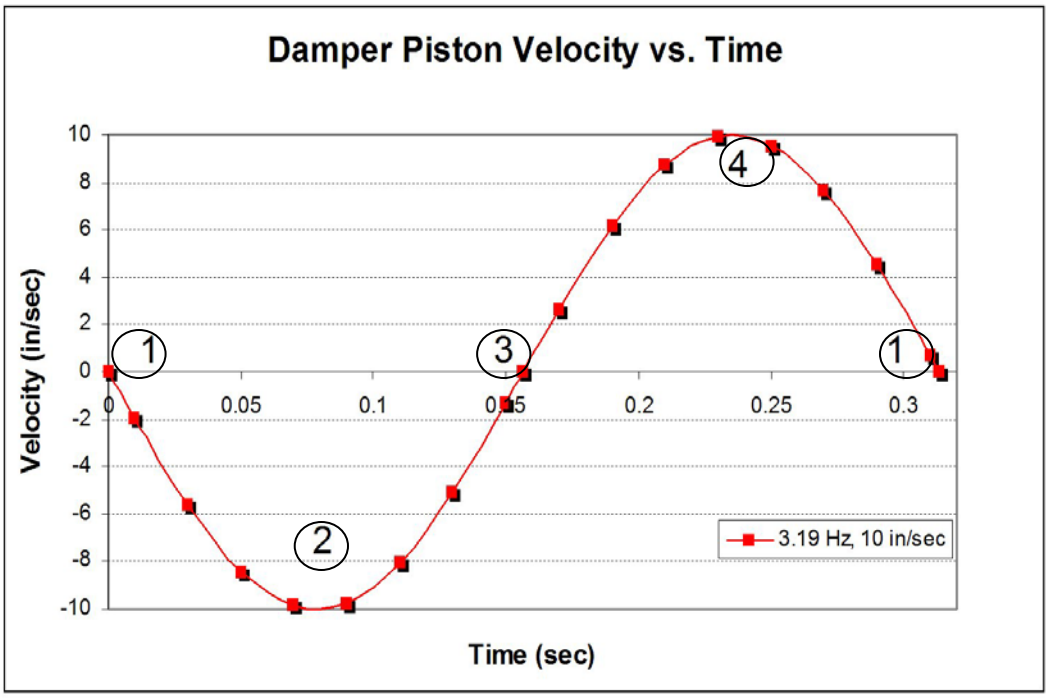

Figure 6: Damper Piston Velocity vs. Time Corresponding to FV Plot

The primary means used to characterize damper performance is the Force vs. Velocity (FV) plot. Figures 4 through 6 show the basic FV plot and the corresponding motion profiles.

Figure 4 shows a Force vs. Velocity plot for a full cycle, compression and rebound strokes. This is sometimes referred to as a Continuous Velocity Plot (CVP). It is important to note the sign conventions for force and velocity. Compression results in negative velocities, while rebound, increasing length, results in positive velocities. In some instances [1], the velocity definitions may be opposite. The convention shown here is used by the Roehrig test dynamometer, and will be used throughout this report.

The convention for forces is to record the force produced by the damper. Rebound forces are negative while compression forces are positive. There are small regions near zero velocities where this is not true. This is due to the hysteretic effects of the damper. The hysteresis shown in Figure 4 is the difference in the force at a given speed when the speed is increasing and when the speed is decreasing. In other words, the damper produces a different force when it is speeding up than when it is slowing down. The term hysteresis is commonly used to refer to this effect and will be used throughout this paper for the difference in forces in the FV plots. However this effect is not the classical hysteresis defined in the scientific literature. The cause of this phenomenon will be examined in the Literature Review section.

Figures 4-6 also have labeled points numbered one through four. These are key points in the motion of the damper. Point one is the beginning of the cycle. The damper is at full extension and has zero starting velocity. From point one to two the damper

begins the compression stroke with increasing speed. At point 2, the maximum negative velocity is achieved. This usually corresponds to the peak force of the compression stroke. The displacement is zero, which means half of the full stroke has been compressed into the damper. From point two to three, the speed begins to decrease. Point three represents the end of the compression stroke. The displacement is at the full negative value, which means that the damper is fully compressed. The speed has returned to zero. Immediately after that point three, the rebound stroke begins with the speed increasing again. At point four, the peak force of the rebound stroke is achieved. The displacement is again at a zero value, so the damper is at extended to half of the total rebound stroke. The cycle then goes from point four back to point one. The rebound continues with the speed of the piston decreasing. At point one, the damper returns to full extension and to zero velocity.

All plots generally remove the gas spring force. Therefore, the force is equal to zero at velocity equal to zero.

The other plot sometimes used to characterize damper performance is the Force vs. Displacement (FD) plot. Figure 7 shows a typical FD plot. This plot is a carryover from the efforts to characterize dampers when all mechanical equipment used measured and charted only Force vs. Displacement.

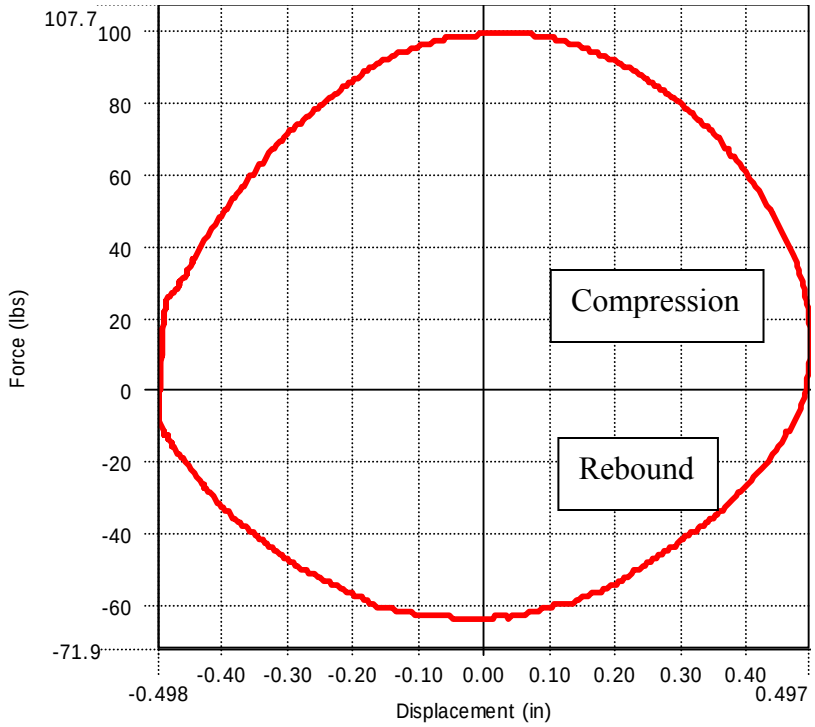

Figure 7: Full Cycle Force vs. Displacement Plot

FD plots use the same force sign convention; positive for compression, negative for rebound. For both compression and rebound, the forces in Figure 7 are not symmetric about the y-axis. The same hysteresis shown in the FV plots is the cause of this asymmetry.

In an attempt to gain understanding, hysteresis can also be examined using a hypothetical ideal spring, a hypothetical ideal damper, and sinusoidal motion input. A hypothetical linear spring will produce a straight line with slope K in an FD plot and an ellipse in and FV plot (see Appendix A). A hypothetical linear damper will produce a straight line with slope C in an FV plot and an ellipse in an FD plot. Hysteresis in an FV plot for an actual damper results when the damper produces spring-like forces.

LITERATURE REVIEW

A literature review was conducted with two major goals. The first goal was to obtain a better understanding of how individual internal components and internal flows had been characterized in the past by studying the development of parametric models for damper characterization.

The second goal of the literature review was to gain an insight into the hysteretic behavior that occurs in characteristic FV plots. Understanding the causes of this phenomena and how it can be minimized are of crucial importance in damper design. Both of these concepts will be addressed in the cited literature.

In 1977, Lang published his Ph.D. dissertation studying the behavior of automotive dampers at high stroking frequencies [1]. The work included creation of one of the first parametric models of a twin tube automotive damper with good agreement to experimental data. This paper is the milestone paper in understanding performance behavior of modern dampers.

The concepts behind Lang's model involved "…the development of a mathematical model of shock absorber performance based upon dynamic pressure flow characteristics of the shock absorber fluid and the dynamic action of the valves" [1]. Lang was one of the first to examine the internal physics of the fluid and the valves in an attempt to model their behavior. The model included the effective compressibility, β', which also accounts for the compliance of the cylinder wall. This aided in correctly modeling one influence on hysteresis. Chamber pressures were also examined.

The model used equations for standard steady orifice flow based on the pressure drop across the flow orifice. The dynamic discharge coefficients and the valve opening forces were found experimentally. A limitation to Lang's model was computing power; his work was completed on an analog computer. For this reason, dynamic discharge coefficients were assumed constant. Good agreement to experimental data was found using this assumption.

Lang then exercised his model to examine factors such as effective fluid compressibility, fluid vapor pressure, and frequency input. A nominal value of effective compressibility, $\beta' = 4.5\,E-6$ in^2/lb, was found. FV plots were created using the nominal value, twice the nominal value, and half the nominal value. It was shown that as effective compressibility increases hysteresis increases, in both high and low speed regions.

Examination of vapor pressure showed the same trend. As the vapor pressure of the damping fluid increases the hysteresis in the FV plot increases because this fluid in the rebound chamber vaporizes at higher pressures. Values from two to ten psi were tested. The hysteresis is caused by the cavitation of the fluid due to the increased vapor pressure values.

Lang's experimentation with input frequencies was particularly valuable. The range of 1-50 Hz was tested. It showed small differences in hysteresis in the 1-10 Hz region and increasing differences in hysteresis for 10-50 Hz range. The increase was most visible in the region affected by the effective compressibility. It was also

determined that inertial effects of the valve parts were negligible compared to other forces due to their small mass.

In conclusion, Lang recommended separation of the gas and fluid in a twin tube chamber in order to control cavitation and frothing in the damper. He also theorized about a rod that travels through both compression and rebound chambers to eliminate the need for any internal gases. Both of these concepts have been applied to modern day high performance dampers.

Reybrouck presented one of the first concise parametric models of a monotube damper [2]. Flow restriction forces were found using empirical relationships that included leak restriction, port restriction and spring stiffness correction factors. Once individual internal forces were found, another empirical relationship was used to calculate the total damping force. Pressure drops across the specific flow restrictions could also be found. These correction factors had some physical meaning, but their values were found through experimentation.

This model showed excellent correlation with experimental data in the 0.5 to 30 Hz range, provided that hysteresis was minimal. Implementation of this model is difficult due to the numerous correction factors necessary for accuracy. There was no discussion about the causes of hysteresis aside from its dependence on frequency.

Reybrouck later extended his model to a twin tube damper and included a more physical representation of hysteresis [3]. It was shown that hysteresis was caused not only by oil compressibility, but the compressibility of gas bubbles transferred from the reserve chamber. It was also shown that reserve chamber pressure greatly affects the

solubility of nitrogen. As the pressure increases the entrapped bubbles are absorbed. This effect should not be neglected for accurate results.

Kim [4] also performed an analysis of a twin tube damper with focus on implementation into a vehicle suspension system. Kim's model [4] included chamber compliance and fluid compressibility which yielded a differential equation for the chamber pressures that was solved using the Runga Kutta Method. Discharge coefficients were experimentally found and applied to the model. Incorporating damping data into a quarter car model, the frequency response of the sprung mass and tire deflection were calculated numerically. Good agreement with experimental data was found for single strokes of the damper, but no full cycle FV plots were included.

Mollica and Youcef-Tuomi presented a monotube damper model created using the bond graph method [5], based on Mollica's M.S. thesis work [6]. This reference concluded five major sources for hysteresis in FV plots.

1. effective compliance of damper fluid,
2. compressibility of the nitrogen gas
3. the resistive fluid damping through piston orifices
4. the resistive friction acting on the floating piston
5. compliance due to the check valve preloads

A simplified model of a damper was created to examine the frequency effects on hysteresis. This simple model showed that for low frequencies the effort is in-phase with fluid flow and velocity. At higher frequencies, the force lags the flow and velocity by 90 degrees. This equates the hysteresis at high frequencies to a phase lag in a control

system. This is similar to the hypothetical spring/damper discussion in the previous section.

Reference [5] also states "Air entrained as bubbles increases effective fluid compliance thereby increasing hysteresis due to additional phase loss occurring at the same input frequency." This shows the importance of eliminating any trapped gas in the damper oil in a monotube damper to reduce hysteresis. This also aids in explaining the general trend of greater hysteresis in twin tube dampers that mix oil and gas in the reserve chamber.

The inertia of the gas piston was found to be negligible. Friction from the gas piston was found to be more important, causing an increase of hysteresis near the zero velocity regions.

Talbott's M.S. thesis in 2002 presents a physical model for an Ohlins NASCAR type monotube racing damper [7]. One major goal of this model was to correlate the model to the real physics of the damper to avoid experimental correction factors used in earlier models. This approach increases ease of implementation to any type of monotube damper with minimal experimentation necessary. Talbott and Starkey also published these findings in SAE paper 2002-01-3337 [8].

Total flow is comprised of valve orifice flow, bleed orifice flow, and piston leakage flow. Flow resistance models were created for each separate flow based on the pressure drop across the orifice, path per Lang's work. Pressure in the gas chamber, P_g, was related to the pressure in the compression chamber, P_c using force balance on the

gas piston. This relation of P_g and P_c was one of the important findings of this modeling method. Talbott assumed the oil and gas in the damper was incompressible.

The other contribution of Talbott was the creation of a shim stack model that predicts the shim stiffness. The model was applicable to a minimum of three shims and a maximum ten. This was the first attempt at any modeling of this shim stack deflection in conjunction with a damper model.

Six non-linear coupled equations were created and solved simultaneously. With all unknowns, the damping force was found from the force balance on the piston assembly.

The model showed good agreement in both FV and FD plots. The low speed regions showed some difference in force due to the hysteresis present in the experimental data. The high speed regions show excellent agreement, particularly after the pre-loaded shim stack opens as a flow path.

DAMPER SPECIFICATIONS

The damper used for this research is a Tanner Externally Adjustable Gen 2 from Tanner Racing Products. It is a gas charged monotube configuration with a floating piston which separates the gas and oil chambers. The primary use for the Tanner Gen 2 is in quarter midget car racing, but their size, price, and range of available damping force make them appropriate for Formula SAE racecars as well. The Tanner Gen 2 is lightweight, relatively inexpensive, and can attain the desired damping forces with interior modifications. Figure 8 shows a three dimensional model of the Tanner Gen 2 damper.

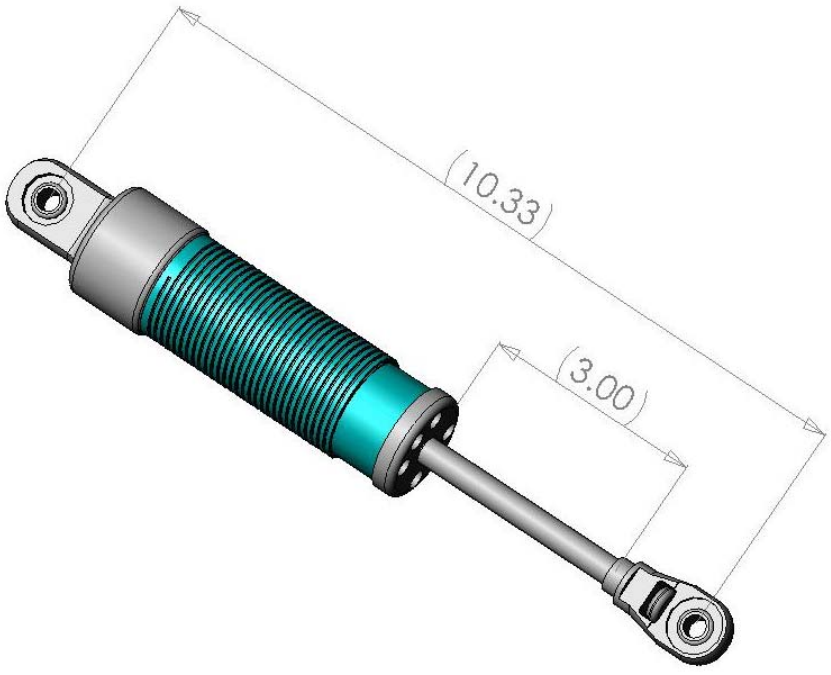

Figure 8: Tanner Gen 2 Damper

The length at maximum extension of the damper is 10.33 inches from centers of the spherical mounting bearings. The stroke of the damper is approx three inches. Outer housing of the damper and end caps are made of aluminum, while the chromed rod is made of polished steel. The end caps are threaded for removal which makes disassembly easy for tuning or rebuild purposes.

The design of the piston and the shims used for controlling the piston orifice flow allow these parts to be manufactured much less expensively than most other racing dampers. The piston is made of machined aluminum and contains six straight orifice flow holes. The piston is shown in Figure 9.

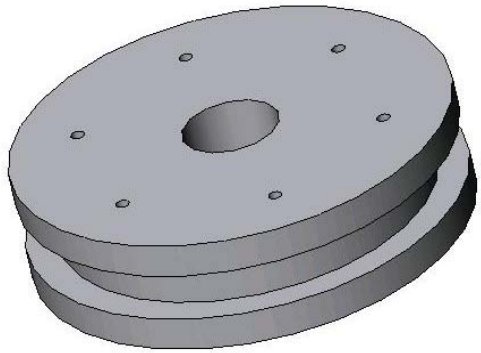

Figure 9: Tanner Gen 2 Aluminum Piston

The piston flow orifices have diameters of .038” and the center hole for mounting the piston on the rod is 0.25” diameter. The groove on the outer diameter of

the cylinder is for the rubber seal between the piston and the cylinder wall. This piston design is less complex than that of an Ohlins or Penske brand damper and this simple design is much less expensive to produce.

Depending on the desired damping levels, pistons are available with the flow orifice diameters from 0.14" (soft damping) to 0.038" (hard damping). Without any shims, the six orifices allow flow in both compression and rebound. A separate shim tuning kit is also available from Tanner racing products; it is shown in Figure 10.

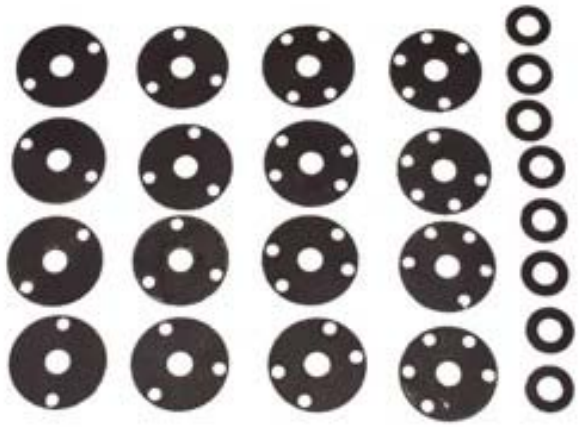

Figure 10: Tanner Racing G2 Carbon Shim Kit [9]

The shims kit from Tanner Racing includes carbon fiber shims. The shims have almost an identical modulus of elasticity and Poisson's ratio to that of steel, but are much lighter in weight. The shims contain holes at locations corresponding to holes in the piston that can be used to create one way flow for compression or rebound. For example, if a two hole shim is used for the compression side of the piston and a three

hole shim for the rebound side of the piston, two one-way paths would exist for rebound and three paths would exist for compression as long as no holes are shared. Also a combination of one way and two way flows can be created. The arrangement of the shims can create numerous possibilities for tuning the Tanner Gen 2 damper. It would also be possible to create shims of varying thicknesses or different materials to achieve desired damping traits.

The threaded needle valve for adjusting the bleed orifice flow has 3.75 turns. The notation of zeros turns is analogous to a fully closed bleed orifice. The larger the number of turns of adjustment, the more the bleed orifice is open. This is a practical consideration since the fully closed position is easy to identify.

The damper fluid used was Tanner Tuned Shock Oil. The properties were unknown for this oil, so typical 5W oil values were used for modeling purposes. Density and viscosity were of primary importance.

DEVELOPMENT OF DAMPER MODEL

Talbott's work with monotube racing dampers was the basis for the following model [7]. The physical basis of each equation will be explained. Modifications to Talbott's method were necessary for modeling of the carbon shims with interior holes.

OVERALL FLOW MODELING

The equations described here are relevant only to the compression stroke of operation, particularly the flow resistance models. For the rebound stroke, the pressure definitions become the opposite and the flow reverses. General operation is the same as shown in Figure 2. The piston rod assembly is pushed into the cylinder and the pressure differential causes flow from the compression chamber to the rebound chamber. Conservation of mass dictates that fluid leaving the compression chamber must enter the rebound chamber.

The total flow rate across the piston is the sum of three different flow paths: bleed orifice flow, valve orifice flow, and piston leakage flow. The major assumption for summation of flow is that the damper oil is incompressible and therefore has constant density. This assumption allows consideration of volumetric rather than mass flow rates. This is expressed in equation (1) and shown in Figure 11. Q is the total volumetric flow rate of the damper in $in^3/\sec$. Q_v is the flow rate through the valves, Q_b is the flow rate through the bleed orifice, and Q_{lp} is the flow rate of leakage past the piston seal

$$Q = Q_v + Q_b + Q_{lp} \tag{1}$$

Boundary C-C can be seen in Figure 11. Equivalent flow across boundary C-C due to rod insertion, Q', is related to velocity regardless of the compression or rebound. This is shown in equation (2). A_c is the area of the piston on the compression side, while A_r is the area of the piston on the rebound side. Area of the rod is A_c minus A_r.

$$Q' = \left(A_c - A_r\right)\dot{x} \tag{2}$$

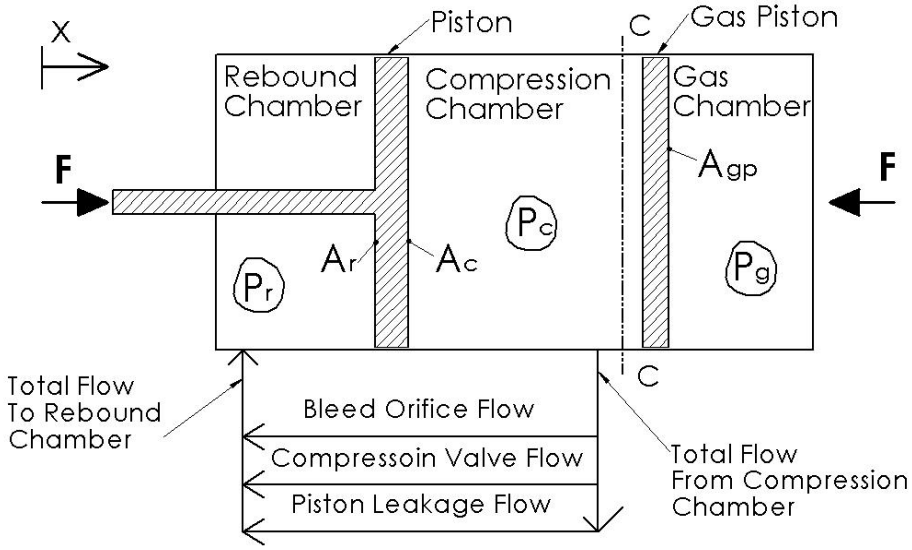

Figure 11: Damper Compression Flow Diagram

Equation (2) shows that the area of the rod is accounted for by the gas chamber. This leads to the total flow rate, Q, being equal to the rod side piston area times the velocity.

$$Q = A_r\dot{x} \tag{3}$$

Combining equations (1) and (3) yields a relation among partial flows and velocity.

$$A_r \dot{x} = Q_v + Q_b + Q_{lp} \tag{4}$$

Now we need the individual flow rates from equation (4).These flows are all driven by the pressure difference, $\Delta p = p_c - p_r$, between the compression and rebound chambers. A Bernoulli's equation can be used to model unsteady flow through a passage of area A. It has the form:

$$Q = AC_d \sqrt{\frac{2\Delta p}{\rho}} \tag{5}$$

C_d is a steady state discharge coefficient and ρ is the density. Lang experimentally modified this term by defining a dynamic discharge coefficient, C_D [1]. C_D is a function of dimensionless parameters including acceleration number, Reynolds number, Cauchy number, and thickness to length ratio.

$$C_D = f\left\{\frac{al}{v^2}, \frac{\mu}{\rho v l}, \beta v^2, \frac{s}{l}\right\} \tag{6}$$

Applying the dynamic discharge coefficient to equation (5) yields:

$$Q = AC_D \sqrt{\frac{2\Delta p}{\rho}} \tag{7}$$

Lang assumed the value for C_D to be constant and found good correlation to experimental data [1]. This model for unsteady flow will be applied to flow in the valves and bleed orifice, and will be assumed turbulent based on Reynolds numbers during operation. The flow is turbulent except in the very low speed region.

BLEED FLOW MODELING

Equation (7) is formulated to find the flow through the adjustable bleed orifice in the piston.

$$Q_b = A_b C_D \sqrt{\frac{2(p_c - p_r)}{\rho}} \tag{8}$$

A_b, Area of the bleed, was determined from measurement of the damper bleed orifice. It is also variable because the bleed valve is adjustable. For different bleed valve settings, more or less bleed area is available. The values for C_D were determined by comparing simulation results to experimental data.

VALVE FLOW MODELING

Modeling of the flow through the piston orifice and the valves is more complex. The flow must be broken up into two parts: flow through the piston orifice and flow contacting the shim stack and exiting. This flow through the shims is referred to as flow through the valves. Two pressure drops are associated with this flow path. Physical orientation of these pressure drops can be seen in Figure 2.

$$\Delta p_{valve} = p_v - p_r \tag{9}$$

$$\Delta p_{po} = p_c - p_v \tag{10}$$

As fluid exits the compression chamber and flows through the piston orifice, the first pressure drop occurs. This is denoted Δp_{po}. The second pressure drop, Δp_{valve}, occurs across the valves after the flow has exited the piston orifice. Obviously, $\Delta p_{po} + \Delta p_{valve}$ is equal to $(p_c - p_r)$.

The flow rate through the piston orifice has the same form as equation (8) with a substitution of equation (10) for the change in pressure term.

$$Q_v = A_o C_D \sqrt{\frac{2\Delta p_{po}}{\rho}} \tag{11}$$

The flow through the piston orifice is equal to the flow through valves due to conservation of mass. Valve flow is driven by the pressure drop shown in equation (9).

$$Q_v = A_{v,\,flow} C_D \sqrt{\frac{2\Delta p_{valve}}{\rho}} \tag{12}$$

The complexity arises when modeling the $A_{v,\,flow}$ term. The flow leaving the piston orifice has contacted the shim stack and essentially turned 90 degrees. For this flow, the flow area is the cylinder wall area defined by the circumference of the shims and height of the shim stack deflection.

$$A_{v,\,flow} = \alpha \pi D_v y \tag{13}$$

In equation (13), πD_v is the circumference of the largest shim in the damper. The α term is the area flow correction factor. Talbott used a value of 0.5 in his model for a damper with three compression holes and three rebound holes [7]. The Tanner Gen 2 damper has a variable number of piston flow orifices. The area flow correction factor is adjusted according to the number of holes used. Substituting equation (13) into equation (12) yields:

$$Q_v = (\alpha \pi D_v y) C_D \sqrt{\frac{2\Delta p_{valve}}{\rho}} \tag{14}$$

where

$$y \propto \frac{(p_v - p_r)A_o}{k} \tag{15}$$

The shim deflection y is an unknown in the system of equations. It can be determined from a force balance on the valve. Figure 12 shows a simplified valve model for the compression stroke.

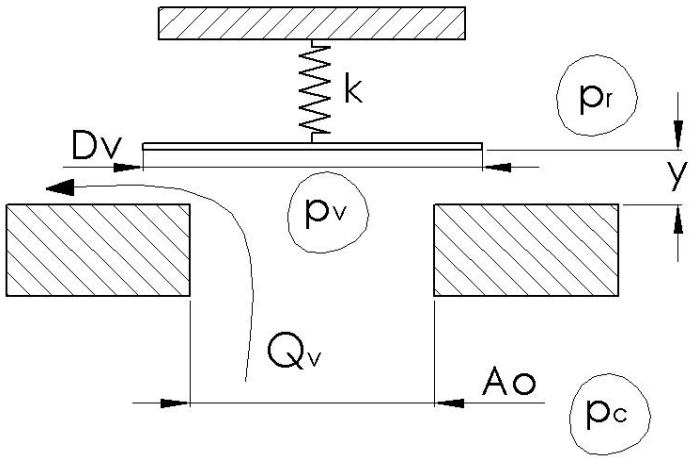

Figure 12: Simplified Compression Stroke Valve Model

The pressure drops across the piston orifice and the valves can be visualized. The shim stiffness, k, must also be determined. The method for finding k will be explained in the Shim Stiffness Modeling section.

In essence, the model show in Figure 12 treats the shim as a linear spring to determine shim deflection, y, and the relation between deflection and force, ky. A force balance on the valve relates the forces; this is shown in Figure 13.

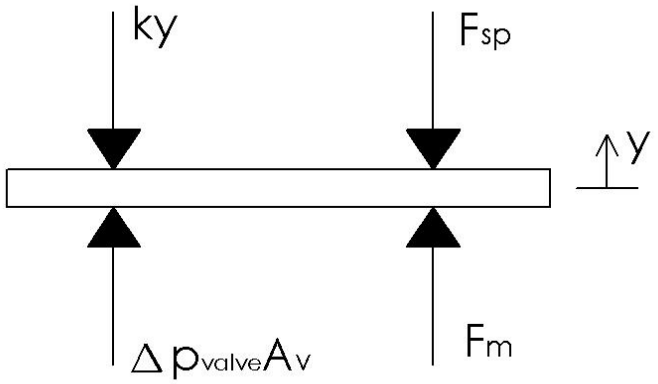

Figure 13: Free Body Diagram of Valve

Summing the forces in the y direction gives equation (16).

$$ky = \Delta p_{valve} A_v + F_m - F_{sp} \tag{16}$$

It is important to note that A_v is the area on which the valve pressure acts. This is not the same as the $A_{v,\,flow}$ term used in equation (13). F_{sp} is the preload spring force. For the Tanner Gen 2 damper, preload on the shims is not possible because of the piston design. A dished piston is required to produce a shim preload and the Tanner Gen 2 piston is flat. A modification to the piston could allow for a preload, and therefore it will be left in the model.

The momentum force, F_m, is derived from the conservation of momentum through the valve. This force arises from the 90 degree direction change of the flow in the valve. The momentum equation in the y direction is:

$$F_m = \rho v_{y,in} Q_{in} - \rho v_{y,out} Q_{out} \tag{17}$$

The velocity out of the valve in the y direction is assumed to be zero, and the velocity in is related to the flow in divided by the area.

$$v_{y,out} = 0 \tag{18}$$

$$v_{y,\,in} = Q_{in} \Big/ A_o = Q_v \Big/ A_o \tag{19}$$

Combining equations (18) and (19) into equation (17) gives:

$$F_m = \rho \frac{Q_v^{\,2}}{A_o} \tag{20}$$

Lang concluded that the velocity out will have a component in the y direction [1]. A correction factor was found experimentally based on actual versus predicted momentum force. The momentum force coefficient, C_f, was found to have a value of 0.3. Combining C_f with equations (16) and (20) gives:

$$ky = \Delta p_{valve} A_v + \rho \frac{Q_v^{\,2}}{A_o} C_f - F_{sp} \tag{21}$$

Equation (21) is the final force balance on the valve. The deflection can be found if the shim stiffness is known.

LEAKAGE FLOW MODELING

The final flow path to model is the leakage of oil between the piston seal and the cylinder. Lang modeled this flow using laminar flow through parallel plates [1]. This assumption is valid because the between cylinder seal and wall is very small (<.004") compared to the length of the flow. The length of the flow is the height of the piston. The equation for this leakage flow is derived from Navier-Stokes equations.

$$Q_{lp} = \left(\frac{\Delta p b^3}{12 \mu l} + \dot{x} \frac{b}{2} \right) \pi D_p = \left(\frac{(p_c - p_r) b^3}{12 \mu l} + \dot{x} \frac{b}{2} \right) \pi D_p \tag{22}$$

The height of the piston in b, while the D_p if the diameter of the piston.

GAS CHAMBER MODELING

In a monotube damper, the gas chamber accounts for the increase of volume caused by the insertion of the piston rod. Talbott assumed the damper oil was incompressible, which makes the gas pressure a function of the piston displacement [7]. Figure 14 shows the forces acting on the gas piston.

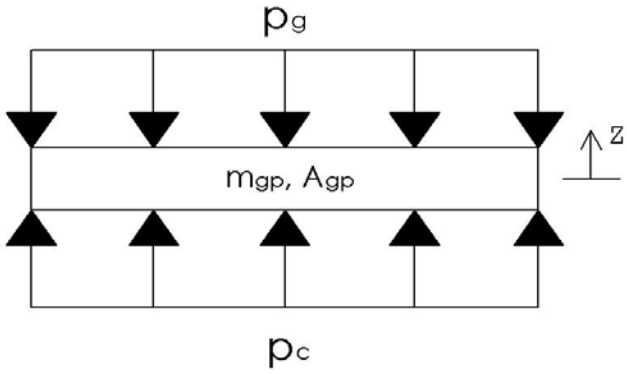

Figure 14: Free Body Diagram of Gas Piston

The pressure in the gas chamber is determined by applying the ideal gas to the chamber.

$$\frac{p_i V_i}{T_i} = \frac{p_f V_f}{T_f} \tag{23}$$

It can be assumed that the initial temperature and final temperature are the same. During testing, the damper is worked until operating temperature is achieved. This temperature varies very little during short periods of testing. Equation (23) becomes:

$$p_f = p_i \frac{V_i}{V_f} \tag{24}$$

Assuming the oil is incompressible, a relation for final volume of the gas chamber can be found.

$$V_f = V_i + \Delta V \tag{25}$$

The gas chamber is modeled as a cylinder and its volume is the product of gas piston area (A_{gp}) and chamber length (L_g). The change in volume is negative for compression and positive for rebound.

$$V_i = A_{gp} L_g \tag{26}$$

$$\Delta V = -A_{rod} x = -(A_c - A_r) x \tag{27}$$

Equation (24) becomes:

$$V_f = A_{gp} L_g - A_{rod} x \tag{28}$$

Assuming that p_{gi} is the initial gas pressure and p_g is that gas pressure at any time, equation (24) becomes:

$$p_g = p_{gi} \frac{A_{gp} L_g}{A_{gp} L_g - A_{rod} x} \tag{29}$$

Now utilizing the force balance on the gas piston from Figure 14, the compression chamber pressure can be found. Gas piston friction is neglected. Using Newton's 2nd law, summation of forces yields:

$$(p_c - p_g) A_{gp} = m_{gp} \ddot{z} \tag{30}$$

With the assumption that the fluid is incompressible, the acceleration of the piston is related to the acceleration of the gas piston.

$$\ddot{z} = \frac{A_{rod}}{A_{gp}} \ddot{x} \tag{31}$$

Combining equations (29), (30), and (31) gives an expression for the compression chamber pressure.

$$p_c = \frac{A_{rod} m_{gp}}{A_{gp}^{\ 2}} \ddot{x} + p_{gi} \frac{A_{gp} L_g}{A_{gp} L_g - A_{rod} x} \tag{32}$$

Equation (32) shows that the compression chamber pressure is a function of piston acceleration, gas pressure, and displacement. It is not a function of piston velocity in this formulation. The acceleration term on the right hand side of equation (31) is much smaller than the p_{gi} term, which effectively shows that p_c is almost equal to p_g.

Talbott states "all of the velocity dependant forces produced by the shock absorber come from pressure variations in the rebound chamber" [7].

DAMPER FORCE MODELING

After the chamber pressures are calculated, the damper force can be found. Summing the forces on the piston assembly yields a relation for the damping force based on the other acting forces. Figure 15 shows the free body diagram of the piston assembly.

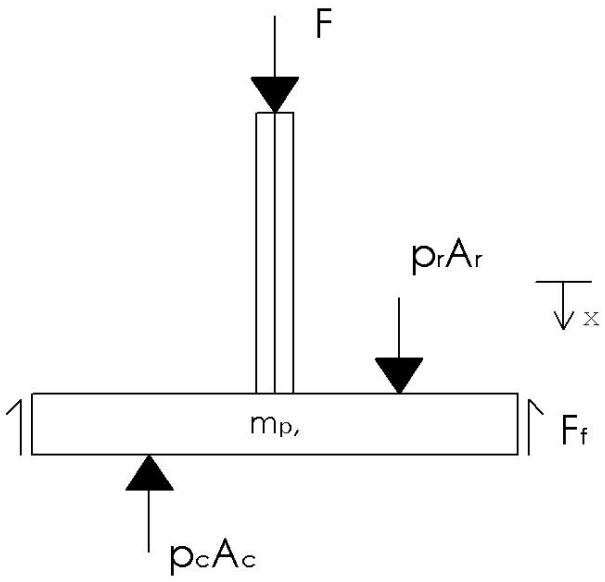

Figure 15: Free Body Diagram of Piston Assembly

Applying Newton's second law, the sum of the forces in the x direction gives equation (33).

$$F + p_r A_r - p_c A_c - F_f = m_p \ddot{x} \tag{33}$$

F is the damper shaft force and F_f is the friction force acting on the piston. The acceleration is calculated from the known sinusoidal input from the damper dynamometer and the pressures are calculated from the model above. The mass of the piston assembly, m_p, includes the piston, the rod, the needle valve and the rod end/spherical bearings and can be measured directly. The areas are also measured parameters. The friction force, F_f, and the gas pressure are calculated by the damper dynamometer from measurements made while the piston is moving very slowly so that the pressure difference (p_c-p_r) is negligible.

The damper shaft force is then the only unknown and can be determined. The damper force found is used in the FV and FD plots to characterize the damper. It is important to note that the mass times acceleration term is relatively small, less than 1 pound at maximum acceleration.

SHIM STIFFNESS MODELING

Deflection of the shim stack in equation (21) is an unknown in the system. Shim deflection is found using a shim stiffness term. This term must be calculated experimentally or analytically. Talbott used equations for the deflection of uniform thickness plates, applied superposition to the system, and found the bottom shim deflection from the loads and reaction forces [7]. A unit pressure load was applied to the bottom shim in the stack, then the deflection was found. The stiffness was calculated using the pressure load times the area of acting pressure divided by the deflection. Shim stiffness has units of pounds per inch (lbs/in), similar to a spring stiffness.

The Tanner Gen 2 damper uses shims with varying number of holes for tuning the damping forces. This posed a difficulty in applying equations for the deflection of uniform thickness plates found in *Formulas for Stress and Strain* [10]. SolidWorks models of the different shims were created. The modulus of elasticity and Poisson's ratio for carbon fiber was used in the shim models. Finite element analysis was then performed to find the shim deflection and calculate the shim stiffness.

The pressure loads in the bottom side of the shim were not distributed over the total area. They were assumed to act between the outer diameter of the shim (1.13") and just inside the holes in the shim (0.65"). Talbott's shim stiffness model used a similar assumption, the pressures acted between the largest shim diameter and the smallest shim diameter [7].

The shim was constrained in the center edge as a fixed boundary. A unit pressure load was applied to the pressure are described above. Figure 16 shows the loads and constraints on the shim.

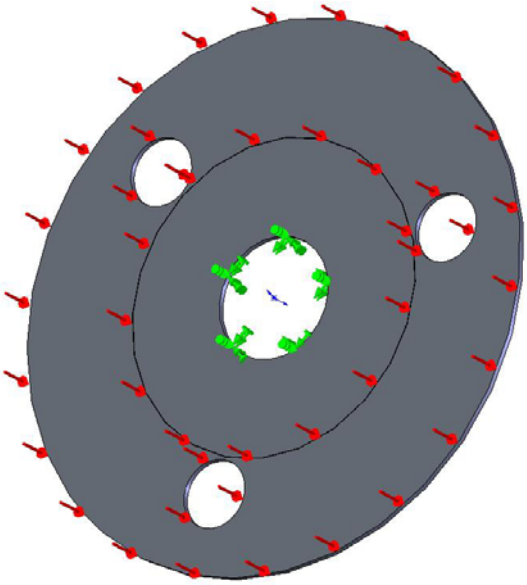

Figure 16: Loads and Constraints for F.E. Three Hole Shim Analysis

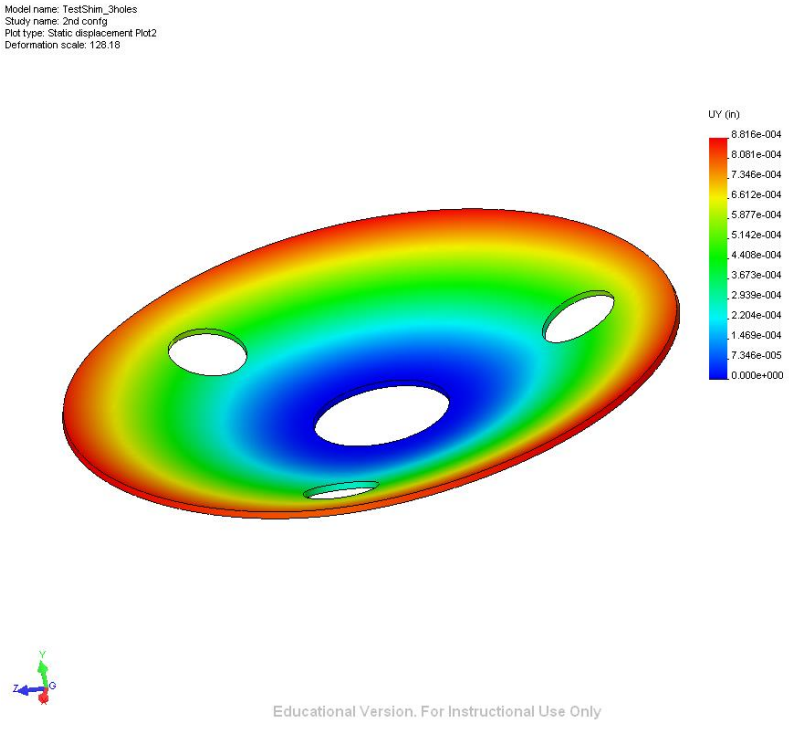

Figure 17: Deflection of Three Hole Shim from F.E. Analysis

Figure 17 shows the results from the finite element analysis from CosmosWorks. The deformation is shown at a scale of 128 to one, for better visualization of the deflection. The color scale ranges from zero in dark blue to 8.8E-4 in red. The displacement shown is the deflection in the Y direction. The maximum value of deflection from the shim was used for the shim stiffness calculation.

Stiffness values were calculated for four different shims thickness values: 0.01", 0.012", 0.015", and 0.02". These are standard shim sizes from manufacturers such as Ohlins. The shim thickness for standard Tanner tuning shims is 0.012". The other values were for a more comprehensive tuning library database.

Shim stiffness values were calculated for five different shim hole configurations: zero, two, three, four, and five holes. Comparison to the shim with no holes demonstrates the effects of holes in the shims on the shim stiffness.

Figure 18 is a plot of stiffness vs. number of holes as calculated using the finite element analysis for varied thickness. An increase in thickness gives an increase in the shim stiffness. The difference in number of holes is shown to be minimal. The percent difference in each thickness case is less than seven percent error for any number of holes tested. This leads to the conclusion that a solid shim can be used to find shim stiffness in most cases, particularly thick shims.

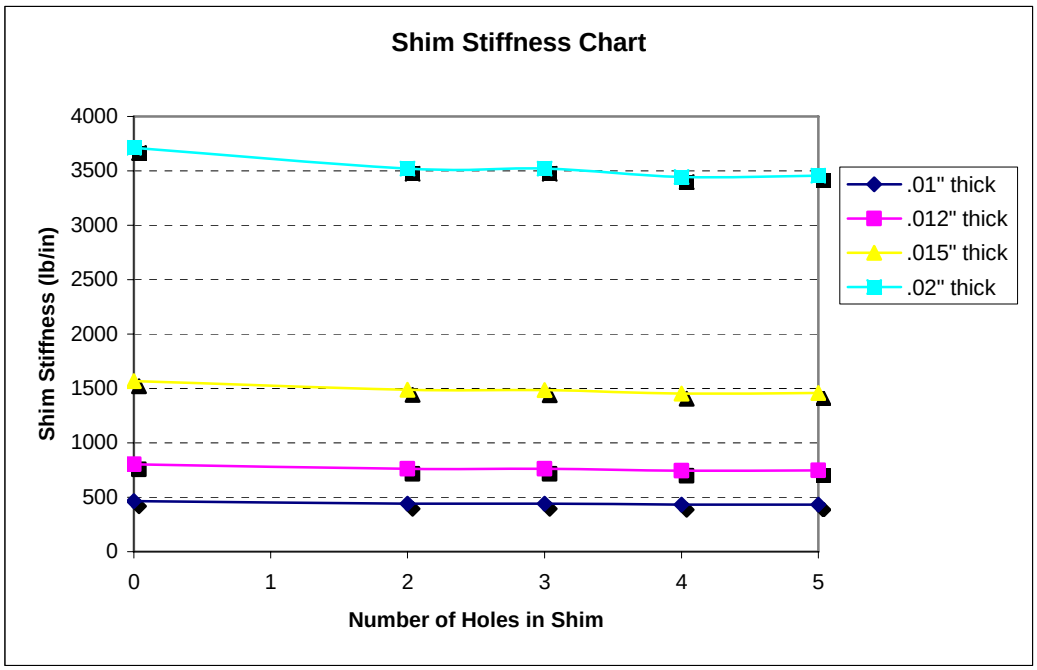

Figure 18: Shim Stiffness Chart for Varied Shim Thickness

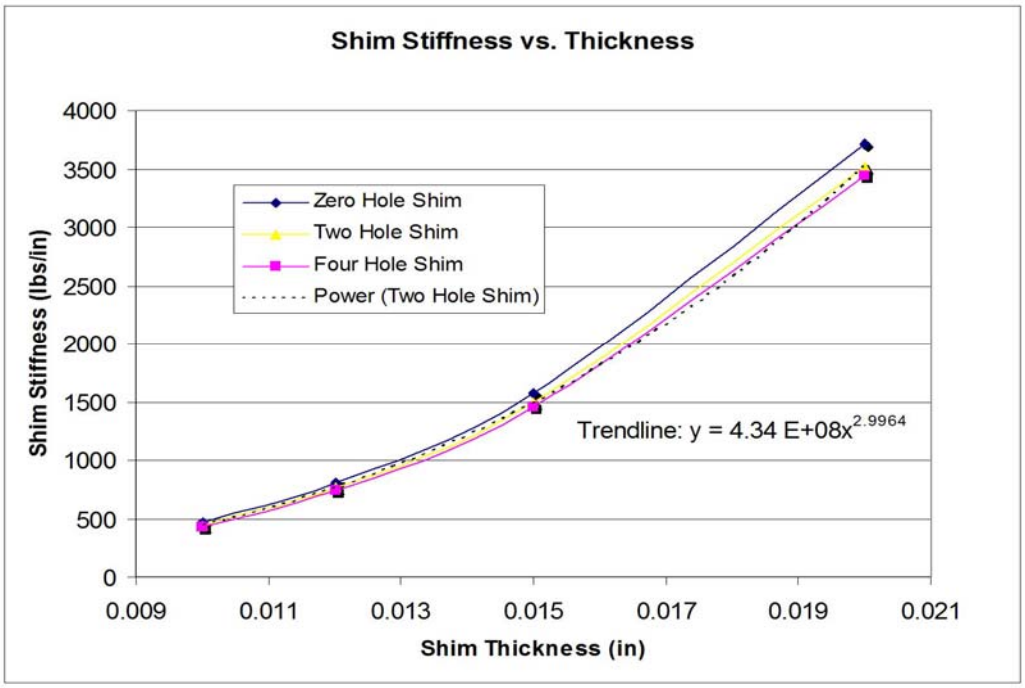

Figure 19: Shim Stiffness as a Function of Shim Thickness.

Figure 19 is a plot of shim stiffness vs. shim thickness. The nonlinear trend displays that stiffness, k, varies as a cube of the shim thickness. This is consistent with the analytical formulation in Roark's [10]. Also this cubic power relation can be examined using a basic cantilever beam; this is shown in Appendix B. The trend line equation was used to find stiffness values for use in the damper program

MODEL SOLUTION METHOD

The physical modeling of forces and resistance leads to a system of six nonlinear coupled equations for the damper: equations (4), (8), (11), (14), (21), and (22). The input is the motion (velocity and position) of the piston with respect to the body.

There are six unknowns from this system of equations, so it can be solved. The unknowns are:

1. Bleed orifice flow rate (Q_b),
2. Valve flow rate (Q_v)
3. Leakage flow rate (Q_{lp})
4. Pressure in the valve (P_v)
5. Pressure in the rebound chamber (P_r)
6. Shim deflection (y)

The remaining pressures in the gas chamber and compression chamber are found using equations (29) and (32), respectively. Once the rebound chamber pressure has been found, equation (33) can be used to find the damper force produced.

The solution approach applied in solving the six coupled equations was Newton's iterative method for solving coupled nonlinear equations. This method was adapted from *Numerical Methods for Engineers and Scientists* by Hoffman [11].

All calculations were performed on a Pentium IV computer with 1.70 GHz processor and 512 MB of RAM. Calculation time was less than fifteen seconds, unless a large number of plots were output from the program.

The general convergence criterion is:

$$\left|\frac{f_i}{A_i}\right| < \varepsilon_i \tag{34}$$

A_i is a user chosen scale factor depending on the function solved. The changes in the independent variables are also tested to avoid infinite loops. The test is:

$$\left|\frac{\Delta x_i}{x_i}\right| < \varepsilon_i \quad for\ |x_i| > 1 \tag{35}$$

or

$$|\Delta x_i| < \varepsilon_i \quad for\ |x_i| < 1 \tag{36}$$

Satisfying inequality (34) indicates a solution. Satisfying inequalities (35) or (36) without satisfying inequality (34) indicates a numerical problem.

EXPERIMENTAL TESTING

EXPERIMENTAL TEST EQUIPMENT

Real damper testing was conducted to obtain experimental data on damper force characteristics. The Tanner Gen 2 damper was tested on a Roehrig Engineering, Inc. model 2VS damper dynamometer. Figure 20 shows the Roehrig dynamometer.

Figure 20: Roehrig Damper Dynamometer [12]

The model 2VS dynamometer has a two hp AC electric motor driving a scotch yoke mechanism. This mechanism produces sine wave displacement of the damper piston with a total stroke of one or two inches. The stroke is set by manually moving a

pin in the scotch yoke. The sine wave displacement equation of the damper piston is defined by the amplitude (half of the stroke), the test frequency, and the phase. This is displayed in equation (37).

$$x(t) = -A_{dyno} \sin(2\pi F_{dyno} t - \pi/2) \tag{37}$$

A_{dyno} is the half stroke (amplitude) and F_{dyno} is the frequency of the motor revolutions. The π/2 phase shift is required because the dynamometer always parks at the position corresponding to full extension of the damper. Installing the damper with the dynamometer parked in this position assures that the damper will not be damaged by being over extended during testing. At start up the damper is cycled through one full compression stroke followed by a full rebound stroke. Zero displacement corresponds to the damper being half compressed. The velocity is determined from the first derivative of displacement, and the acceleration from the second derivative. Equations (38) and (39) show these derivatives.

$$\dot{x}(t) = -A_{dyno} 2\pi F_{dyno} \cos(2\pi F_{dyno} t - \pi/2) \tag{38}$$

$$\ddot{x}(t) = A_{dyno} (2\pi F_{dyno})^2 \sin(2\pi F_{dyno} t - \pi/2) \tag{39}$$

Figures 21, 22, and 23 show the sinusoidal motion profiles for an amplitude of 0.5 inch (one inch stroke) and frequencies of1.59 Hz and 3.19 Hz.

In Figure 21 shows the displacement of the damper piston vs. time. Figure 22 shows the velocity of the piston vs. time and Figure 23 shows the acceleration of the piston vs. time. These profiles are used in the damper model computations.

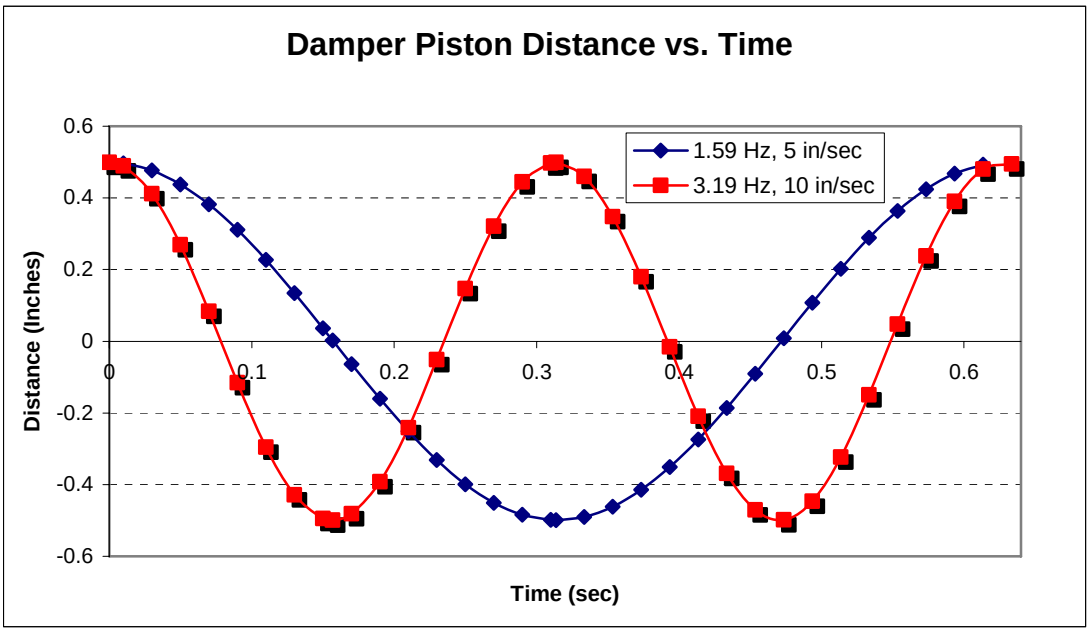

Figure 21: Damper Piston Distance vs. Time Profile

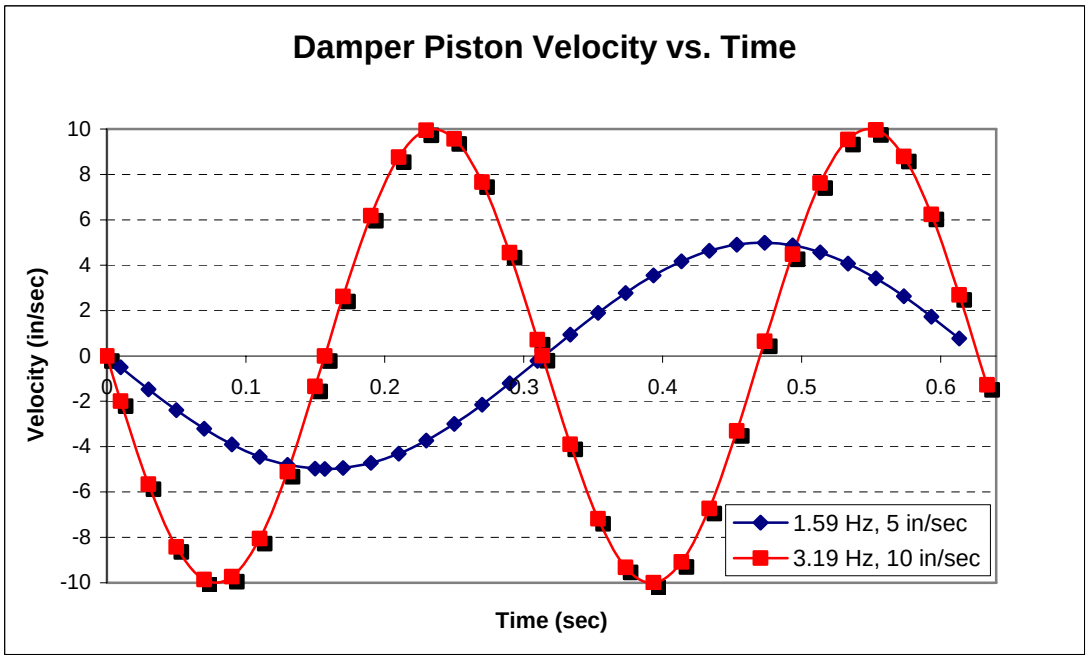

Figure 22: Damper Piston Velocity vs. Time Profile

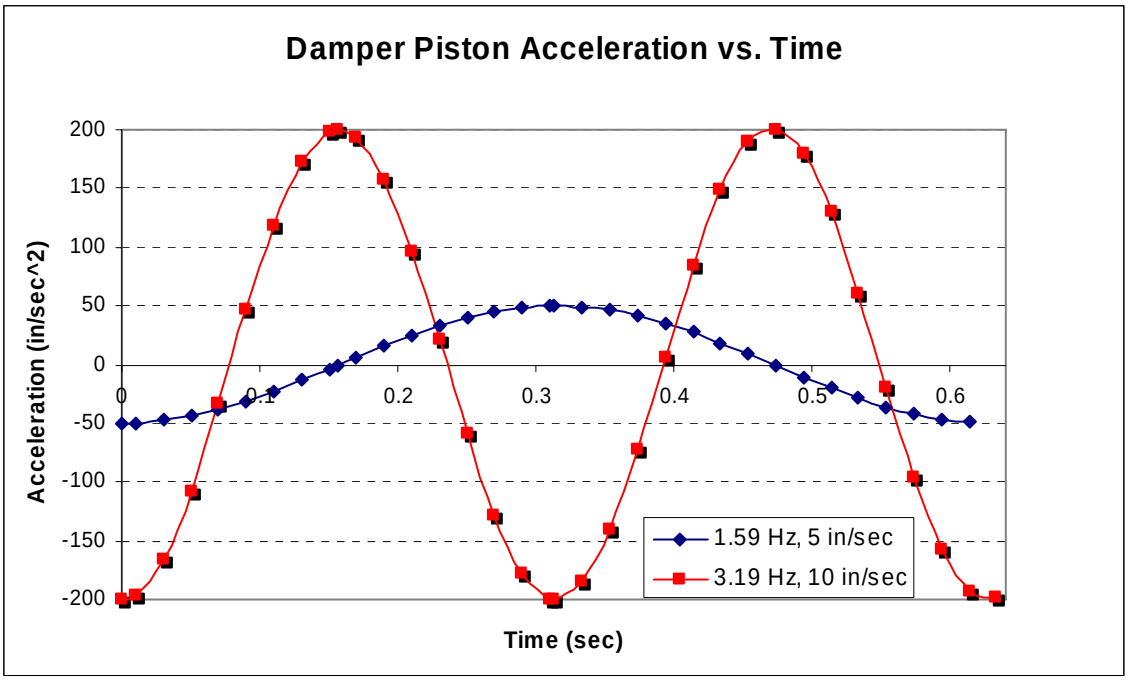

Figure 23: Damper Piston Acceleration vs. Time Profile

Data for velocity and displacement in the dynamometer comes from velocity and displacement transducers. This data is measured, stored, and output for FD and FV plots on the dynamometer software. The forces are sensed by a load cell mounted in the load path for the cylinder end of the damper. The rod end of the damper is pinned to the scotch yoke mechanism to drive the piston rod assembly. The dynamometer also has an infrared temperature sensor to measure the temperature of the damper body to ensure standard warm up temperatures. There are mounting clevises for both ends of the damper to ensure that there is no backlash in the mounting. Any play in the mounting of the damper will appear in the FD plots.

The dynamometer is controlled by Roehrig software running on a PC. Communication between the dynamometer and the computer is through a USB connection. Analog to digital conversion for force and motion data are internal to the dynamometer.

The minimum and maximum velocities are 0.05 and 11.39 in/sec, respectively. The program allows the user to select the maximum speed and the testing frequency is calculated based on stroke and desired speed. The maximum load capacity for the load cell is 1250 pounds at 10 in/sec.

TESTING METHOD

In order to obtain the correct data for correlating the damper model to experimental data, a specific series of test were performed. Four different configurations were tested and all are described below. In all cases, the stroke tested was one inch. All tests were performed at 90 ºF ± 3 ºF. The damper was given time to cool between individual tests. The gas spring force is removed from all testing and model data.

The gas pressure of each test was 60 psi. Low pressure in the nitrogen filling tank and low precision of the gage used to charge the damper caused errors in pressure. The actual pressure value was tested on the dynamometer using a 0.05 in/sec cycle. The values from the experimental data were used in the model correlation. The test pressure for each test appears on the FV and FD plots.

At the beginning of each test run, a low speed friction cycle was conducted to find the experimental value for the friction force. This friction value was used in model

correlation. All recoded data was stored and exported as text files for input into Microsoft Excel.

In the first test setup configuration, solid shims were placed over the valve orifices in the piston to block valve flow for both the compression and rebound strokes. This allowed only flow through the bleed orifice and the piston seal gap. Results were used for bleed orifice correlation. The bleed adjustment was set to full open setting (3.75 turns). Maximum velocities of 4, 6, 8, and 10 in/sec were tested. When testing velocities below 4 in/sec, the data becomes very erratic due to the sampling rate. For that reason all testing was conducted at or above 4 in/sec (1.275 Hz).

The second test setup was the "as received" configuration of the damper, i.e. no shims blocking the valve orifice flow. It will be denoted as the no shim 6C6R configuration, meaning six unrestricted flow paths in compression and rebound. This test was conducted to correlate unrestricted valve flow with and without bleed flow. In this case, there are six flow paths in compression and rebound through the piston. The initial configuration was tested with fully open and fully closed bleeds. Two velocities were tested: 5 in/sec (1.59 Hz) and 10 in/sec (3.19 Hz).

The third test setup was the 3C3R configuration. This notation means that three shimmed flow paths exist in the piston for the compression and rebound strokes. This test was conducted to obtain data for modeling the fully complex damper with shim restrictions. 5 in/sec and 10 in/sec velocities were tested. Both speeds were tested with a fully open and fully closed bleed orifice.

The fourth test setup was 2C4R configuration. This is a variant of the third test setup. The notation means that two shim controlled flow paths exist in the compression stroke, while four shim controlled flow paths exist in rebound. Five in/sec and ten in/sec velocities were tested. Both speeds were tested with a fully open and fully closed bleed orifice.

RESULTS

A basic analysis of damping forces required for a Formula SAE racecar is located in Appendix C.

BLEED ORIFICE CORRELATION

The bleed orifice is open at all times during damper operation, so it important to accurately model this particular flow path. In the Tanner Gen 2 damper, the bleed orifice dominates the flow at all speeds because its flow area is larger than the piston orifice flow paths.

In other racing damper, Ohlins for instance, the bleed orifice is generally smaller than the piston orifices.

For example, the bleed orifice at full open has a diameter of .104" in which is a bleed flow area of 8.50e-3 in^2. The flow area of six 0.038" diameter piston orifices is 6.8e-3 in^2. The 25% larger flow area of the bleed orifice shows its importance at all speeds in this particular damper.

To simulate the solid shims in the damper experimentation, the piston orifice diameter was set to zero. This forced the internal flow to travel through either the bleed orifice or the piston seal gap. Knowing that the flow through the piston seal gap is an order of magnitude less than the orifice flow, this method of correlation of bleed only flow is acceptable.

Equation (18) is the flow equation for the bleed orifice. All of the variables in the equation are measured or calculated except the dynamic discharge coefficient, C_D. Fine tuning the value of this coefficient is the technique used to correlate the model flow

to the experimental flow. The starting value for the correlation was $C_D = 0.7$, per Lang's work [1].

Reasonable correlation was found using two different values for C_D. At maximum speeds of higher than 6 in/sec, a value of 0.68 correlated well. At speeds lower than 6 in/sec, a value of 0.61 was used to obtain good correlation between model and experimental data. These values are used in all modeling configurations in the remainder of this research.

Figures 24 and 25 show FV and FD data for the bleed only configuration tested at 6 in/sec (1.913 Hz). The gas pressure for this test run was 46 psi.

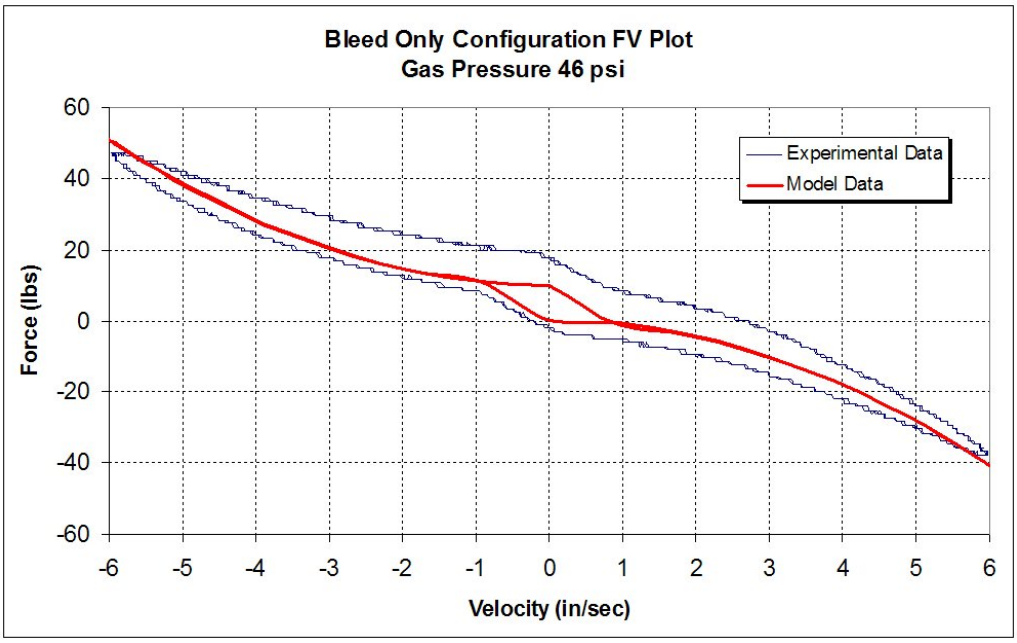

Figure 24: FV Plot, Bleed Only Configuration, 6 in/sec, $p_g = 46$ psi, $C_{D,b} = 0.61$

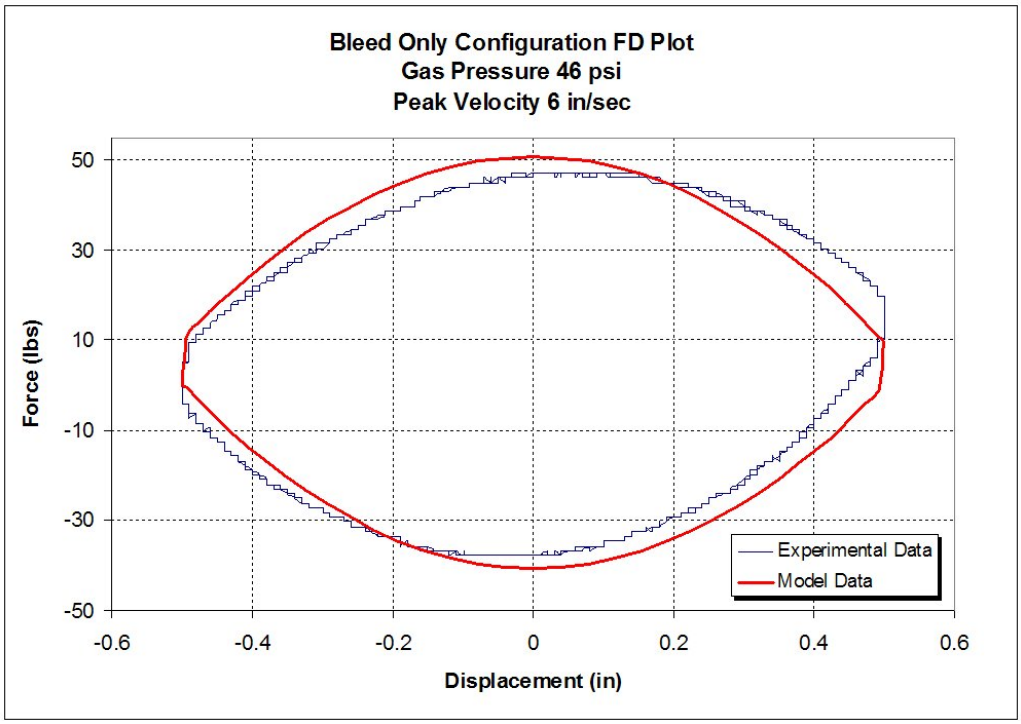

Figure 25: FD Plot, Bleed Only Configuration, 6 in/sec, $p_g = 46$ psi, $C_{D,b} = 0.61$

In Figure 24, the model data is directly plotted over the experimental data. Reasonable agreement is found using $C_D = 0.61$. The general nonlinear trend and magnitude of the forces are similar. One reason the model does not precisely match the experimental data is the absence of fluid compressibility in the model, which can cause the hysteresis. Compressibility is the major cause of the difference in forces when accelerating and decelerating, i.e. hysteresis. Compressibility is the primary cause of hysteresis because the frequency in this case is relatively low, and inertia effects have a small magnitude (less than 1 pound). The maximum width of the hysteresis loop is approximately 10 pounds over the range of velocity.

The small loop at low velocities in the model data is due to the reversal of coulomb friction term in the transition from compression to rebound. This loop represents the behavior at speeds less than 1 in/sec quite well.

Figure 25 shows the same force data in the FD domain. The hysteresis in Figure 24 is represented by the force axis asymmetry in the Figure 25. At higher values of positive displacement in the FD plot, force values differ by up to 10 pounds. This implies that the model does not accurately capture the "spring" effects of the damper. The majority of the data has less than 5 pounds difference from model to experimental.

Figures 26 and 27 show FV and FD data for the bleed only configuration tested at 10 in/sec (3.19 Hz). The gas pressure for this test run was 46 psi. The dynamic discharge coefficient used was $C_D = 0.68$. With the increase in maximum speed, the FV and FD data show an increase in force. The gap in the FV plot due to hysteresis is approximately 10 pounds difference from 1 in/sec to 8 in/sec, positive or negative.

Both Figures 26 and 27 show very good agreement with the nonlinear trend of force data and magnitudes of force data. The maximum difference from model to experimental forces is approximately 10 pounds. The difference of force in Figure 27 appears to be less than in Figure 25. The differences are approximately the same, but the larger values of forces at higher speeds make it appear this way.

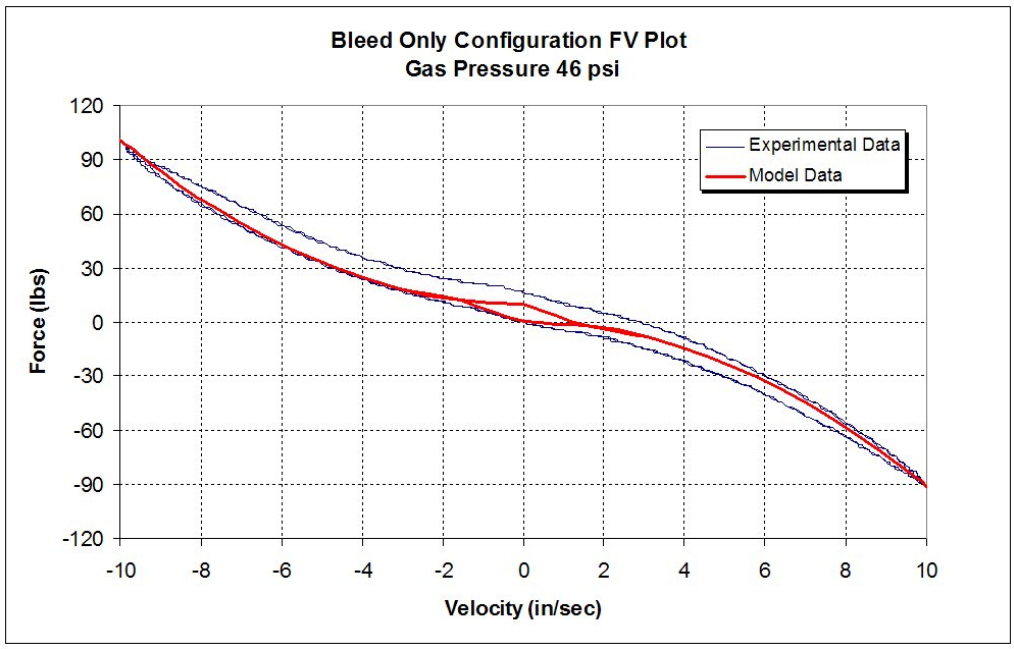

Figure 26: FV Plot, Bleed Only Configuration, 10 in/sec, p_g = 46 psi, $C_{D,b}$ = 0.68

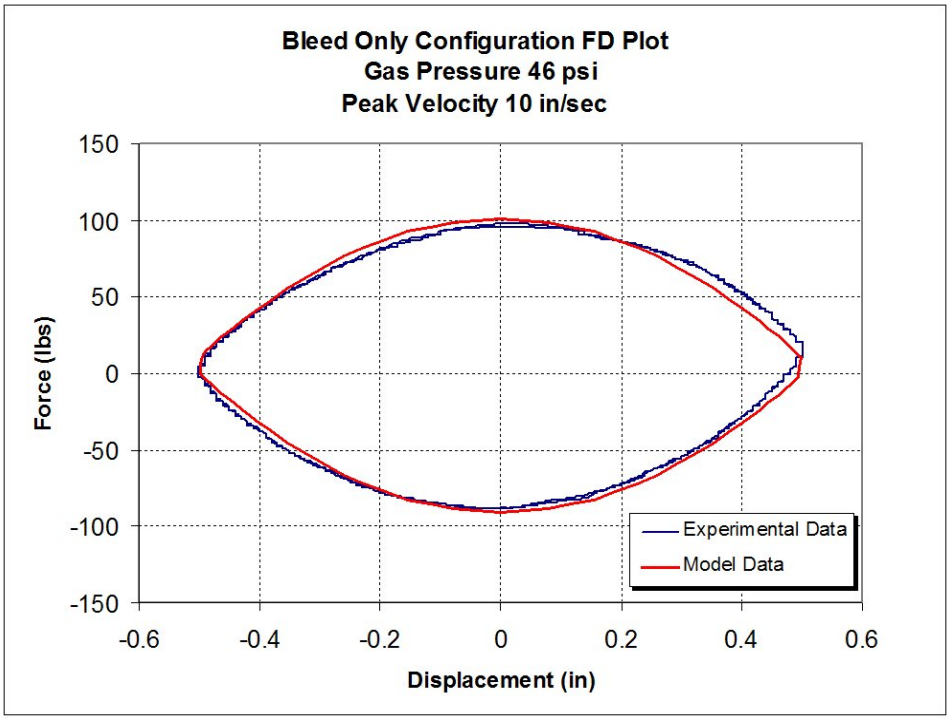

Figure 27: FD Plot, Bleed Only Configuration, 10 in/sec, p_g = 46 psi, $C_{D,b}$ = 0.68

The logical next step to correlate the model data to the experimental data would be to experimentally measure the compression and rebound chamber pressures. This would require pressure taps in each chamber of the damper and equipment to record this pressure information. Experimental data for chamber pressure would provide insight into the damper operation, but this method was beyond the scope of this research. Measured pressure could also be used to evaluate the accuracy of the dynamometer tests to determine gas pressure and seal friction.

By reducing the dynamic discharge coefficient for the lower testing speeds, the flow resistance is increased. This appears to show that the model underestimates force values at lower test speeds. Values, 0.61 and 0.68, for the discharge coefficient are with in reason according to Lang's research [1].

The model data also has the trend of correlating better when the piston is slowing down from maximum speeds. It would seem the inertial effects would be the cause, but the magnitude of these effects is less than 0.5 pounds at the largest value of acceleration.

UNRESTRICTED VALVE ORIFICE CORRELATION

The initial configuration of the damper was tested with 6 piston orifices with no shim restriction. A simplified model was created without the inclusion of equations (14) and (21). The first tests modeled were 5 and 10 in/sec velocities with a fully closed bleed orifice. These allowed for the correlation of the dynamic discharge coefficient for the unrestricted valve flow.

The value for C_D for the valves was set to 0.7 per Lang's work again [1]. Exercising the model and matching nonlinear force behavior, the final value of C_D was

set to 0.71. Again, the model forces more accurately represent the force data when the piston is slowing down from peak speed. The gas pressure of the 5 in/sec closed bleed test was 32 psi. The gas pressure of the 10 in/sec closed bleed test was 30 psi.

Figures 28 and 29 display the 5 in/sec 6C6R configuration tests for the fully closed bleed.

Agreement between model and experimental forces is very reasonable. In Figure 28, the maximum difference in model data to experimental data is approximately 10 pounds when the piston is speeding up in compression.

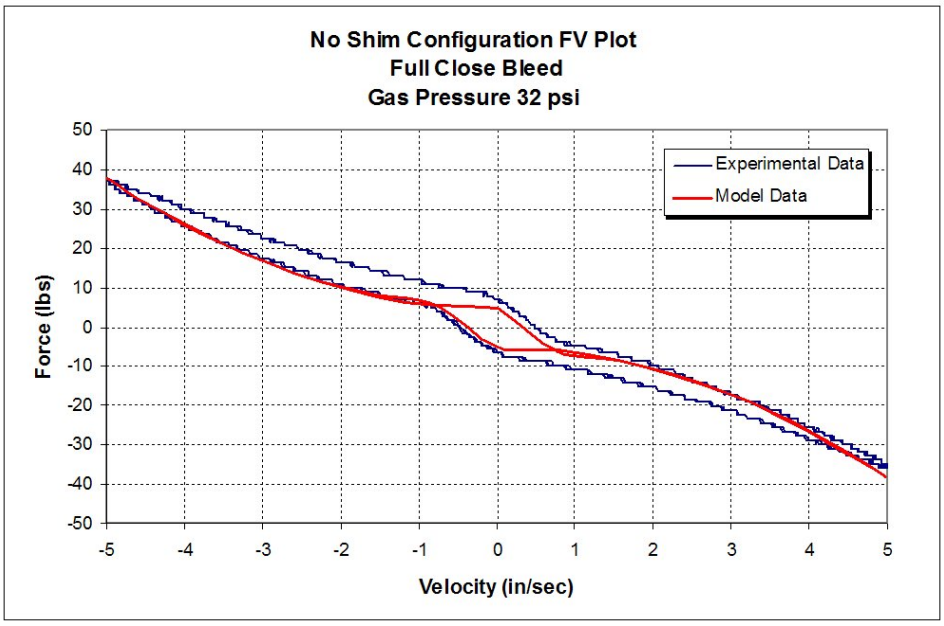

Figure 28: FV Plot, No Shim 6C6R Configuration, 5 in/sec, Bleed Closed, p_g = 32 psi, $C_{D,v}$ = 0.71

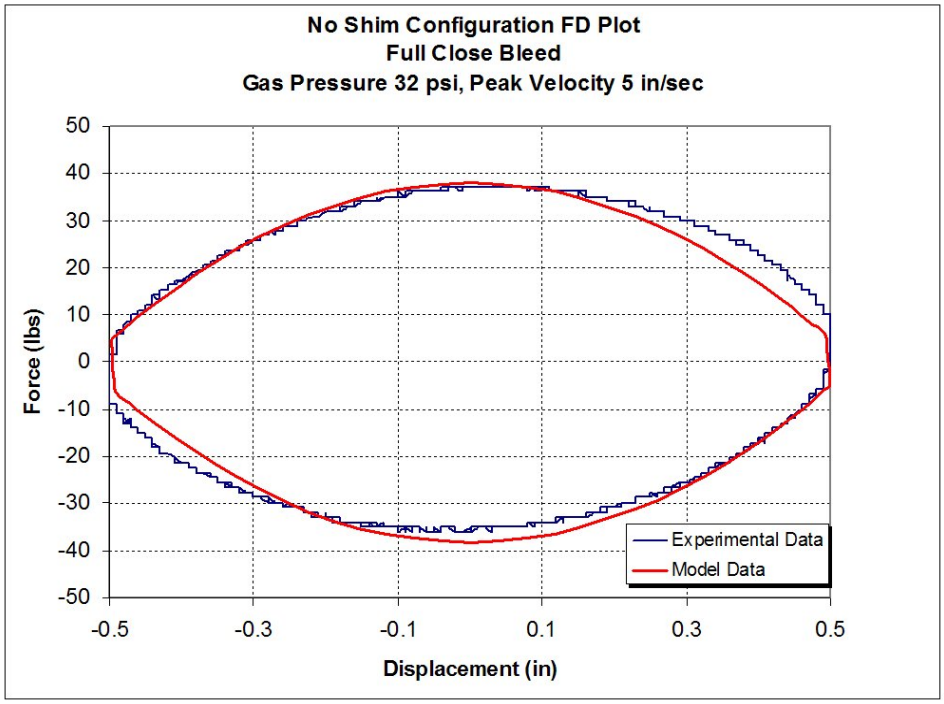

Figure 29: FD Plot, No Shim 6C6R Configuration, 5 in/sec, Bleed Closed, p_g = 32 psi, $C_{D,v}$ = 0.71

Figure 29 also shows good agreement in elliptical trend of FD plot. The area of most disagreement is at large positive values of displacement, which corresponds to acceleration in the compression stroke. At the large values of displacement, the velocity is near zero, so the pressure difference is not creating the force. The gas spring effects of the damper and the friction are the most likely causes of this difference.

Figure 30 displays the 10 in/sec 6C6R configuration FV test for the fully closed bleed. The dynamic discharge coefficient CD = 0.71 was used for 10 in/sec and the gas pressure was 30 psi.

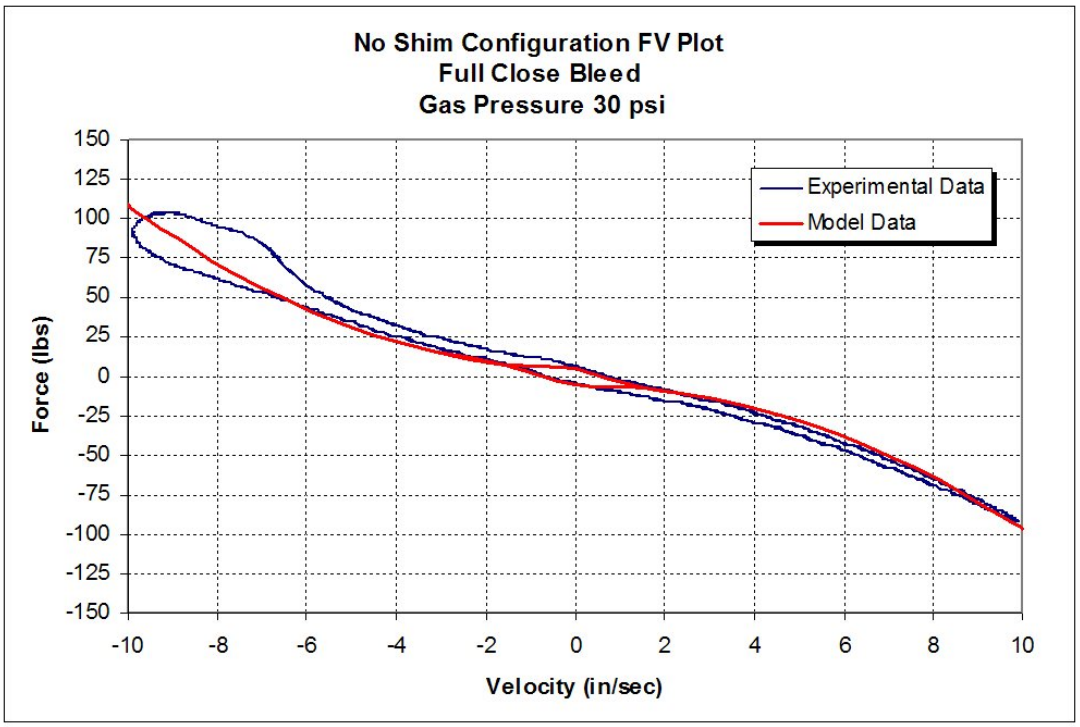

Figure 30: FV Plot, No Shim 6C6R Configuration, 10 in/sec, Bleed Closed, p_g = 30 psi, $C_{D,v}$ = 0.71

Figure 30 has good correlation between model and experimental data except at large negative velocities. This portion of the FV plot corresponds to the high speed compression of the piston. The large hysteresis loop is probably caused by cavitation of the damper oil in the rebound chamber during compression. The model predicts negative pressure in this region, which is impossible. Thus the assumptions used in deriving the model are not valid in this region, and will not predict this effect. In the actual damper, the oil may be vaporizing because the pressure drops below the vapor pressure in the rebound chamber. This would obviously increases the hysteretic effects.

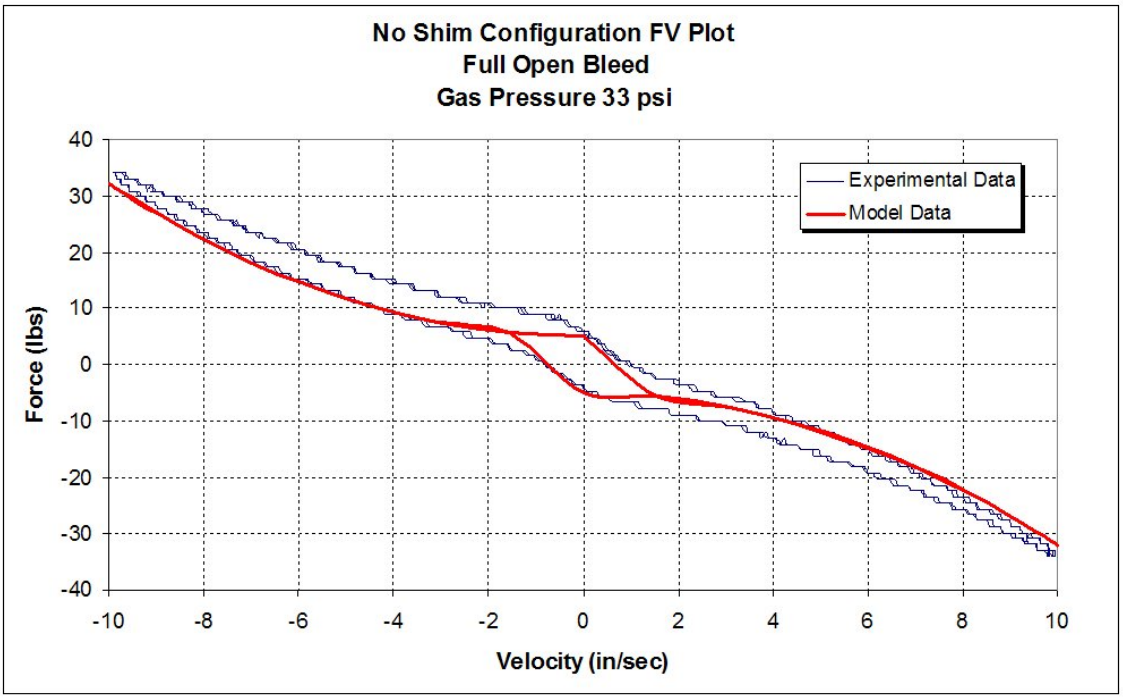

Figure 31: FV Plot, No Shim 6C6R Configuration, 10 in/sec, Bleed Open, p_g = 33 psi, $C_{D,v}$ = 0.71

With confidence in the dynamic discharge coefficients for both the bleed orifice and the valves, overall validation was explored. Figure 31 shows the No Shim configuration at 10 in/sec with a fully open bleed. The gas pressure was 33 psi. This figure shows good agreement between model and experimental results in general trend of nonlinear forces. The dynamic discharge coefficients found by isolating flow paths worked well together in representing the nonlinear force trend. In this case of combined bleed and valve flows, the forces during decelerations phases correspond much better to the model than those of acceleration.

Even with the absence of the fluid compressibility, the largest difference in force is approximately five pounds for this configuration. The low speed region, less than 2 in/sec, has excellent agreement in this case. The magnitude of the forces in this low speed region is approximately five pounds. The friction force used in the model for this test was set at five pounds, so this means the modeling of constant coulomb friction is a reasonable assumption. At low speeds, the majority of the damping forces are caused from the friction in the damper.

RESTRICTED VALVE ORIFICE CORRELATION

The final correlation that was performed involved a damper with bleed and valve flow, and the presence of shims to restrict the valve flow. This correlation is full verification with all the modeled systems of the damper present.

The 3R3C was the first correlated using the dynamic discharge coefficients from the isolated flow correlations. Figures 32 and 33 show FV and FD plots for the 3C3R configuration tested at 5 in/sec with a gas pressure of 24 psi. The value of C_D for the bleed was 0.68 and C_D for the valve flow was 0.71.

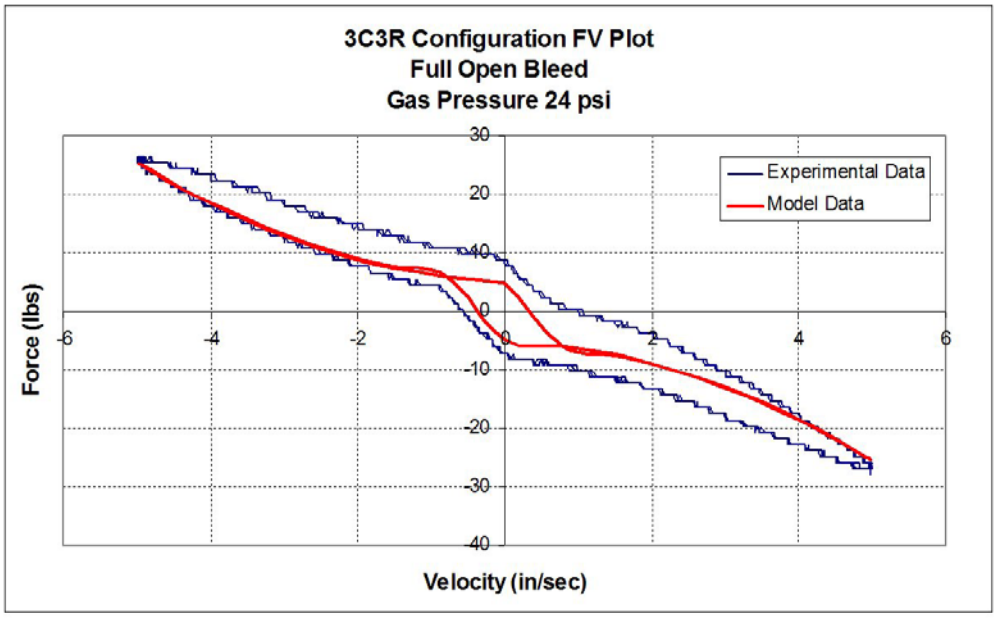

Figure 32: FV Plot, 3C3R Configuration, 5 in/sec, Bleed Open, $p_g = 24$ psi, $C_{D,v} = 0.71$, $C_{D,b} = 0.61$

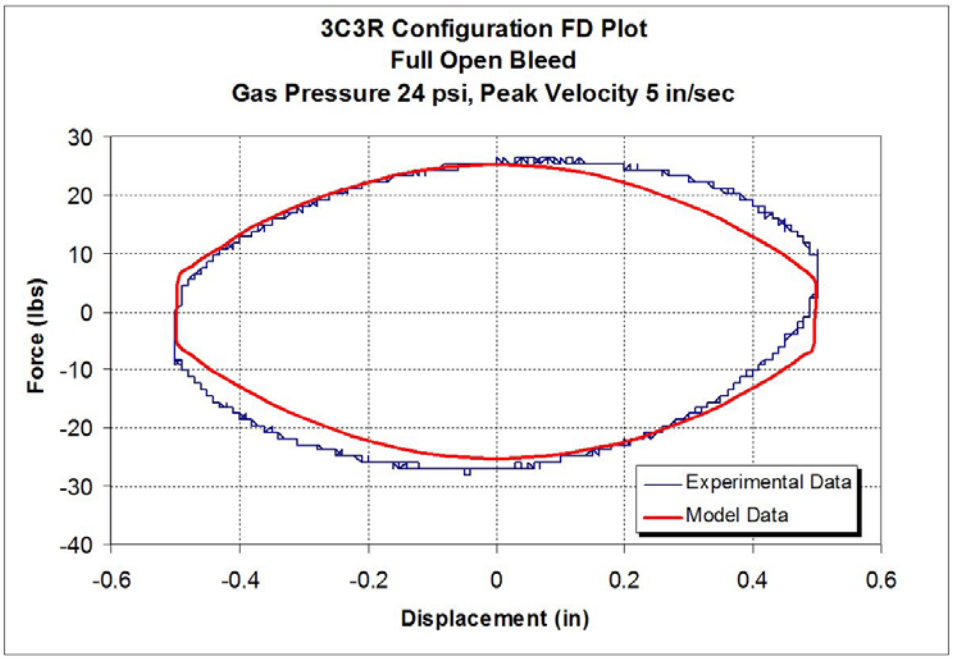

Figure 33: FD Plot, 3C3R Configuration, 5 in/sec, Bleed Open, $p_g = 24$ psi, $C_{D,v} = 0.71$, $C_{D,b} = 0.61$

The correlation of the 3C3R model configuration to the experimental is very good. In Figure 32, the general nonlinear force trends are present, and the maximum difference in model to experimental data is 6 pounds.

In Figure 33, the 3C3R FD plot shows good general agreement. Both the experimental and model data have the fast force transfer at the maximum displacements. The difference in the values is again caused by the hysteresis in the FV plot.

Figures 34 and 35 show FV and FD plots for the 3C3R configuration tested at 10 in/sec with a gas pressure of 24 psi. The value of CD for the bleed was 0.61 and CD for the valve flow was 0.71.

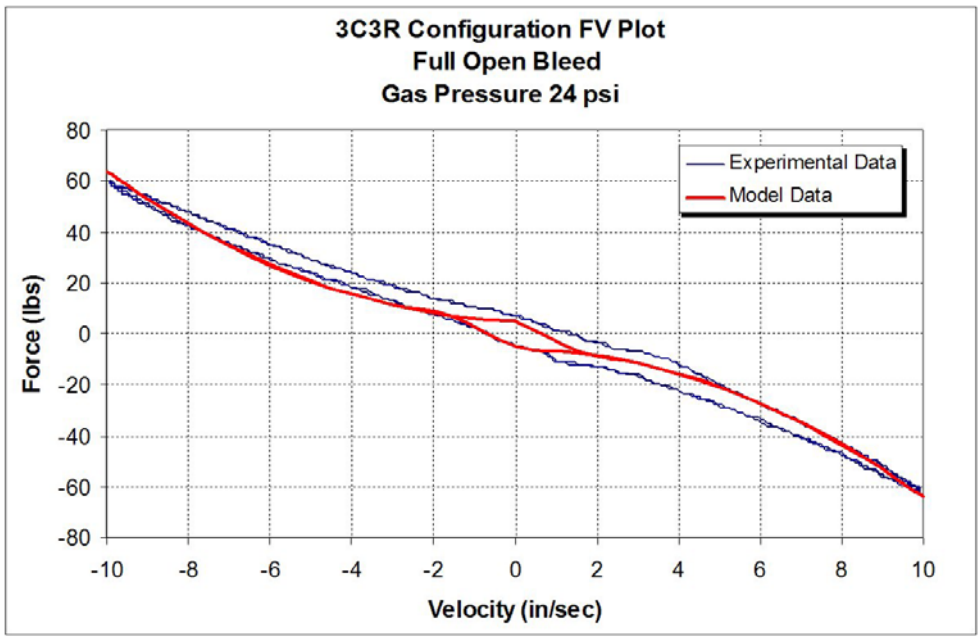

Figure 34: FV Plot, 3C3R Configuration, 10 in/sec, Bleed Open, $p_g = 24$ psi, $C_{D,v} = 0.71$, $C_{D,b} = 0.68$

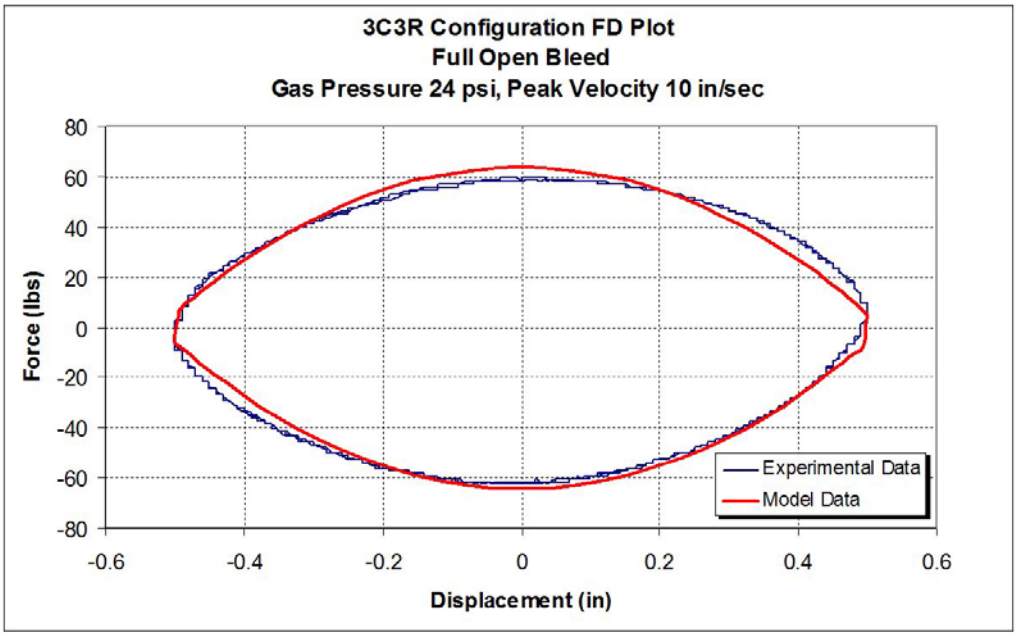

Figure 35: FD Plot, 3C3R Configuration, 10 in/sec, Bleed Open, $p_g = 24$ psi, $C_{D,v} = 0.71$, $C_{D,b} = 0.68$

In Figure 34, the maximum difference in force for the cycle is 8 pounds at -5 in/sec. The peak compression force is slightly high, but the difference in value is only 2 pounds. Figure 35 displays good correlation for the model and experimental data. The general trend of the displacement is followed by the model with a slight discrepancy in the accelerating compression region (upper right side).

For both high and low velocities, the dynamic discharge coefficients for the bleed and the valves correlate well in a fully configured damper that includes internal shims for flow restriction. The 3C3R configuration had very reasonable correlation, but for an additional check the 2C4R configuration will be examined for the same type of correlation.

Figures 36 and 37 show the FV and FD plots of 2C4R configuration tests at 10 in/sec with 52 psi gas pressure. The dynamic discharge coefficients used for the 3C3R configuration worked equally well for the 2C4R configuration for adequate correlation

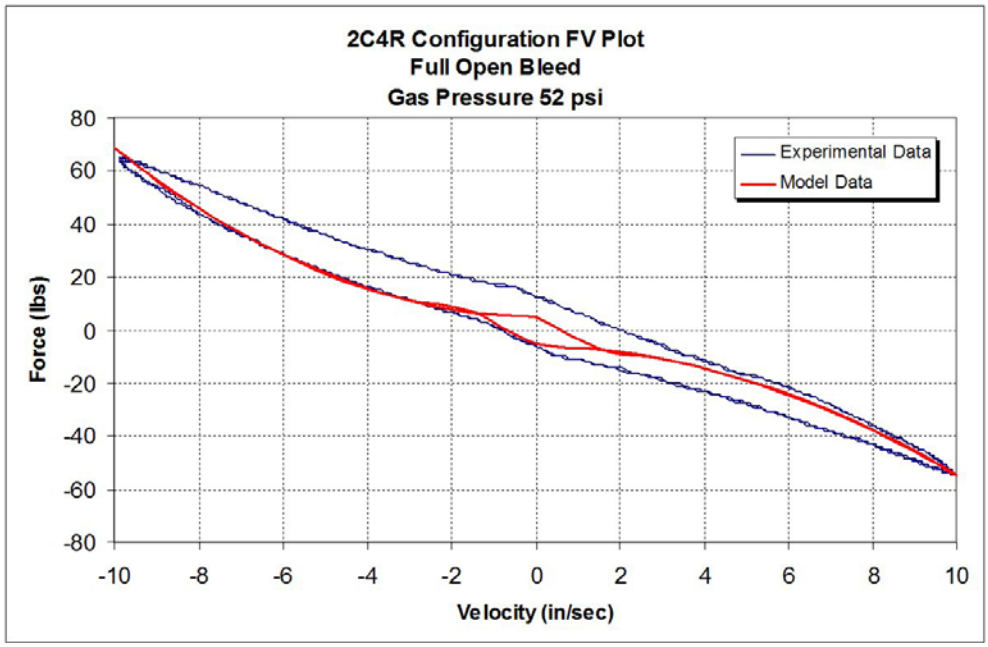

Figure 36: FV Plot, 2C4R Configuration, 10 in/sec, Bleed Open, $p_g = 52$ psi, $C_{D,v} = 0.71$, $C_{D,b} = 0.68$

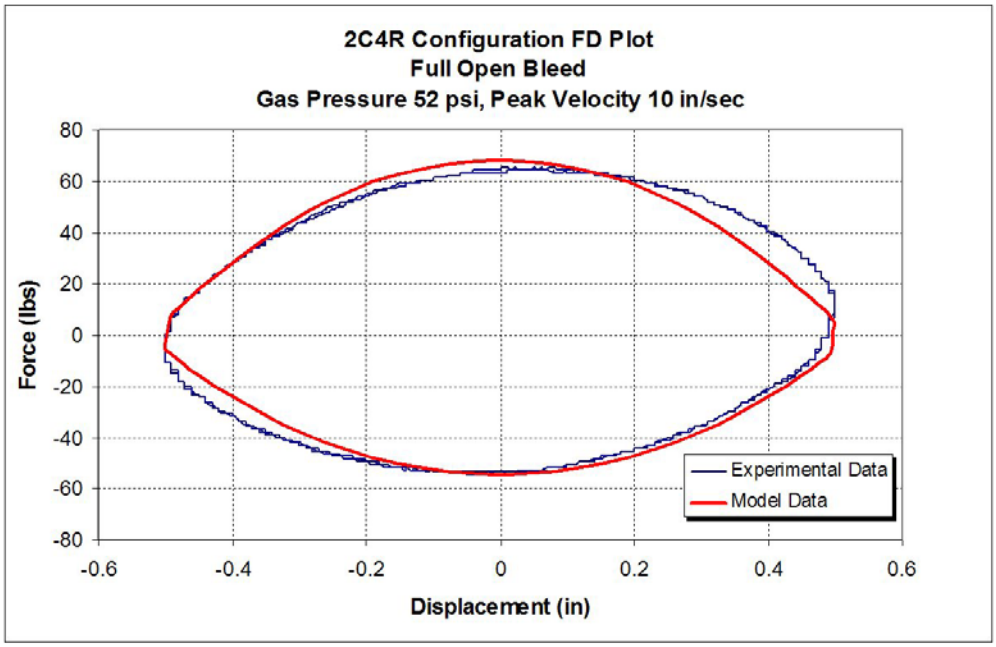

Figure 37: FD Plot, 2C4R Configuration, 10 in/sec, Bleed Open, $p_g = 52$ psi, $C_{D,v} = 0.71$, $C_{D,b} = 0.68$

In Figure 36, the same nonlinear force trends are observed as in Figure 34. The compression forces increase by 6 pounds at the peak compression velocity over the value of 58 pounds in the 3C3R configuration. This is expected because the reduction in number of compression flow orifices.

The correlation of the damper model to experimental data was conducted by adjustment of C_D, the dynamic discharge coefficient for the bleed orifice and the valve orifices. With a working model, the internal workings of the damper can be explored.

INTERNAL OPERATIONS OF DAMPER

With a correlated model pressures, flow rates and shims deflections can be calculated and analyzed. The 2C4R configuration was used with a gas pressure of 48 psi and a maximum speed of 5 in/sec. Figure 38 shows the internal chamber pressures for the 2C4R configuration test.

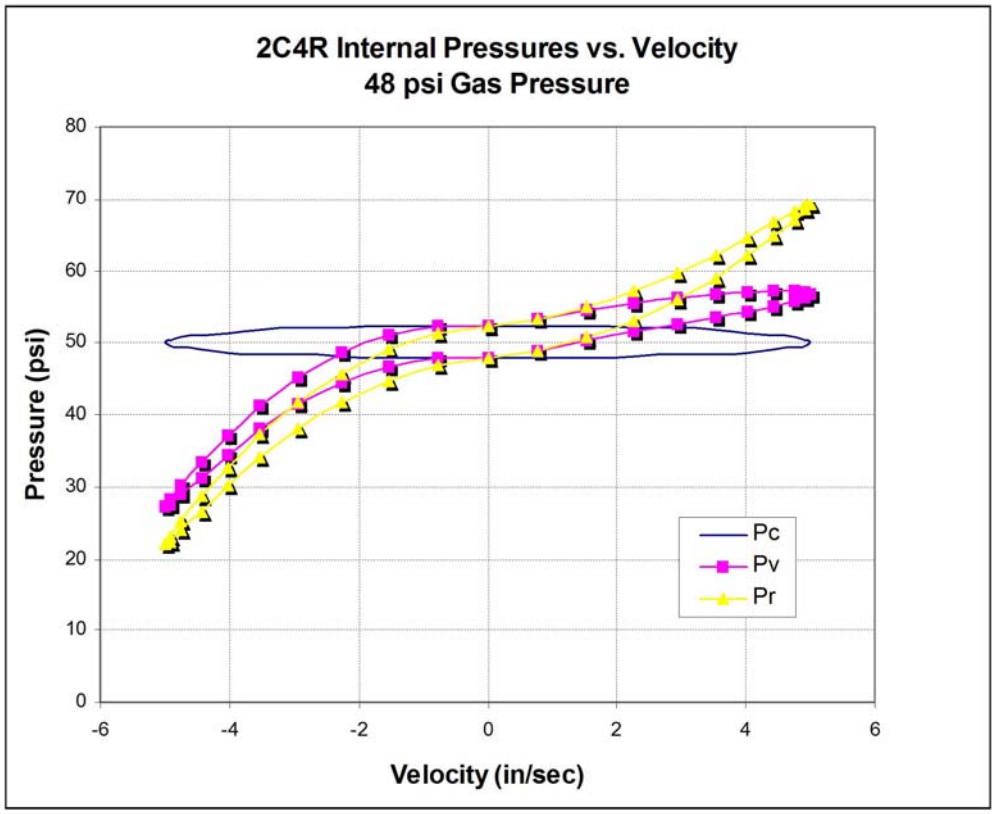

Figure 38: 2C4R Configuration Internal Pressure Plot

Figure 38 shows that the chamber pressure is relatively independent of velocity, remaining almost constant at 50 psi. This implies that the pressure in the rebound chamber is the controlling factor of the FV relationship of a damper. During

compression the pressure in the valve, P_v, is nearly equal to rebound chamber pressure, P_r. The major pressure drop is across the orifice in the compression case. For rebound, P_v is approximately half the vale of P_r. In the compression case the piston orifices are restricting flow, while in rebound the restriction is much less. This is logical because two orifices are open for compression and four are open for rebound.

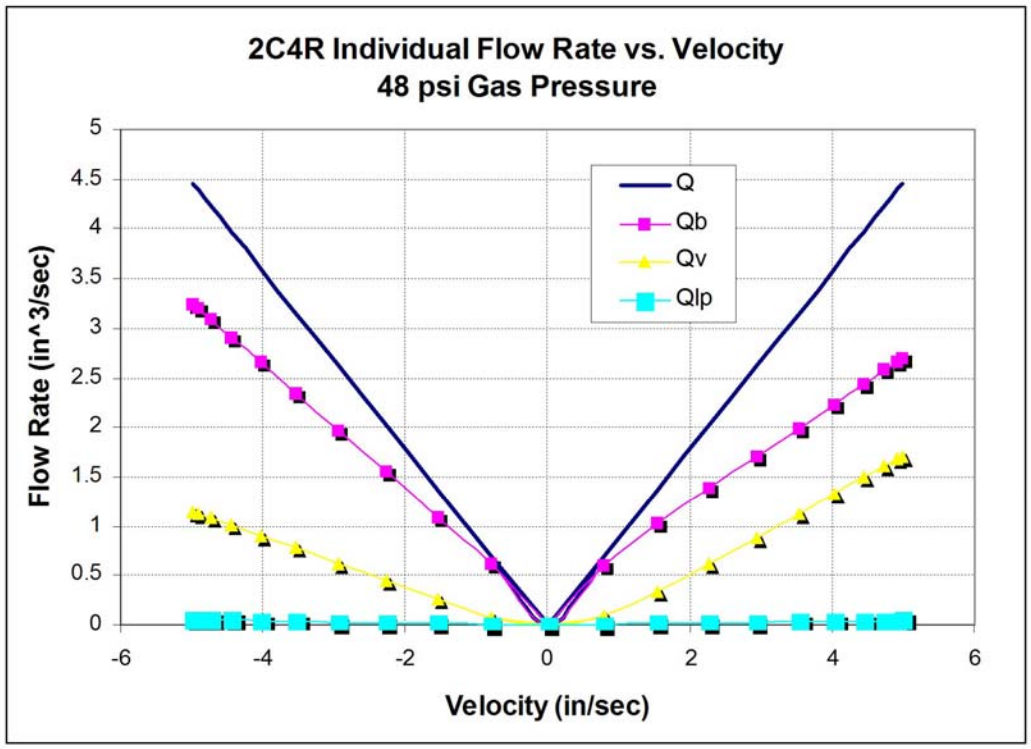

Figure 39: 2C4R Configuration Internal Flow Rate Plot

Figure 39 shows the flow rates of the three flow paths in the damper and the total flow rate. The total flow rate is the sum of the flow rates through the flow paths. Two orifice holes for the compression stroke yield less valve flow than four orifices in the

rebound stroke. The increase in valve flow in rebound in turn decreases the bleed orifice flow for the rebound stroke. Figure 39 also demonstrates the piston leakage flow is an order of magnitude lower than any of the other two flows. Neglecting this flow would not be an unreasonable assumption in the creation of the model.

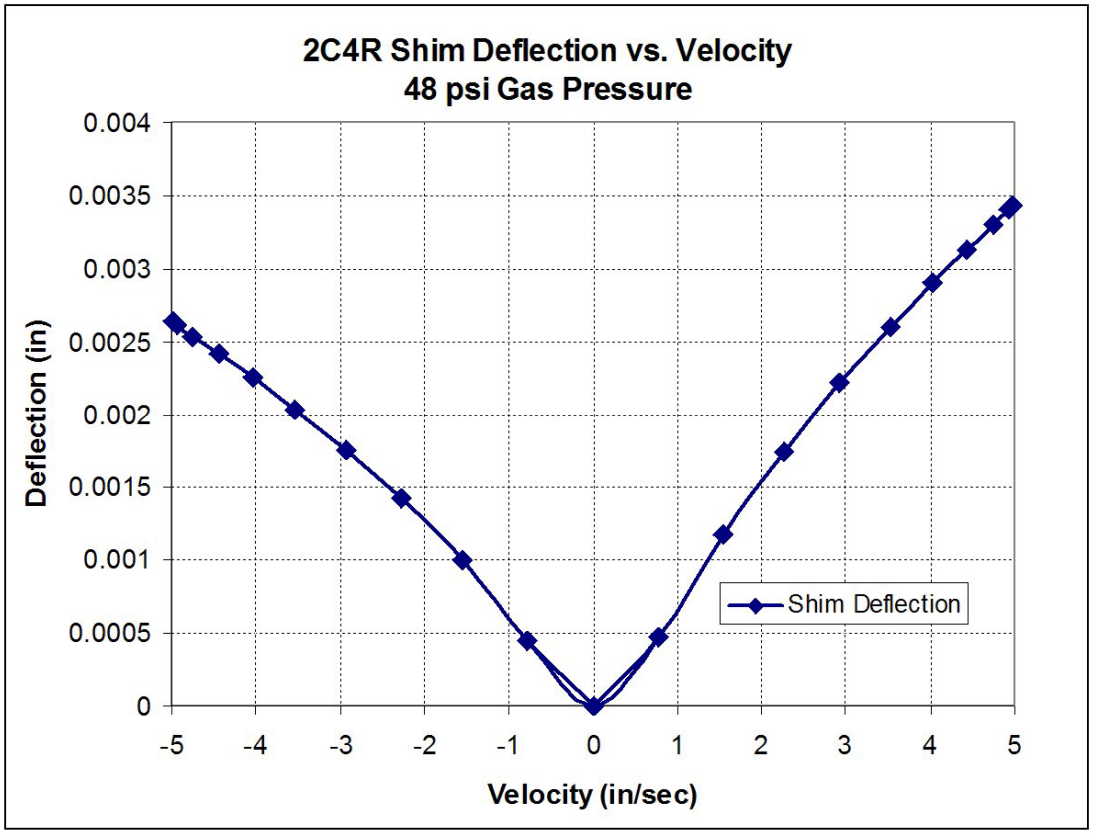

Figure 40: 2C4R Configuration Shim Deflection Plot

Figure 40 shows the shim deflection related to the velocity of the piston. More deflection occurs in rebound where four flow paths exist. This is consistent with Figure

39, where there is more valve flow during rebound. Since there is no preload in the design of the tanner piston, they begin to deflect as soon as motion is imposed.

Knowledge of these internal pressures, flow rates and deflections give an insight to the physics inside a damper. An understanding in these areas can lead to better damper tuning and design.

DAMPER PARAMETER STUDY

Obtaining a correlated model gives one the ability to exercise the model in a study of many variables in the damper. All major variables were examined to assess their sensitivity in operation. These variables include bleed orifice diameter, number of piston orifices, diameter of the valves, shim stiffness, density.

BLEED ORIFICE DIAMETER

The first parameter investigated was the bleed orifice diameter.

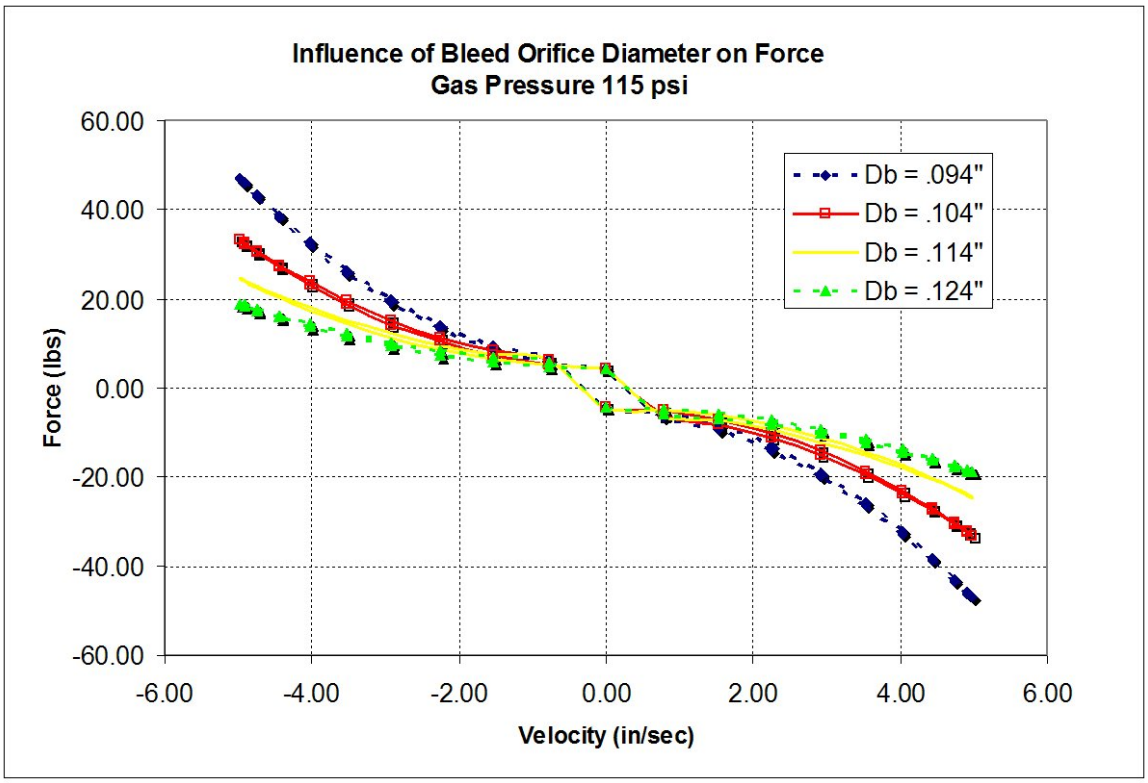

Figure 41: Influence of Bleed Orifice Diameter on Force

Figure 41 shows the change of damper force by changing the diameter of the bleed orifice. The bleed only configuration was used for this test. By reducing the diameter from 0.104" to 0.094" the peak force in compression changes from 32 pounds to 47 pounds. Reducing the diameter another 0.01" would no doubt cause a great increase in the damping force. This is cautionary because the rebound chamber pressure can quickly go below the vapor pressure and cause cavitation of the damper oil. This will cause an erratic increase in the damping force. Creating a larger bleed orifice only lessens the flow resistance and creates less damping force.

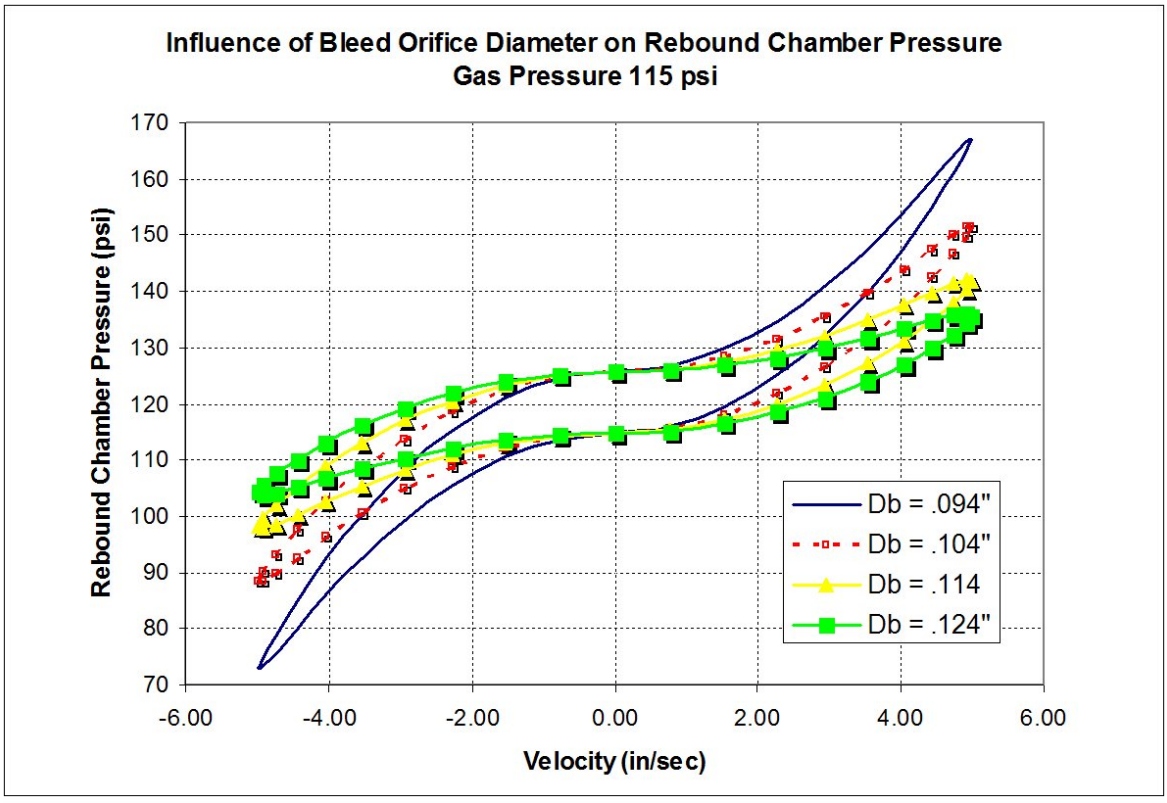

Figure 42: Influence of Bleed Orifice Diameter on Rebound Chamber Pressure

Figure 42 shows the rapid change of the rebound chamber pressure in compression if the flow is restricted. The pressure drops to 72 psi for the 0.094" D_b from 88 psi for 0.104" D_b at -5in/sec velocity. Understanding how to adjust the bleed orifice and avoid cavitation is important in damper tuning. This also shows the importance of maintaining a relatively high gas chamber pressure. If the gas chamber pressure is too low, cavitation will occur at lower input speeds. Actual modification of the bleed orifice is possible, but would require extensive modification to the piston rod design and the needle valve.

BLEED ORIFICE ADJUSTMENT

The next parameter investigated was the adjustability of the needle valve to control the size of the bleed orifice. The 3C3R configuration was used for this test. The total adjustment of the valve is 3.75 turns, with zero turns corresponds to a fully closed bleed orifice. As the adjustment turns increase the area of the bleed flow increases. The flow areas were calculated for one, two, three turns of adjustment. The fully open bleed area value corresponds to 3.75 turns.

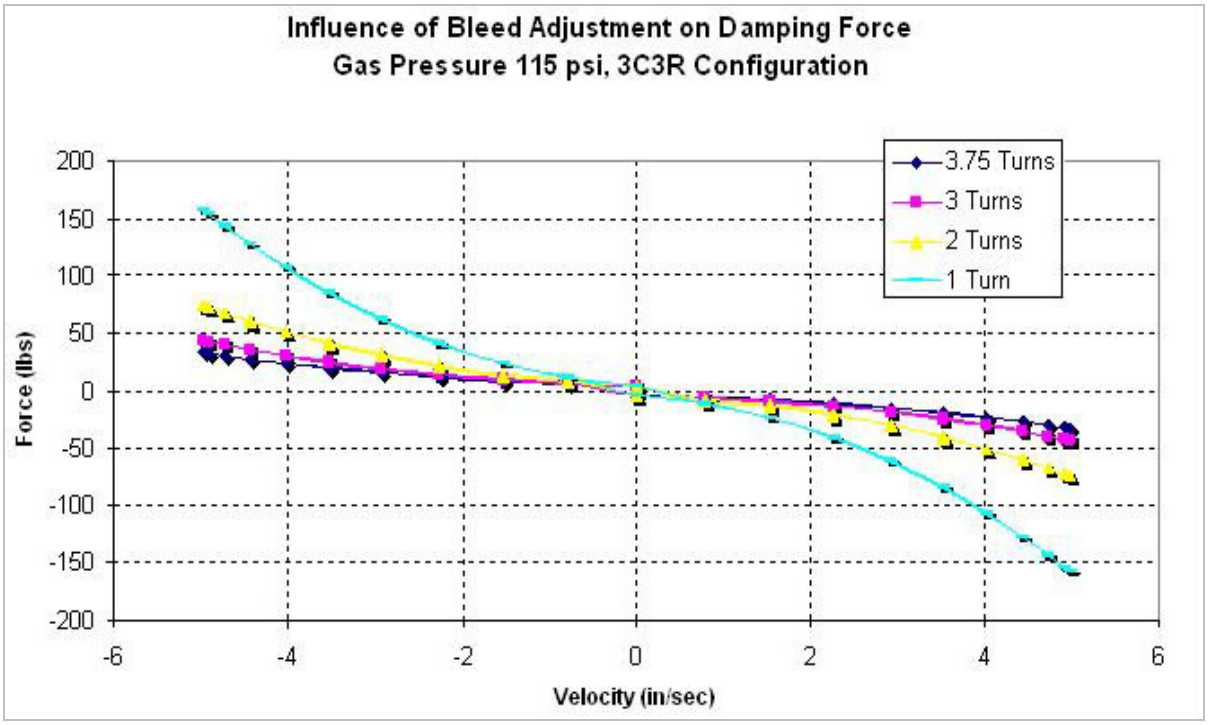

Figure 43: Influence of Bleed Adjustment on Damping Force

Figure 43 displays the great influence that the bleed adjustment has on the damping force. For 3.75 turns in the 3C3R configuration, the peak force is 25 pounds in compression. One turn of the adjustment gives a damping force of 155 pounds in compression. This is most effective way to increase the damping force and is the only way without disassembly of the damper. The warning from the previous section still applies; if the rebound chamber pressure becomes too low cavitation can occur in the oil causing hysteresis.

NUMBER OF PISTON ORIFICES

The number of piston holes was examined using the initial no shim configuration. The test was conducted with the bleed open and closed. Standard orifice diameters of 0.038" were tested. This is shown in Figures 44 and 45.

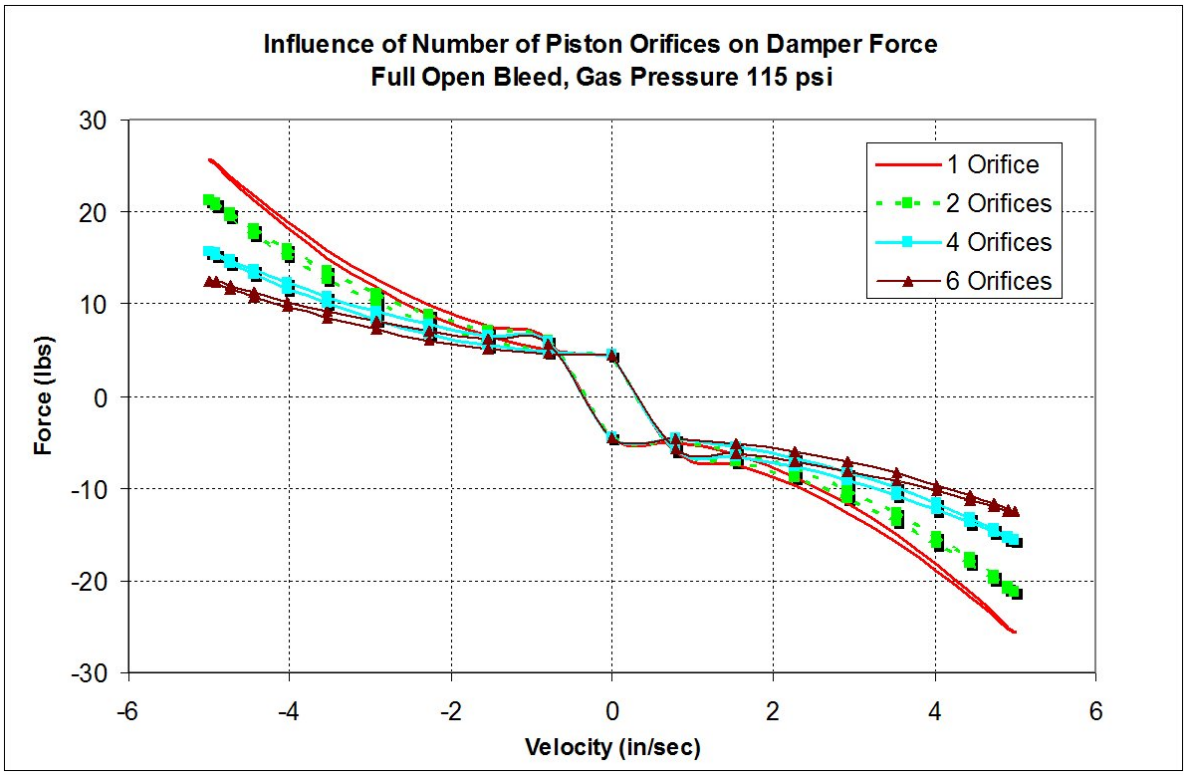

Figure 44: Influence of Number of Piston Orifices on Damper Force with Open Bleed

Figure 44 shows the results of the test run with a fully open bleed valve. It shows an increase in force at peak velocity from 12 pounds for six orifices to 25 pounds for one orifice. It is evident that the open bleed is dominating the flow in this case. Reducing the number of holes has a minor effect because their diameter is still small in

comparison to the bleed flow area. In the case where the bleed is fully open, reducing the number of piston orifices is not of great benefit in increasing damping force.

Figure 45 shows the results of the test run with the bleed valve fully closed. This forces the primary flow to travel through the orifices that are being reduced in number. A greater affect on the damping force is seen.

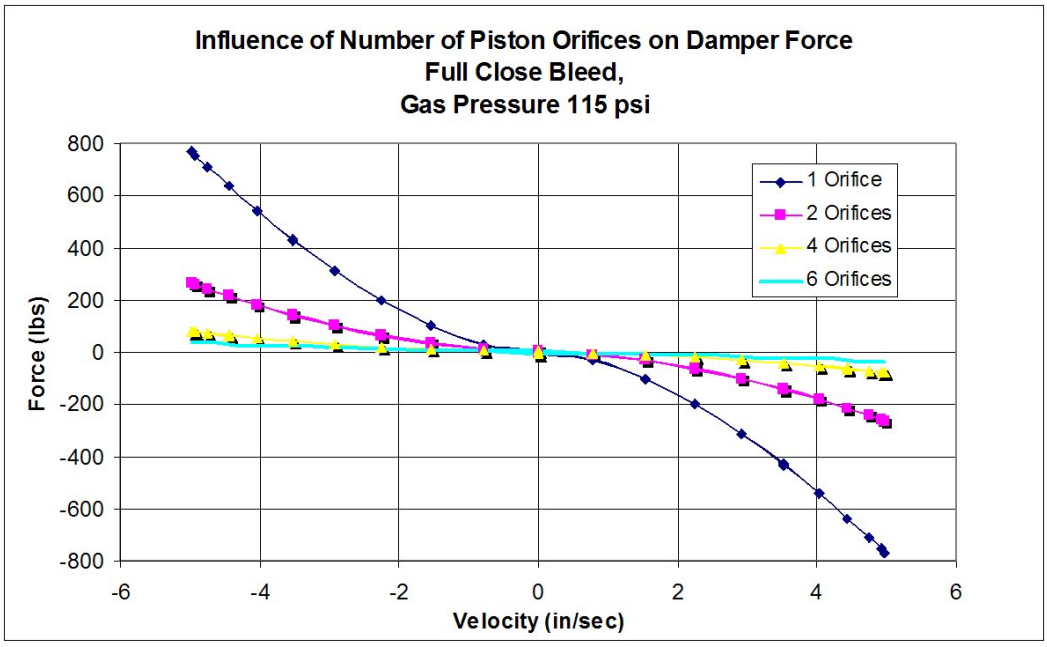

Figure 45: Influence of Number of Piston Orifices on Damper Force with Closed Bleed

The increase in force is much more dramatic with the reduction of orifices. The difference in peak force from four orifices to two is 200 pounds. This becomes more than a 400 lb difference when reducing number of holes from two to one. It is more than likely that the case of one orifice will have cavitation in the compression stroke because

of the highly restricted flow. This can be examined using a simplified version of equation (33). Neglecting acceleration terms and friction equation (33) becomes:

$$F = p_c A_c - p_r A_r \tag{40}$$

Solving for rebound pressure yields:

$$p_r = \frac{p_c A_c - F}{A_r} = \frac{F_{crit} - F}{A_r} \tag{41}$$

Where F_{crit} is the value of critical force where the pressure change from a negative to positive value. Using equation 41 and assuming p_c equal to p_g, the rebound chamber pressures were found. For the one and two orifice cases, the pressures solved for were negative. One orifice gave a value of -731 psi for p_r, while the two orifice case gave a value of -162 psi. In both of these cases, the model assumptions are not valid due to the cavitation that is occurring. For the four orifice case, the rebound pressure was found to be 44 psi. This positive value would avoid cavitation and the model is valid in this circumstance. The value of F_{crit} is 115 pounds, which is logical because the area of the piston is approximately one in^2. This shows that the gas pressure value is directed related to the forces that can be produced without causing cavitation. The user can now understand how to avoid cavitation to achieve a required peak damping force.

If the bleed orifice is reduced through the adjustment and the desired damping is still not achieved, reducing the number of flow paths in the piston can cause an additional increase in the damper force.

VALVE ORIFICE DIAMETER

The next parameter studied was the diameter of the valve orifices. Two configurations were used when experimenting with the valve orifice diameter. Initial no shim and 3C3R configurations were used. The initial no shim configuration was tested with the full bleed closed with the 6 standard piston orifices. The 3C3R configuration was used in order to investigate the change in diameter in a system with fewer orifices and shim restrictions.

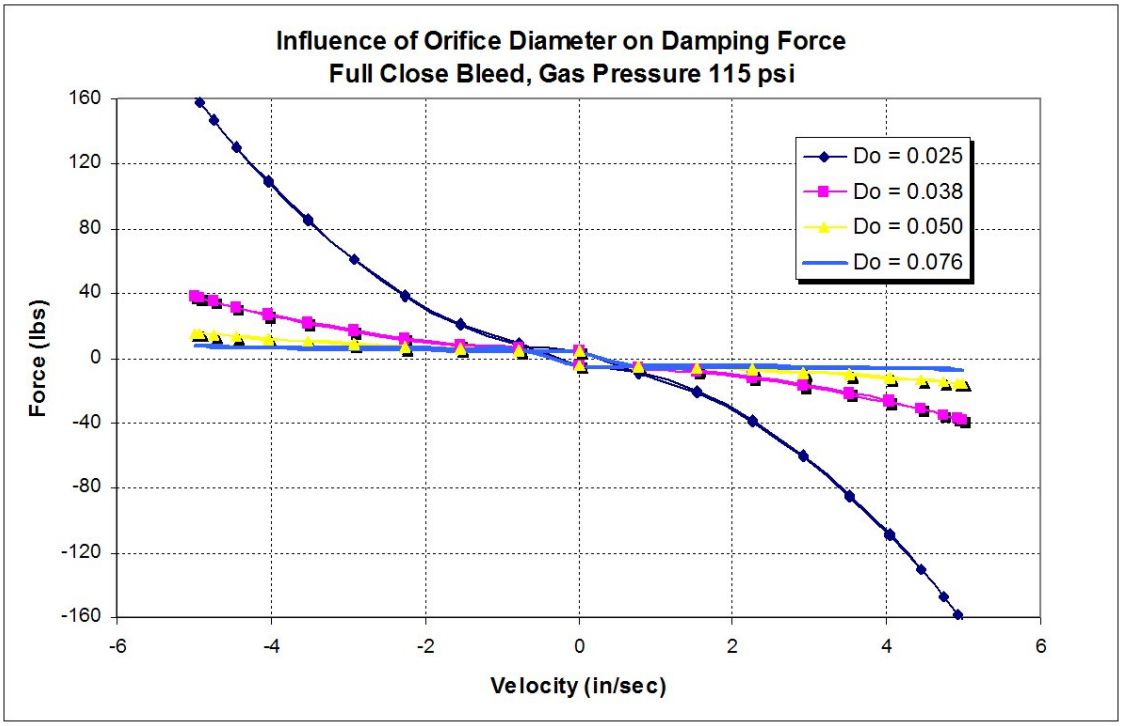

Figure 46: Influence of Orifice Diameter on Damping Force, No Shims, Full Close Bleed

Figure 46 shows the great increase in damping forces when the orifice diameter is reduced. Maximum compression force for Do = 0.038" was 40 pounds and for Do =0.025" was 160 pounds. The force is a very nonlinear function of the orifice diameter. Examining the larger diameter values of 0.050" and 0.076", little difference appears in the forces. It is also important to note that the 160 pounds of peak force exceeds the F_{crit} value of 115 lbs for this gas pressure setting. Reduction of the orifice size can also lead to cavitation of the fluid in the compression stroke, if the valves are the primary flow paths.

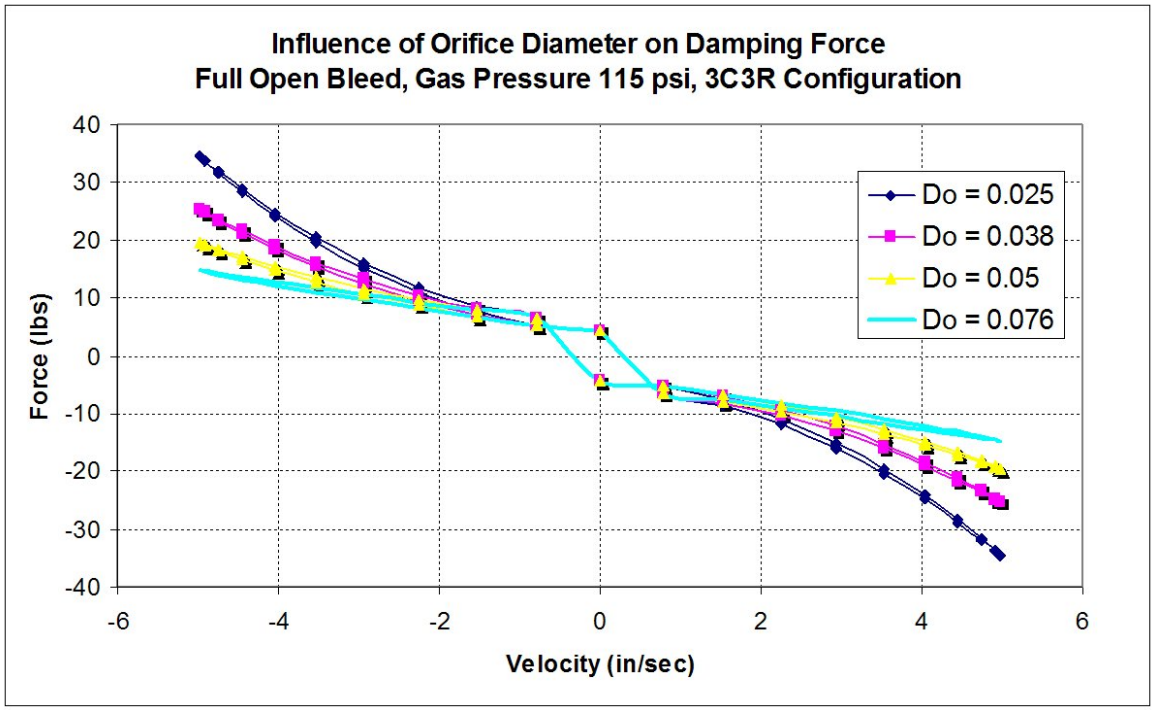

Figure 47: Influence of Orifice Diameter on Damping Force, 3C3R, Full Open Bleed

Figure 47 shows how the change in orifice diameter affects a damper with fully open bleed orifice and shim flow restrictions. Because the bleed is the largest flow area, the reduction in orifice diameter has less of an affect that in Figure 46. An increase of 10 pounds occurs at the maximum negative velocity in the transition from Do = 0.038" to Do =0.025". The decrease in orifice diameter has minimal effect because of the size of the bleed orifice.

With the usage of piston blanks, different orifices in the piston could be made with minimal machining effort. Standard small size drill bits are commercially available. Reduction in orifice size is a good method for increasing force from the damper as long as cavitation is considered.

SHIM STIFFNESS

The shim stiffness of four different shim thickness values was examined. The four shim thickness values tested were: 0.01", 0.012", 0.015", and 0.02". The 3C3R configuration was used to test the different shim stiffness values.

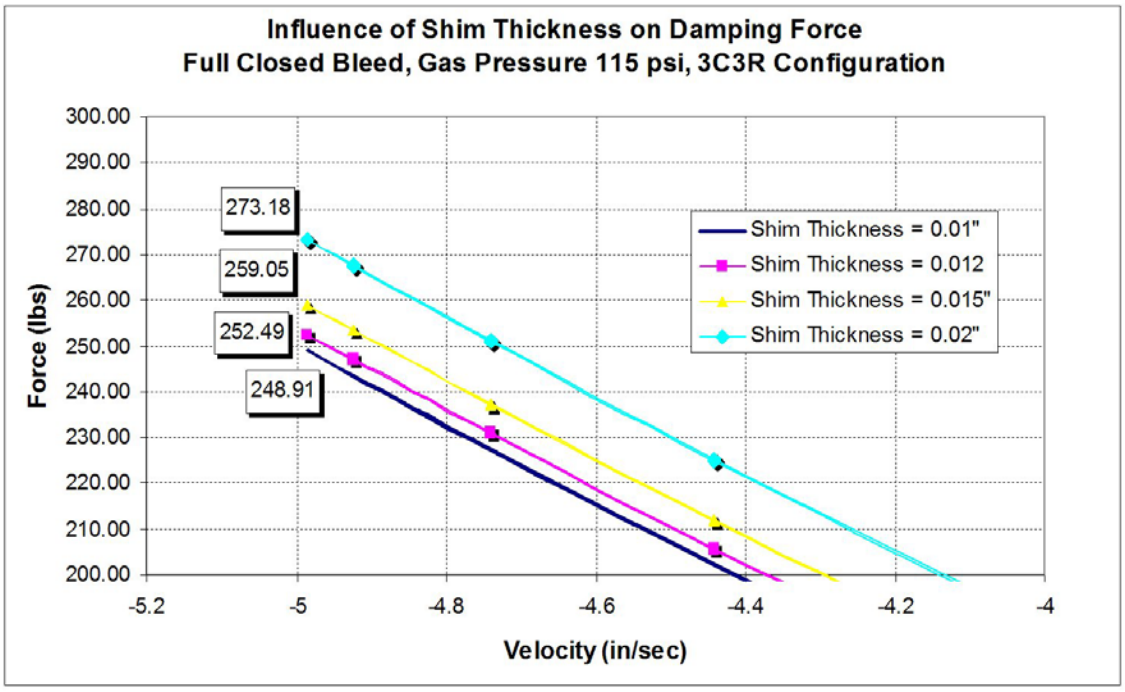

Figure 48: Influence of Shim Thickness on Peak Compression Forces

Figure 48 shows the peak forces during the compression stroke on the FV plot for the varying shim thickness values. This test was conducted at fully closed bleed to create the largest pressure differentials across the shims. The thickness of the shims has a moderate effect on the maximum forces that are produced. A difference of 24.27 pounds occurs in peak force value from the 0.01 inch shim to the 0.02 inch shim at the maximum speed. The same force trend occurs in the rebound stroke. Using thicker shims for tuning the damper is a method to achieve small increases in the force compared to the overall magnitude. In this case a 24.27 pound increase occurs in an approximately 250 pound overall peak force range. This is roughly a ten percent gain in peak damping forces.

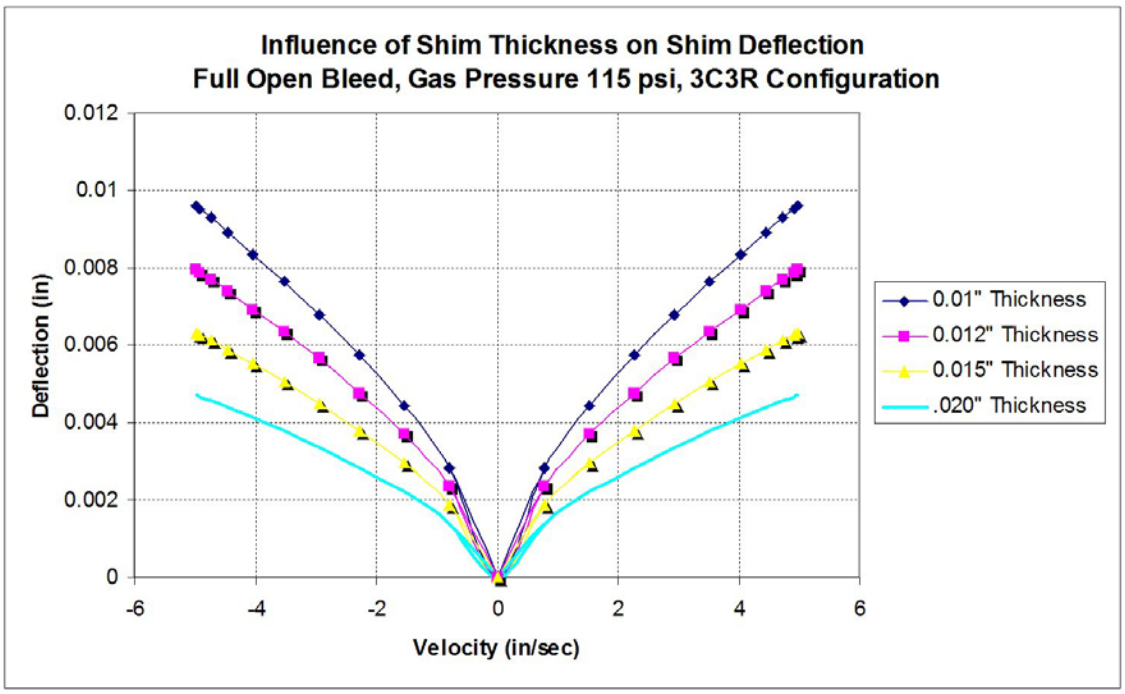

Figure 49: Influence of Shim Thickness on Shim Deflection

Figure 49 shows the shim deflection for the four shim thickness values. The thicker the shim, the less deflection and flow through the valve. A greater deflection occurs with a thinner shim, as would be expected. In terms of general tuning of this damper, using the bleed adjustment should be the primary method. Once the magnitude of forces are achieved using the bleed, the piston orifices can be restricted or unrestricted as desired.

FLUID DENSITY

The density of the damper oil was also investigated. The affects of change in density can be seen in Figure 50.

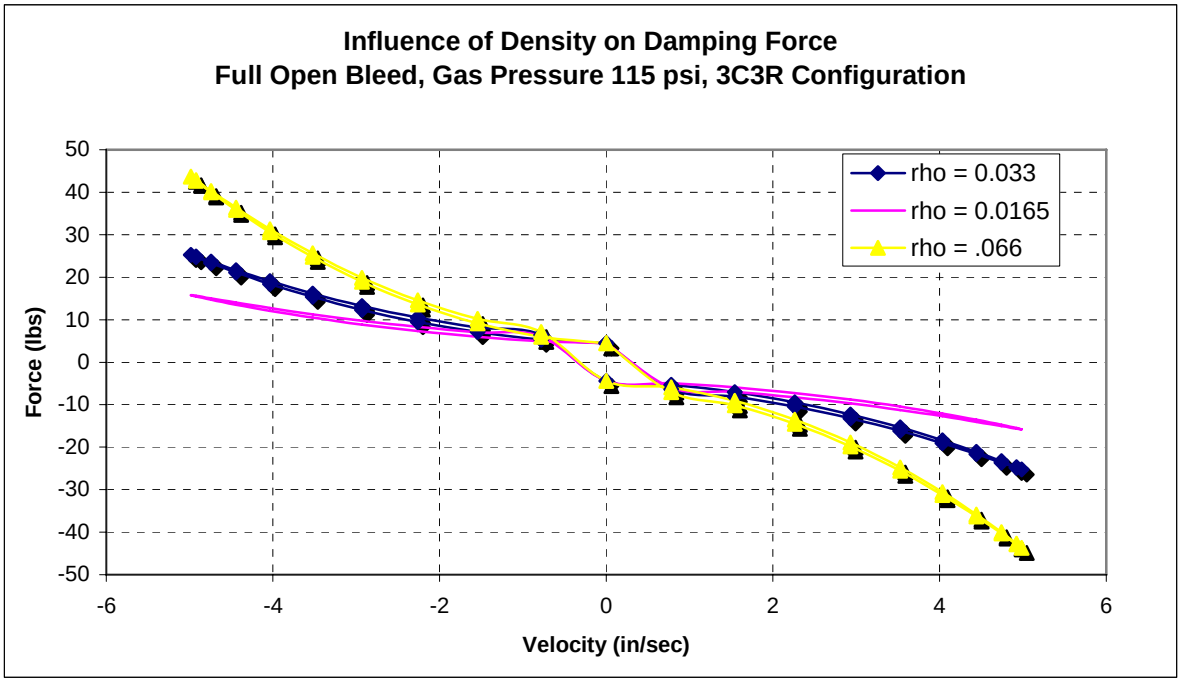

Figure 50: Influence of Density on Damping Force

The nominal value of 5W mineral oil was used in all previous model calculation. This is a value of 0.033 lb/in^3. Twice and half this nominal value were input into the model to see the effects of fluid density on the damping force.

The reduction of density causes a decrease in the damping force. This is caused the less dense fluid flowing with less resistance through the orifices. This would also have an effect on the kinematic viscosity of the system. The less dense the oil, the less

the value of dynamic viscosity will be. In other words, the resistance to flow will decrease and reduce the damping forces.

PRESSURE CHAMBER COMPLIANCE

In the investigation of hysteresis in the damper, the effect of chamber compliance has been included in the compressibility term, β'. Knowing the inner and outer geometry of the damper, an order of magnitude calculation of the strain on the chamber wall due to internal pressures can be performed.

Assuming the housing is a perfect cylinder, basic hoop stress can be calculated for given pressures. The threads on the outside of the housing were neglected. Once the hoop stress was found, the strain was found from Hooke's law. Then the change in radius can be found.

Table 1: Change in Radial Diameter Due to Internal Pressure

Pressures (psi)	Hoop Stress (psi)	Strain (in/in)	Radial Change (in)	Inner Radius (in)	Inner Diameter (in)
0	0	0.00E+00	0.00E+00	0.56750	1.13500
25	115.8163265	1.16E-05	6.57E-06	0.56751	1.13501
50	231.6326531	2.32E-05	1.31E-05	0.56751	1.13503
100	463.2653061	4.63E-05	2.63E-05	0.56753	1.13505
500	2316.326531	2.32E-04	1.31E-04	0.56763	1.13526
1000	4632.653061	4.63E-04	2.63E-04	0.56776	1.13553

From Table 1, it can be seen that inner diameter has very little change at even extreme internal pressures. From zero psi to 1000 psi, the change in diameter is only

0.06%. This basic calculation implies that the compliance of the chamber wall can be neglected with little or no change in the results.

TIME STEPS SAMPLED IN PROGRAM

In all previous FV plots in the research a loop appeared in the low speed regions. This was the product of the number of time steps sampled for the cycle of motion. The number of time steps used for all previous calculations was 40 per cycle. Figure 51 shows the influence of increasing the number of time steps and the effect on the interior loop.

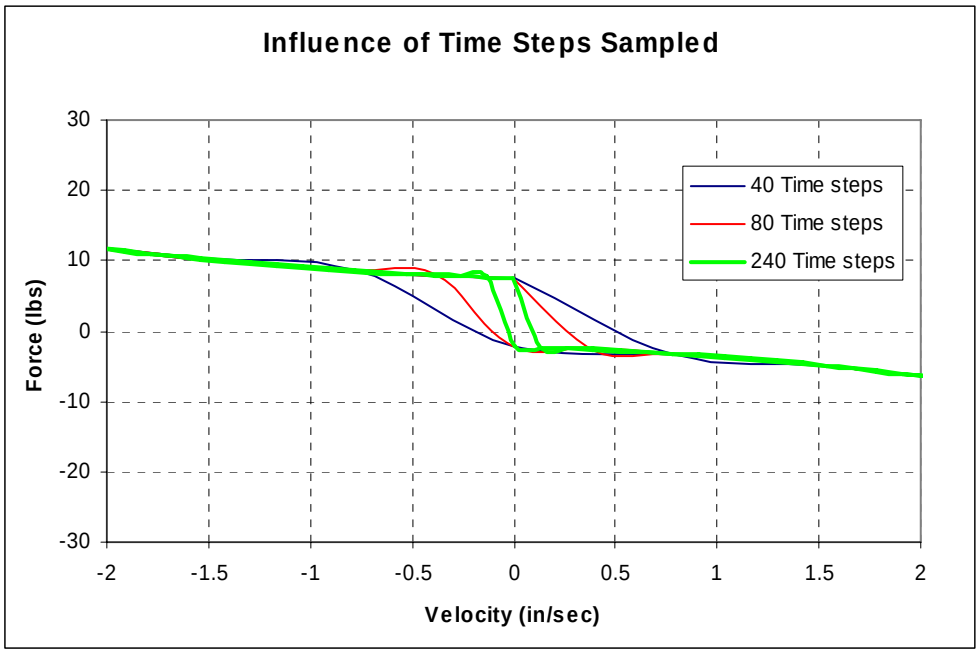

Figure 51: Influence of Number of Time Steps Sampled in Program

Figure 51 shows how the increase of time steps reduces the size of the low speed loop. For 40 time steps, the first velocity used for force calculation in compression was

-0.77 in/sec. For 240 time steps, the first velocity used for force calculation in compression was -0.13 in/sec. The increase of time steps allows for a more detailed investigation of speeds with magnitude less than 0.5 in/sec. The pressures at lower speeds can also be investigated with more clarity. The gas "spring" effects still remain the challenge to model in the low speed regions, as seen in the correlation data.

CONCLUSIONS AND RECOMMENDATIONS

CONCLUSIONS

A parametric model for predicting damper performance was successfully created and correlated to experimental damper data. The model was shown to be applicable to numerous possible configurations of the damper. The model produces FV and FD plots with good agreement with respect to the magnitude of the force and the nonlinear trend of the forces. An interesting observation is that the model correlates well to the portions of the velocity cycle when the damper piston is decreasing in velocity.

The primary mechanism for force generation is the change in pressure in the rebound chamber, since the compression chamber is almost constant. The gas pressure dictates the compression chamber pressure. To avoid cavitation of the fluid, the gas chamber pressure must be set so the rebound chamber pressure never drops below zero for the desired maximum compression force. This is not a concern in the rebound stroke because the rebound chamber pressure increases above the compression chamber pressure.

The model does not predict hysteresis. The exclusion of compressibility of the fluid may be one cause of its absence.

The holes in the shims have little effect on the shim stiffness. The shim stiffness also varies as the cube of the thickness. The holes may have an effect on the flow area, but this is difficult to quantify.

The parameter study showed the dominate variable in the force characteristics was the bleed orifice area and the bleed adjustment. Reducing piston orifice size or

number can have a large impact on damping forces, but the possibility of cavitation must always be accounted for. A basic critical force can be found and used a starting point for predicting cavitation during the compression stroke.

For use as a design tool in Formula SAE applications would be of great use in suspension design and reduction of damper testing time.

RECOMMENDATIONS

The inclusion of compressibility into the model would have the largest benefit. The difficulty lies in that the system model with compressibility is defined by a partial differential equation and the current solution method is not applicable.

Testing with real shims of varying thickness could better help correlate the shim stiffness model. Also, additional testing for cavitation while varying gas pressure would be beneficial.

The presence of the shims in the valve system will cause a change in discharge coefficients. An increase in the accuracy of the valve modeling is necessary for increased accuracy. One possibility would be modeling these two flows as one system to more accurately portray the behavior of the system.

An experimental and analytical study of the factors that influence coulomb friction forces would be of great practical use. Racecar designers and tuners spend a great deal of time and money to eliminate coulomb friction. Factors that could be investigated are pressure, seal material, seal construction, lubricant, etc. Quantifying the relative importance of each factor would be of great benefit.

REFERENCES

[1] Lang H.H., *A Study of the Characteristics of Automotive Hydraulic Dampers at High Stroking Frequencies*, Ph.D. Dissertation, University of Michigan, Ann Arbor, 1997.

[2] Reybrouck K.G., *A Non Linear Parametric Model of an Automotive Shock Absorber*, SAE Technical Paper Series 940869, 1994.

[3] Duym S.W., Steins R., Baron G.V., Reybrouck K.G., *Physical Modeling of the Hysteretic Behaviour of Automotive Shock Absorbers*, SAE Technical Paper Series 970101, 1997.

[4] Kim D., *Analysis of Hydraulic Shock – Absorber and Implementation on the Vehicle Suspension Systems*, M.S. Thesis, Seoul National University, S. Korea, 1993.

[5] Mollica R., Youcef-Toumi K., A *Nonlinear Dynamic Model of a Monotube Shock Absorber*, Proceedings of the American Control Conference, Albuquerque, NM, June 1997, pp. 704-708.

[6] Mollica R., *Nonlinear Dynamic Model and Simulation of a High Pressure Monotube Shock Absorber Using the Bond Graph Method*, M.S. Thesis, Massachusetts Institute of Technology, Cambridge, MA, 1997

[7] Talbott M.S., *An Experimentally Validated Physical Model of a High Performance Automotive Damper*, M.S. Thesis, Purdue University, Lafayette, IN, 2002

[8] Talbott M.S., Starkey J., *An Experimentally Validated Physical Model of a High Performance Mono-Tube Damper*, SAE Technical Paper Series 2002-01-3337, 2002.

[9] Tanner Racing Products, 2006, "G2 Carbon Shim Kit 85602", 15 May, 2006. http://www.tannerracing.com/

[10] Roark R.J., Young W.C., *Formulas for Stress and Strain*, 5th Edition, McGraw-Hill, New York, pp.324-343, 1975.

[11] Hoffman J.D., *Numerical Methods for Engineers and Scientists*, 2nd Edition, Marcel Dekker, Inc., New York, 2001.

[12] Roehrig Engineering Inc, 2006, "Model 2VS Damper Dynamometer", 15 May, 2006. http://www.roehrigengineering.com/cart/home.php?cat=1/

APPENDIX A

HYPOTHETICAL SPRING AND DAMPER ANALOGY

For a sinusoidal motion, the displacement and velocity is given as:

$$x = A\sin(\omega t) \tag{42}$$

$$\dot{x} = \omega A\cos(\omega t) \tag{43}$$

The forces for a hypothetical ideal linear spring and damper are:

$$F_{spring} = -Kx = -KA\sin(\omega t) \tag{44}$$

$$F_{damper} = -C\dot{x} = -C\omega A\cos(\omega t) \tag{45}$$

Consider an FV plot for the spring. Equations (43) and (44) can be rearranged to yield:

$$\frac{\dot{x}}{\omega A} = \cos(\omega t) \tag{46}$$

$$\frac{F_{spring}}{-KA} = \sin(\omega t) \tag{47}$$

From trigonometry:

$$1 = \cos^2 + \sin^2 = \left(\frac{\dot{x}}{\omega A}\right)^2 + \left(\frac{F_{spring}}{-KA}\right)^2 \tag{48}$$

Equation (48) is a parabola with coordinates $\dot{x}$ and F_{spring}. Thus the FV plot for a hypothetical linear spring is an ellipse. Figures 52 – 55 show the FV and FD trends for the hypothetical linear spring and damper found using equations (42)-(45).

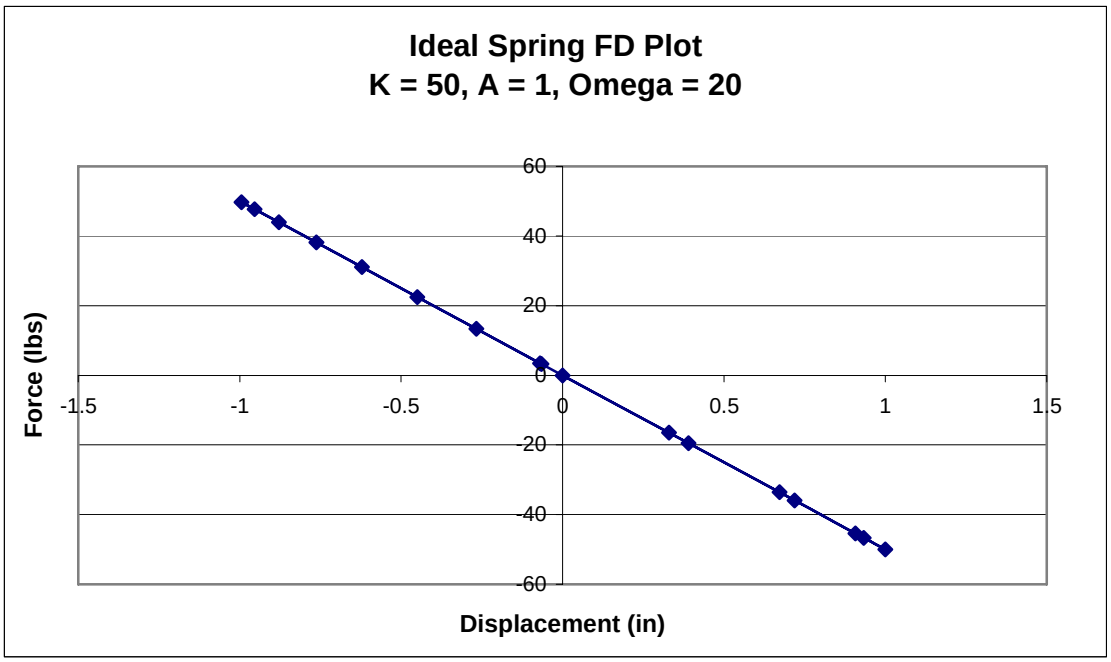

Figure 52: Hypothetical Ideal Spring FD Plot

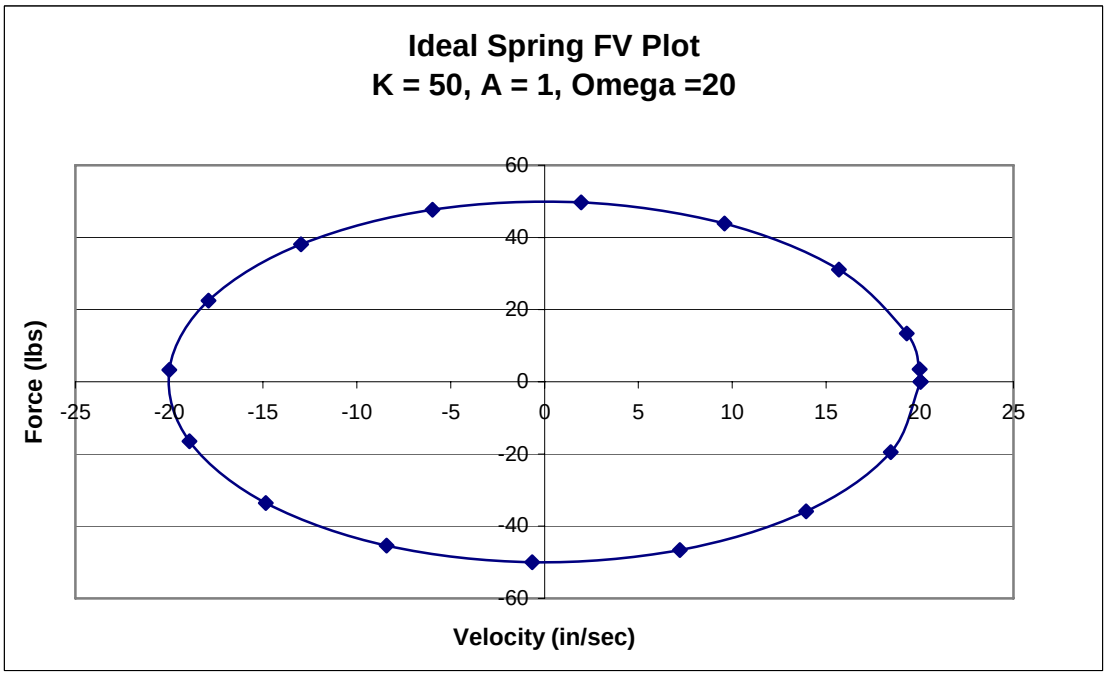

Figure 53: Hypothetical Ideal Spring FV Plot

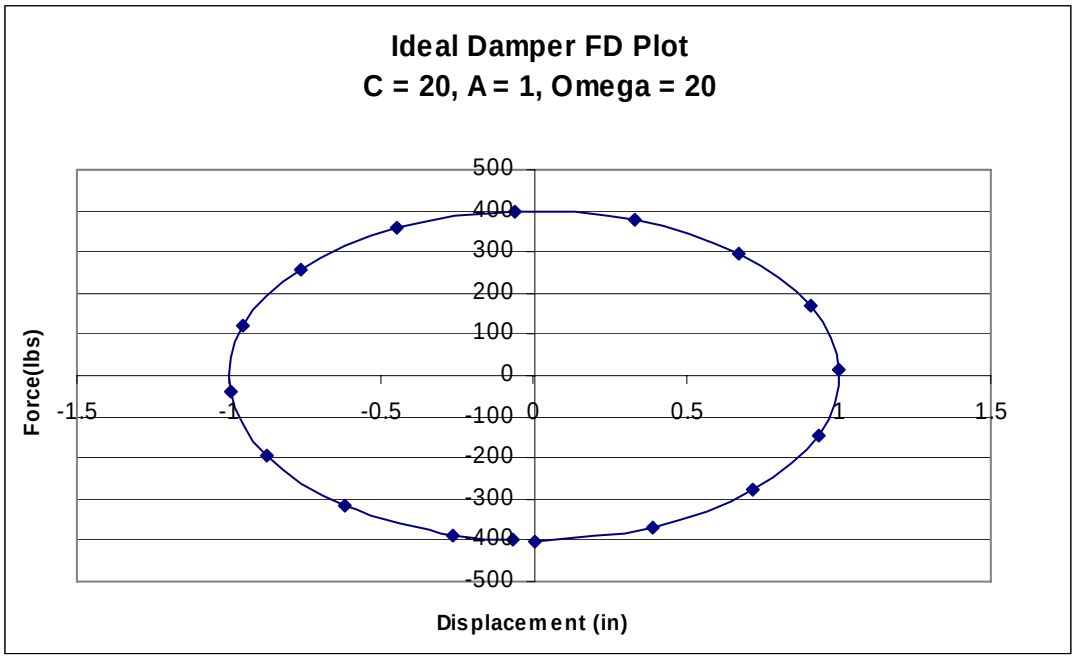

Figure 54: Hypothetical Ideal Damper FD Plot

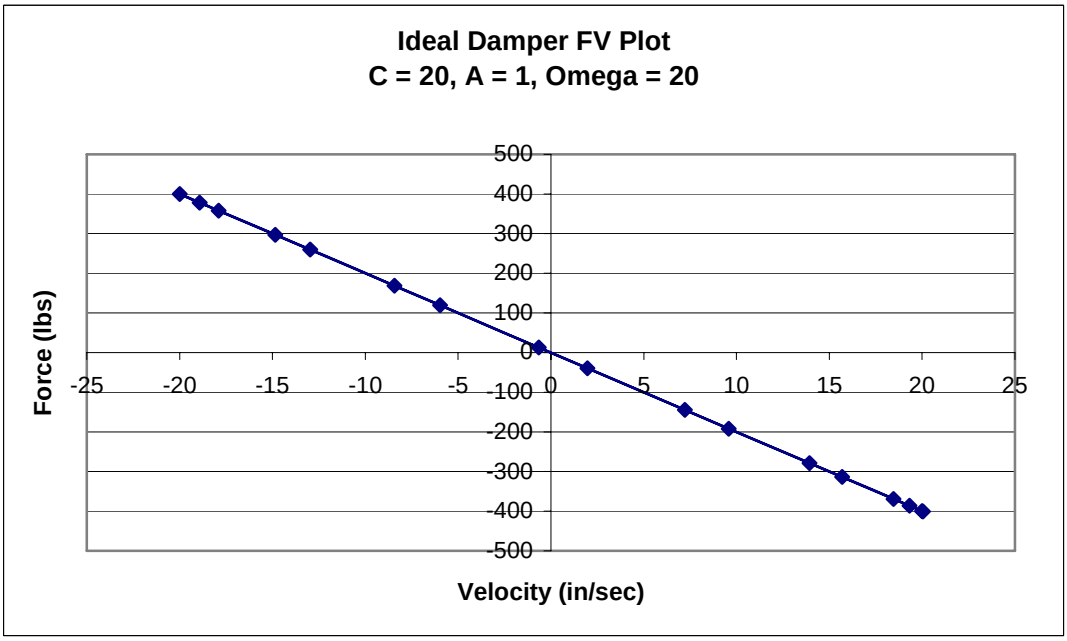

Figure 55: Hypothetical Ideal Damper FV Plot

APPENDIX B

CUBIC RELATION OF STIFFNESS TO THICKNESS

The relation between shim stiffness was shown to have a cubic relation to the shim thickness. This can be explored using a basic cantilever beam because deflection of the beam and the disk are similar in nature.

The deflection of the cantilever is known to be:

$$\delta = \frac{PL^3}{3EI} \tag{49}$$

P is the load, L is beam length, E is elastic modulus, and I is the moment of inertia. Equation (50) is the relation for the moment of inertia. b is the width and t is the thickness of the beam.

$$I = \frac{bt^3}{12} \tag{50}$$

Combining equations (49) and (50) gives:

$$\delta = \frac{4PL^3}{Ebt^3} \tag{51}$$

To find an equivalent stiffness of the beam, divide the load by the deflection.

$$k = \frac{P}{\delta} = P / \frac{4PL^3}{Ebt^3} = \frac{Ebt^3}{4L^3} = C_1 t^3 \tag{51}$$

Equation 51 shows that the effective stiffness is proportional to the thickness of the beam cubed. This shows the similarity to the fixed disk deflection of the shims. C_1 is a general constant if all other input variables are unchanged.

Also, an examination of the formulas for flat circular plates of constant thickness in *Formulas for Stress and Strain* [10] also show this thickness cubed relation. A multiple term equation is used to find the deflection of a pressure loaded circular disk with a fixed inner radius. A plate constant is used in appears in these terms and is shown in equation 52.

$$D = \frac{Et^3}{12(1-v^2)} \tag{52}$$

This plate constant appears in the denominator of the deflection equation, and in the numerator of the equivalent stiffness. So the analytical calculation of the deflection and stiffness are also relative to the thickness cubed. This again shows the curve fit to the FEA results are valid for usage in the program to find a stiffness value.

APPENDIX C

DAMPING REQUIRED FOR FSAE CAR

The following is an order of magnitude calculation for the range of damping forces necessary for the 2006 TAMU Formula SAE racecar. This was done to verify the feasibility of the damper choice.

Assuming a natural frequency of 2.5 Hz, equation (53) is the conversion to radians/sec.

$$\omega_n = 2\pi f_n = 2\pi(2.5) = 15.7 \frac{rad}{\sec} \tag{53}$$

From the natural frequency, the stiffness, k, of a one wheel system can be found if the mass in known. Assuming a 600 pound car evenly distributed front to rear and left to right, the wheel load is 150 pounds.

$$\omega_n^2 = \frac{k}{m} = \frac{k}{(W/g)} = \frac{kg}{W} \tag{54}$$

$$\Rightarrow k = \frac{\omega_n^2 W}{g} = \frac{(15.7)^2 150}{386} = 96 \frac{lbs}{in} \tag{55}$$

Assuming a critically damped system, the damping coefficient can be found using equation (56).

$$c = 2\sqrt{km} = 2\sqrt{96\, lbs/in \;\; \frac{150\, lbs}{386\, in/\sec^2}} = 12 \frac{lb}{(in/\sec)} \tag{56}$$

The damping force can be found by multiplying the damping coefficient by the desired velocity. Figure 56 shows the trend of damping as velocity increases.

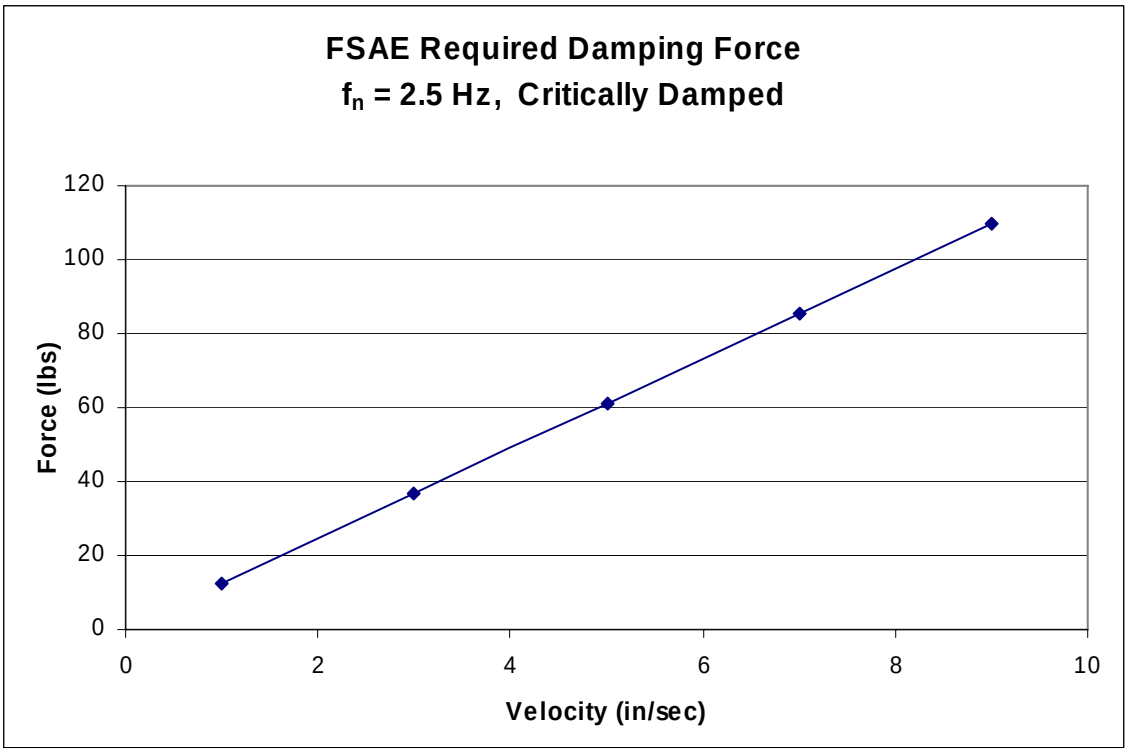

Figure 56: Range of Required Damping Force for FSAE Racecar

Figure 56 shows the general range of forces necessary for critical damping for a FSAE damper. The maximum force shown is 110 pounds at 9 in/sec. The Tanner Gen 2 damper is more than capable of creating these damping forces as long as the gas pressure is large enough to prevent fluid cavitation.

APPENDIX D

COMPUTER PROGRAM

```
%this is a prelimanry program for shock absorber compression stroke
%inputs are known physical variables, motion profiles, gas pressure and
%compression chamber pressure
clc
clear all
close all
%%%%%%%%%%%%%%%%%%%%%%%%%%%%%%%%%%%%%%%%%%%%%%%%%%%%%%%%%%%%%%%%%%%%%%%%%
%%
%define the motion profiles in vectors
timesteps = 240; %steps in a cycle minus one
Freq = 1.59; %Hz
Amp = .499 %in
cycle = Freq^-1;
halfcycle = cycle/2;
incoftime =cycle/timesteps;

Timevec = zeros(timesteps+1,1);
%For the comp cycle, where vel is pos; and rebound where vel is neg
for j = 2:1:timesteps+1
    Timevec(j,1) = Timevec(j-1,1) + incoftime;
    %this will change for diff # of time steps
end
%the compression cycle is for step 1 through step (timesteps/2 + 1)
%the rebound is the remaining steps to timesteps + 1
%max displacement is 1", split into positive 1/2" and negative 1/2"
Xvec = zeros(timesteps+1,1);
for j = 1:1:timesteps+1
    Xvec(j,1) = Amp * sin(Freq*2*pi*Timevec(j) - pi/2);
end
% figure (1)
% plot(Timevec,Xvec,'-b*')
% xlabel('Time (sec)')
% ylabel('Displacement (in)')
% title('Cycle Displacement Profile vs. time')
%Velocity
Xdot = zeros(timesteps+1,1);
for j = 1:1:timesteps+1
    Xdot(j,1) = (Amp*2*pi*Freq )* cos(Freq*2*pi*Timevec(j) - pi/2);
end
% figure (2)
% plot(Timevec,Xdot,'-b*')
% xlabel('Time (sec)')
% ylabel('Velocity (in/sec)')
% title('Cycle Velocity Profile')
%acceleration
Xdotdot = zeros(timesteps+1,1);
for j = 1:1:timesteps+1
```

```
    Xdotdot(j,1) = -(Amp*2*pi*Freq )*(2*pi*Freq ) *
sin(Freq*2*pi*Timevec(j) - pi/2);
end
% figure (3)
% plot(Timevec,Xdotdot,'-b*')
% xlabel('Time (sec)')
% ylabel('Acceleration (in/sec^2)')
% title('Cycle Aceleration Profile')
%%%%%%%%%%%%%%%%%%%%%%%%%%%%%%%%%%%%%%%%%%%%%%%%%%%%%%%%%%%%%%%%%%%%%%%%%%%%%%%
%define values for gas pressue and compression chamber pressure
%initial gas pressure
Pgasi =24;% psi standard
Dgp = 1.39; % Diameter gas piston in
Agp = pi*(Dgp/2)^2; %in^2
Lg = .80; %in
Drod = .375; %diameter rod in
Arod = pi*(Drod/2)^2;
mgp = .0273; %mass gas piston, lbs
slugs = 386.4; %slugs in in/sec^2 for proper unit conversion
%gas pressure for the cycle
Pgas = zeros(timesteps+1,1);
for j = 1:1:timesteps+1
Pgas(j) = Pgasi * (Agp*Lg)/(Agp*Lg-Arod*Xvec(j));
end
%pressure in the compression chamber during compression stroke
Pc = zeros(timesteps+1,1);
for j=1:1:timesteps+1
    Pc(j) = Pgas(j) + (Arod/Agp^2)* (mgp/slugs) * Xdotdot(j);
end
% figure (4)
% hold on
% plot(Xdot, Pc,'-rx')
% plot(Xdot,Pgas,'-b*')
% title('Compression Chamber Pressure & Gas Pressure Compression
Stroke')
% xlabel('Velocity in/sec^2')
% ylabel('Pressure Compression Chamber, Pc, lbs/in^2')
% legend('Pc', 'Pgas')
%
%%%%%%%%%%%%%%%%%%%%%%%%%%%%%%%%%%%%%%%%%%%%%%%%%%%%%%%%%%%%%%%%%%%%%%%%%%%%%%%
%%
%Examine total flow from equation
%constant inputs
Dpis = 1.13; %diameter of piston, inches
Apis = pi*(Dpis/2)^2;
Ar = Apis-Arod;
Q = zeros(timesteps+1,1);
%for positive velocity
for j = 1:1:timesteps/2+1
Q(j) = Ar*Xdot(j);
end
%for negative velocity, %all flows will have positive values
for j = timesteps/2+2:1:timesteps+1
    Q(j) = Ar*-Xdot(j);
```

```
end
% figure(5)
% plot(Xdot,Q)
% title('Total Flow, Q, for compression Stroke vs. Velocity')
% xlabel('Velocity in/sec')
% ylabel('Total Flow, Q, in^3/sec')
%%%%%%%%%%%%%%%%%%%%%%%%%%%%%%%%%%%%%%%%%%%%%%%%%%%%%%%%%%%%%%%%%%%%%%%%%%%%%%%%
%%%
%Define the storage for the solved values,
%at X = 0 in beginning, Pc = Pv = Pr, y = 0, and Qb, Qlp, & Qv = 0
Pr = zeros(timesteps+1,1); %Vector for Pressure in Rebound chamber
Pr(1) = Pc(1); %equal pressure at time zero
Pv = zeros(timesteps+1,1); %Vector for Pressure in valve
Pv(1) = Pc(1); %equal pressure at time zero
y = zeros(timesteps+1,1); %Shim deflection vector
y(1)=0;
Qv = zeros(timesteps+1,1);
Qv(1)=0;
Qb = zeros(timesteps+1,1);
Qb(1)=0;
Qlp = zeros(timesteps+1,1);
Qlp(1)=0;
%%%%%%%%%%%%%%%%%%%%%%%%%%%%%%%%%%%%%%%%%%%%%%%%%%%%%%%%%%%%%%%%%%%%%%%%%%%%%%%%
%%%%%
%Define the equations for interative solving, 6 eq's 6 unknowns
%%%common labels, v = valve, o = orifice, b = bleed orifice, lp =
leakage
%Initial guesses for unknowns for the first calculation
Pv(2) = 26.24; %pressue in the valving, psi
Pr(2) = 26.07; %pressure in the rebound chamber, psi
Qv(2) = 0.08;   %Valve Flow, in^3/sec
Qb(2) = .35 ;  %Bleed Orifice Flow, in^3/sec
Qlp(2) = 0.0025 ; %Seal Flow, in^3/sec
y(2) = .0005; %Shim deflection, in
%
%%%%%%%%%%%%%%%%%%%%%%%%%%%%%%%%%%%%%%%%%%%%%%%%%%%%%%%%%%%%%%%%%%%%%%%%%%%%%%%%
%%
%COMPRESSION STROKE ITERATIONS
for j = 2:1:timesteps/2  %one more count gives infinite iterations
    %define the initial guesses for the iteration loops
    if j == 2
       Qvi = Qv(2);
       Qbi = Qb(2);
       Qlpi =Qlp(2);
       yi = y(2);
       Pvi = Pv(2);
       Pri =Pr(2);
   else
       Qvi = Qv(j-1);
       Qbi = Qb(j-1);
       Qlpi = Qlp(j-1);
       yi = y(j-1);
       Pvi = Pv(j-1);
       Pri = Pr(j-1);
```

```
    end
 %%%%All constant Inputs from each equation for the compression
stroke%%%
 %%%%%%
 %EQ1, Ar prevoiusly defined
 %%%%%%
 %EQ2
 Dv1 = 1.13;%inch %Diameter of compression valve,i.e. Dia of largest
Shim
 Cdv1 = 0.71;%dynamic discharge coeff for valve : 1=compression stroke
 rho = 0.0330; % fluid density of mineral oil lbm/in^3 about 5W oil
wieght
 %%%%%%
 %EQ3,
 %assume large diameter holes for compression stroke
 Do1 = .0375;%.14; %in, Diameter of compression orifice
 Ao1 =  3*pi*(Do1/2)^2; %area of orifice flow, 3 holes
 %from shim model estimate Av
 Rop = .240; %in %  found by modeling shim and estimating pressure area
 %based on top shim diameter in multi shim stack
 a3 = .565; %in % same method as Rop. this is large shim radius
 Av =  .5 * (pi*a3^2 - pi*Rop^2);
 %1/2 of annular area of acting pressue on shim
 Cf = 0.3; %momentum coefficent, exp found by Lang
 Fsp = 0;  %spring preload on shims, set to zero for start
 k1 =800; %lbf/in spring constant of shims,
 %%%%%%%
 %EQ4, Ao1,rho,slugs previously defined
 Cdo1 = .71; %dynamic discharge coeff for orifice, 1 = compression
 %%%%%
 %EQ5  %rho, slugs previously defined
 Db1 = .104 ; %measured diameter of bleed orifice
 Ab1 = (pi *(Db1/2)^2);
 Cdb1 = .61; %Bleed orifice dynamic discharge coeff, 1=compression
 %%%%%
 %EQ6
  b = .003; %leakage gap, measured estimate, inches
 %%no slugs needed in this case for the mu, if in lbm/(in*sec)then it
does
 mu = 2.5*10^-5;  % this is corrected into lbf*sec/in^2
 l = .30; %this is length of leak
%%%%%%%
count = 1;
%EQ1: sums of total flows
f1 = Qvi + Qbi + Qlpi - Xdot(j)*Ar;  %f1 = 0
%partial derivatives
df1dQv = 1;
df1dQb = 1;
df1dQlp = 1;
df1dy = 0;
df1dPv = 0;
df1dPr = 0;
```

```
%EQ2: valve flow equation to shim
f2 = .5*pi*Dv1*yi*Cdv1*sqrt(2*slugs*(Pvi-Pri)/rho) - Qvi;  %f2 = 0

%partial derivatives
df2dQv = -1;
df2dQb = 0;
df2dQlp = 0;
df2dy = .5*pi*Dv1*Cdv1*sqrt(2*slugs*(Pvi-Pri)/rho);
df2dPv=(pi*Dv1*yi*Cdv1*sqrt(2))/(4*(rho/slugs)*sqrt(slugs*(Pvi-
Pri)/rho));
df2dPr=-(pi*Dv1*yi*Cdv1*sqrt(2))/(4*(rho/slugs)*sqrt(slugs*(Pvi-
Pri)/rho));

%EQ3: Force balance on the valve
f3 = (Pvi-Pri)*Av + Cf*(rho/slugs)*(Qvi^2/Ao1) - Fsp - k1*yi;  %f3=0
%partial derivatives
df3dQv = 2*Cf*(rho/slugs)*(Qvi/Ao1);
df3dQb = 0;
df3dQlp =0;
df3dy = -k1;
df3dPv = Av;
df3dPr = -Av;

%EQ4: Orifice flow rate equation to valve
f4 = Ao1*Cdo1*sqrt(2*slugs*(Pc(j)-Pvi)/rho) - Qvi;%f4=0
%partial derivatives
df4dQv= -1;
df4dQb = 0;
df4dQlp = 0;
df4dy = 0;
df4dPv = (-Ao1*Cdo1*sqrt(2))/(2*(rho/slugs)*sqrt(slugs*(Pc(j)-
Pvi)/rho));
df4dPr = 0;

%EQ5: Bleed Orifice equation
f5 = Ab1*Cdb1*sqrt(2*slugs*(Pc(j)-Pri)/rho) - Qbi;%f5=0
%partial derivatives
df5dQv = 0;
df5dQb = -1;
df5dQlp = 0;
df5dy= 0;
df5dPv =0;
df5dPr = (-Ab1*Cdb1*sqrt(2)) / (2*(rho/slugs)*sqrt(slugs*(Pc(j)-
Pri)/rho));

%EQ6: Seal leakage Equation
f6 = pi*Dpis*( b^3*(Pc(j)-Pri)/(12*mu*l) + Xdot(j)*b/2) - Qlpi; %f6=0
%partial derivatives
df6dQv = 0;
df6dQb = 0;
df6dQlp = -1;
df6dy = 0;
df6dPv = 0;
```

```
df6dPr = -b^3*pi*Dpis/(12*mu*l);

%iterativly solve the system A*Delta = f
%build f vector
f = [-f1;-f2;-f3;-f4;-f5;-f6];

%build the A matrix
A(1,:) = [df1dQv,df1dQb,df1dQlp,df1dy,df1dPv,df1dPr] ;
A(2,:) = [df2dQv,df2dQb,df2dQlp,df2dy,df2dPv,df2dPr] ;
A(3,:) = [df3dQv,df3dQb,df3dQlp,df3dy,df3dPv,df3dPr] ;
A(4,:) = [df4dQv,df4dQb,df4dQlp,df4dy,df4dPv,df4dPr] ;
A(5,:) = [df5dQv,df5dQb,df5dQlp,df5dy,df5dPv,df5dPr] ;
A(6,:) = [df6dQv,df6dQb,df6dQlp,df6dy,df6dPv,df6dPr] ;

Delta = A^-1*f;
%reassign the unknowns
       Qvi = Qvi + Delta(1,1);
       Qbi = Qbi + Delta(2,1);
       Qlpi =Qlpi + Delta(3,1);
       yi = yi + Delta(4,1);
       Pvi = Pvi + Delta(5,1);
       Pri =Pri + Delta(6,1);

%%%%%%%%%%%%%%%%%%%%%%%%%%%%%%%%%%%%%%%%%%%%%%%%%%%%%%%%
while max(abs(Delta))>.0001 | max(abs(f))>.00001
    %EQ1: sums of total flows
f1 = Qvi + Qbi + Qlpi - Xdot(j)*Ar; %for loop here  %f1 = 0
%partial derivatives
df1dQv = 1;
df1dQb = 1;
df1dQlp = 1;
df1dy = 0;
df1dPv = 0;
df1dPr = 0;

%EQ2: valve flow equation to shim
f2 = .5*pi*Dv1*yi*Cdv1*sqrt(2*slugs*(Pvi-Pri)/rho) - Qvi;  %f2 = 0
%partial derivatives
df2dQv = -1;
df2dQb = 0;
df2dQlp = 0;
df2dy = .5*pi*Dv1*Cdv1*sqrt(2*slugs*(Pvi-Pri)/rho);
df2dPv=(pi*Dv1*yi*Cdv1*sqrt(2))/(4*(rho/slugs)*sqrt(slugs*(Pvi-
Pri)/rho));
df2dPr=-(pi*Dv1*yi*Cdv1*sqrt(2))/(4*(rho/slugs)*sqrt(slugs*(Pvi-
Pri)/rho));

%EQ3: Force balance on the valve
f3 = (Pvi-Pri)*Av + Cf*(rho/slugs)*(Qvi^2/Ao1) - Fsp - k1*yi;  %f3=0
%partial derivatives
df3dQv = 2*Cf*(rho/slugs)*(Qvi/Ao1);
df3dQb = 0;
```

```
df3dQlp =0;
df3dy = -k1;
df3dPv = Av;
df3dPr = -Av;

%EQ4: Orifice flow rate equation to valve
f4 = Ao1*Cdo1*sqrt(2*slugs*(Pc(j)-Pvi)/rho) - Qvi;%f4=0
%partial derivatives
df4dQv= -1;
df4dQb = 0;
df4dQlp = 0;
df4dy = 0;
df4dPv = (-Ao1*Cdo1*sqrt(2)) / (2*(rho/slugs)*sqrt(slugs*(Pc(j)-
Pvi)/rho));
df4dPr = 0;

%EQ5: Bleed Orifice equation
f5 = Ab1*Cdb1*sqrt(2*slugs*(Pc(j)-Pri)/rho) - Qbi;%f5=0
%partial derivatives
df5dQv = 0;
df5dQb = -1;
df5dQlp = 0;
df5dy= 0;
df5dPv =0;
df5dPr = (-Ab1*Cdb1*sqrt(2)) / (2*(rho/slugs)*sqrt(slugs*(Pc(j)-
Pri)/rho));

%EQ6: Seal leakage Equation
f6 = pi*Dpis*( b^3*(Pc(j)-Pri)/(12*mu*l) + Xdot(j)*b/2) - Qlpi; %f6=0
%partial derivatives
df6dQv = 0;
df6dQb = 0;
df6dQlp = -1;
df6dy = 0;
df6dPv = 0;
df6dPr = -b^3*pi*Dpis/(12*mu*l);

%iterativly solve the system A*Delta = f for Delta
%build f vector
f = [-f1;-f2;-f3;-f4;-f5;-f6];
%build the A matrix
A(1,:) = [df1dQv,df1dQb,df1dQlp,df1dy,df1dPv,df1dPr] ;
A(2,:) = [df2dQv,df2dQb,df2dQlp,df2dy,df2dPv,df2dPr] ;
A(3,:) = [df3dQv,df3dQb,df3dQlp,df3dy,df3dPv,df3dPr] ;
A(4,:) = [df4dQv,df4dQb,df4dQlp,df4dy,df4dPv,df4dPr] ;
A(5,:) = [df5dQv,df5dQb,df5dQlp,df5dy,df5dPv,df5dPr] ;
A(6,:) = [df6dQv,df6dQb,df6dQlp,df6dy,df6dPv,df6dPr] ;
%solve the matrix system
Delta = A^-1*f;
      %reassign the unknowns
       Qvi = Qvi + Delta(1);
       Qbi = Qbi + Delta(2);
       Qlpi =Qlpi + Delta(3);
```

```
        yi = yi + Delta(4);
        Pvi = Pvi + Delta(5);
        Pri =Pri + Delta(6);

        %this pulls the real part of the complex solution
        Qv(j) = real(Qvi);
        Qb(j) = real(Qbi);
        Qlp(j) =real(Qlpi);
        y(j) = real(yi);
        Pv(j) = real(Pvi);
        Pr(j) =real(Pri);


    count = count + 1;

end
end %end of first for loop for compression iteration

%%%%%%%%%%%%%%%%%%%%%%%%%%%%%%%%%%%%%%%%%%%%%%%%%%%%%%%%%%%%%%%%%%%%%%%%%%
%%%
%%%begin of the rebound stroke
%% Pr > Pv > Pc, the velocity is negative in this region according to
EQ's
%at v = o the pressures are assumed to equalize, assign the values from
Pc
Pr(timesteps/2+1)=Pc(timesteps/2+1);
Pv(timesteps/2+1)=Pc(timesteps/2+1);
%%%%%%%%%%%%%%%%%%%%%%%%%%%%%%%%%%%%%%%%%%%%%%%%%
%%%common labels, v = valve, o = orifice, b = bleed orifice, lp =
leakage
%Initial guesses for unknowns for the Rebound calculation
Pv(timesteps/2 + 2) = 32.9; %pressue in the valving, psi
Pr(timesteps/2 + 2) = 32.1; %pressure in the rebound chamber, psi
Qv(timesteps/2 + 2) = 0.5;   %Valve Flow, in^3/sec
Qb(timesteps/2 + 2) = 0.5 ;  %Bleed Orifice Flow, in^3/sec
Qlp(timesteps/2 + 2) = 0.005 ; %Seal Flow, in^3/sec
y(timesteps/2 + 2) = .002; %Shim deflection, in
%%%%%%%%%%%%%%%%%%%%%%%%%%%%%%%%%%%%%%%%%%%%%%%%%%%%%%%%%%%%%%
 %%%%All constant Inputs from each equation for the Rebound stroke%%%
 %%%%%%
 %EQ1, Ar prevoiusly defined
 %%%%%%
 %EQ2  slugs, rho prevoiusly defined
 Dv2 = 1.13;%inch %Diameter of comp valve,i.e. Diameter of largest Shim
 Cdv2 = 0.71;%dynamic discharge coeff for valve : 2 = rebound stroke
 %%%%%%%%%
 %EQ3, Cf, Rop, a3, Av, Fsp prevoiusly defined
 %assume smaller diameter holes for rebound stroke
 Do2 = .0375; %in, Diameter of rebound orifice
 Ao2 =  3*pi*(Do2/2)^2; %area of orifice flow, 4 holes
 k2 = 800; %lbf/in spring constant of shims, this is an initial guess
%from shim model estimate Av,
% % %  Rop = .240; %in
```

```
% % % this was found by modeling shim and estimating pressure area
% % %  %based on top shim diameter in multi shim stack
% % %  a3 = .565; %in % same method as Rop. this is large shim radius
% % %  Av =  .5 * (pi*a3^2 - pi*Rop^2);
% % %  1/2 of annular area of acting pressue on shim
% % %  Fsp = 0;  %spring preload on shims, set to zero for start
%%%%
%EQ4, Ao1,rho,slugs previously defined
 Cdo2 = .71; %dynamic discharge coeff for orifice, 2 = Rebound
%%%%%
%EQ5  %rho, slugs previously defined
 Db2 = .104; %measured diameter of bleed orifice
 Ab2 = pi *(Db2/2)^2;
 Cdb2 =0.61; %Bleed orifice dynamic discharge coeff, 2=Rebound
%%%%%
 %EQ6 %b,mu,l previously defined
%
%%%%%%%%%%%%%%%%%%%%%%%%%%%%%%%%%%%%%%%%%%%%%%%%%%%%%%%%%%%%%%%%%%%%%%%%%%%%%%%
%%
%REBOUND STROKE ITERATIONS
for j = (timesteps/2 + 2):1:timesteps   %loop over time steps
    %define the initial guesses for the iteration loops
    if j == (timesteps/2 + 2)
       Qvi = Qv(timesteps/2 + 2);
       Qbi = Qb(timesteps/2 + 2);
       Qlpi =Qlp(timesteps/2 + 2);
       yi = y(timesteps/2 + 2);
       Pvi = Pv(timesteps/2 + 2);
       Pri =Pr(timesteps/2 + 2);
   else
       Qvi = Qv(j-1);
       Qbi = Qb(j-1);
       Qlpi = Qlp(j-1);
       yi = y(j-1);
       Pvi = Pv(j-1);
       Pri = Pr(j-1);
    end
count = 1;
%NOTE:
%all the equations and partials are overwritten for the rebound stroke,
%should be ok though
%EQ1: sums of total flows
f1 = Qvi + Qbi + Qlpi - (-Xdot(j))*Ar;  %f1 = 0 %negative cause neg vel
%partial derivatives
df1dQv = 1;
df1dQb = 1;
df1dQlp = 1;
df1dy = 0;
df1dPv = 0;
df1dPr = 0;

%EQ2: valve flow equation to shim
f2 = .5*pi*Dv2*yi*Cdv2*sqrt(2*slugs*(Pvi-Pc(j))/rho) - Qvi;  %f2 = 0
```

```
%partial derivatives
df2dQv = -1;
df2dQb = 0;
df2dQlp = 0;
df2dy = .5*pi*Dv2*Cdv2*sqrt(2*slugs*(Pvi-Pc(j))/rho);
df2dPv=(pi*Dv2*yi*Cdv2*sqrt(2))/(4*(rho/slugs)*sqrt(slugs*(Pvi-
Pc(j))/rho));
df2dPr =0;

%EQ3: Force balance on the valve
f3 = (Pvi-Pc(j))*Av + Cf*(rho/slugs)*(Qvi^2/Ao2) - Fsp - k2*yi;  %f3=0
%partial derivatives
df3dQv = 2*Cf*(rho/slugs)*(Qvi/Ao2);
df3dQb = 0;
df3dQlp =0;
df3dy = -k2;
df3dPv = Av;
df3dPr = 0;

%EQ4: Orifice flow rate equation to valve
f4 = Ao2*Cdo2*sqrt(2*slugs*(Pri-Pvi)/rho) - Qvi;%f4=0
%partial derivatives
df4dQv= -1;
df4dQb = 0;
df4dQlp = 0;
df4dy = 0;
df4dPv = (-Ao2*Cdo2*sqrt(2)) / (2*(rho/slugs)*sqrt(slugs*(Pri-
Pvi)/rho));
df4dPr = (Ao2*Cdo2*sqrt(2)) / (2*(rho/slugs)*sqrt(slugs*(Pri-
Pvi)/rho));

%EQ5: Bleed Orifice equation
f5 = Ab2*Cdb2*sqrt(2*slugs*(Pri-Pc(j))/rho) - Qbi;%f5=0
%partial derivatives
df5dQv = 0;
df5dQb = -1;
df5dQlp = 0;
df5dy= 0;
df5dPv =0;
df5dPr = (Ab2*Cdb1*sqrt(2)) / (2*(rho/slugs)*sqrt(slugs*(Pri-
Pc(j))/rho));

%EQ6: Seal leakage Equation
f6 = pi*Dpis*( b^3*(Pri-Pc(j))/(12*mu*l) + (-Xdot(j))*b/2) - Qlpi;
%f6=0
%partial derivatives
df6dQv = 0;
df6dQb = 0;
df6dQlp = -1;
df6dy = 0;
df6dPv = 0;
df6dPr = b^3*pi*Dpis/(12*mu*l);
```

```
%iterativly solve the system A*Delta = f
%build f vector
f = [-f1;-f2;-f3;-f4;-f5;-f6];
%build the A matrix
A(1,:) = [df1dQv,df1dQb,df1dQlp,df1dy,df1dPv,df1dPr] ;
A(2,:) = [df2dQv,df2dQb,df2dQlp,df2dy,df2dPv,df2dPr] ;
A(3,:) = [df3dQv,df3dQb,df3dQlp,df3dy,df3dPv,df3dPr] ;
A(4,:) = [df4dQv,df4dQb,df4dQlp,df4dy,df4dPv,df4dPr] ;
A(5,:) = [df5dQv,df5dQb,df5dQlp,df5dy,df5dPv,df5dPr] ;
A(6,:) = [df6dQv,df6dQb,df6dQlp,df6dy,df6dPv,df6dPr] ;

Delta = A^-1*f;
%reassign the unknowns
       Qvi = Qvi + Delta(1,1);
       Qbi = Qbi + Delta(2,1);
       Qlpi =Qlpi + Delta(3,1);
       yi = yi + Delta(4,1);
       Pvi = Pvi + Delta(5,1);
       Pri =Pri + Delta(6,1);
%%%%%%%%%%%%%%%%%%%%%%%%%%%%%%%%%%%%%%%%%%%%%%%%%%%%%%%%    Start newton
iterations
while max(abs(Delta))>.01 | max(abs(f))>.01
%EQ1: sums of total flows
f1 = Qvi + Qbi + Qlpi - (-Xdot(j))*Ar;  %f1 = 0 negative cause neg vel
%partial derivatives
df1dQv = 1;
df1dQb = 1;
df1dQlp = 1;
df1dy = 0;
df1dPv = 0;
df1dPr = 0;

%EQ2: valve flow equation to shim
f2 = .5*pi*Dv2*yi*Cdv2*sqrt(2*slugs*(Pvi-Pc(j))/rho) - Qvi;  %f2 = 0
%partial derivatives
df2dQv = -1;
df2dQb = 0;
df2dQlp = 0;
df2dy = .5*pi*Dv2*Cdv2*sqrt(2*slugs*(Pvi-Pc(j))/rho);
df2dPv=(pi*Dv2*yi*Cdv2*sqrt(2))/(4*(rho/slugs)*sqrt(slugs*(Pvi-
Pc(j))/rho));
df2dPr =0;

%EQ3: Force balance on the valve
f3 = (Pvi-Pc(j))*Av + Cf*(rho/slugs)*(Qvi^2/Ao2) - Fsp - k2*yi;  %f3=0
%partial derivatives
df3dQv = 2*Cf*(rho/slugs)*(Qvi/Ao2);
df3dQb = 0;
df3dQlp =0;
df3dy = -k2;
df3dPv = Av;
df3dPr = 0;
```

```
%EQ4: Orifice flow rate equation to valve
f4 = Ao2*Cdo2*sqrt(2*slugs*(Pri-Pvi)/rho) - Qvi;%f4=0
%partial derivatives
df4dQv= -1;
df4dQb = 0;
df4dQlp = 0;
df4dy = 0;
df4dPv = (-Ao2*Cdo2*sqrt(2)) / (2*(rho/slugs)*sqrt(slugs*(Pri-
Pvi)/rho));
df4dPr = (Ao2*Cdo2*sqrt(2)) / (2*(rho/slugs)*sqrt(slugs*(Pri-
Pvi)/rho));

%EQ5: Bleed Orifice equation
f5 = Ab2*Cdb2*sqrt(2*slugs*(Pri-Pc(j))/rho) - Qbi;%f5=0
%partial derivatives
df5dQv = 0;
df5dQb = -1;
df5dQlp = 0;
df5dy= 0;
df5dPv =0;
df5dPr = (Ab2*Cdb1*sqrt(2)) / (2*(rho/slugs)*sqrt(slugs*(Pri-
Pc(j))/rho));

%EQ6: Seal leakage Equation
f6 = pi*Dpis*( b^3*(Pri-Pc(j))/(12*mu*l) + (-Xdot(j))*b/2) - Qlpi;
%f6=0
%partial derivatives
df6dQv = 0;
df6dQb = 0;
df6dQlp = -1;
df6dy = 0;
df6dPv = 0;
df6dPr = b^3*pi*Dpis/(12*mu*l);

%iterativly solve the system A*Delta = f
%build f vector
f = [-f1;-f2;-f3;-f4;-f5;-f6];
%build the A matrix
A(1,:) = [df1dQv,df1dQb,df1dQlp,df1dy,df1dPv,df1dPr] ;
A(2,:) = [df2dQv,df2dQb,df2dQlp,df2dy,df2dPv,df2dPr] ;
A(3,:) = [df3dQv,df3dQb,df3dQlp,df3dy,df3dPv,df3dPr] ;
A(4,:) = [df4dQv,df4dQb,df4dQlp,df4dy,df4dPv,df4dPr] ;
A(5,:) = [df5dQv,df5dQb,df5dQlp,df5dy,df5dPv,df5dPr] ;
A(6,:) = [df6dQv,df6dQb,df6dQlp,df6dy,df6dPv,df6dPr] ;

Delta = A^-1*f;
%reassign the unknowns
       Qvi = Qvi + Delta(1,1);
       Qbi = Qbi + Delta(2,1);
       Qlpi =Qlpi + Delta(3,1);
       yi = yi + Delta(4,1);
       Pvi = Pvi + Delta(5,1);
       Pri =Pri + Delta(6,1);
```

```
    Qv(j) = real(Qvi);
       Qb(j) = real(Qbi);
       Qlp(j) =real(Qlpi);
       y(j) = real(yi);
       Pv(j) = real(Pvi);
       Pr(j) =real(Pri);
    count = count + 1

end
end %end of rebound iteration loop

%This defines the last Pv, Pr for graphing
Pr(timesteps+1)=Pc(timesteps+1);
Pv(timesteps+1)=Pc(timesteps+1);
%%%%%%%%%%%%%%%%%%%
%Now calculate the Damping Forces
DampingF = zeros(timesteps+1,1);
Ffric = 5; %lbs of seal friction
Mpassm = .335 ; %Measured piston/rod assembly mass
%%%%%%%%%%%%%%%%%%%
%calc the damping force, account correctly for constant friction
for j = 1:1:timesteps/2
    DampingF(j) = - Pr(j)*Ar + Pc(j)*Apis + Ffric +
Mpassm*Xdotdot(j)/slugs;
end

for j = timesteps/2+1 : 1 : timesteps
    DampingF(j) = -Pr(j)*Ar + Pc(j)*Apis -
Ffric+Mpassm*Xdotdot(j)/slugs;
end

DampingF(timesteps+1) = - Pr(timesteps+1)*Ar + Pc(timesteps+1)*Apis
+ Ffric + Mpassm*Xdotdot(timesteps+1)/slugs;

%Note: you must divive the mass by slugs !!!!!!!!!
%%%%%%%%%%%%%%%%%%%%%%%%%%%%%%%%%%%%%%%%%%%%%%%%%%%%%%%%%%%%%%%%%%%%%%%
figure(555)
hold on
plot(Xdot, Pr,'-b')
plot(Xdot, Pv, '-r')
plot(Xdot, Pc, '-g')
legend('Pr', 'Pv','Pc')
%
% figure(556)
% hold on
% plot(Xdot,Q,'-r')
% plot(Xdot,Qv,'-g')
% plot(Xdot,Qb,'-b')
% plot(Xdot,Qlp, '-c')
% legend('Q','Qv','Qb','Qlp')
```

```
% figure(777)
% plot(Xdot, DampingF, '-b');
% xlabel('Velocity, in/sec')
% ylabel('Damping Force, lbf')
% title('Damper Force vs. Velocity')
%
%
% figure(888)
% plot(Xvec, DampingF, '-b');
% xlabel('Displacement, in')
% ylabel('Damping Force, lbf')
% title('Damper Force vs. Displacement')

%reverse the velocity vector for different velocity definition
RevXvec = zeros(timesteps+1,1);
for j = 1:1:timesteps+1
    RevXvec(j) = -Xvec(j);
end

figure(998)
plot(RevXvec, DampingF, '-b');
xlabel('Velocity, in/sec')
ylabel('Damping Force, lbf')
title('Damper Force vs. Velocity')

RevXdot = zeros(timesteps+1,1);
for j = 1:1:timesteps+1
    RevXdot(j) = -Xdot(j);
end
figure(999)
grid
hold on
plot(RevXdot, DampingF, '-b');
xlabel('Velocity, in/sec')
ylabel('Damping Force, lbf')
title('Damper Force vs. Velocity')
```

VITA

Name:	Kirk Shawn Rhoades
Address:	8303 Tierra Serena Pl. NE
	Albuquerque, NM 87122
Email Address:	ksrhoad@tamu.edu
Education:	B.S., Mechanical Engineering, University of New Mexico, 2004
	M.S. Mechanical Engineering, Texas A&M University, 2006